ลักษณะเฉพาะของสายแร่ที่สัมพันธ์กับการเกิดแร่ทองคำความสมบูรณ์สูงจากบ่อเอตะวันออกของแหล่งทองคำชาตรี จังหวัดพิจิตรและเพชรบูรณ์ ประเทศไทย

นางสาวภิญญาพัชญ์ รงคะพิมลพงศ์

วิทยานิพนธ์นี้เป็นส่วนหนึ่งของการศึกษาตามหลักสูตรปริญญาวิทยาศาสตรมหาบัณฑิต
สาขาวิชาธรณีวิทยา ภาควิชาธรณีวิทยา
คณะวิทยาศาสตร์ จุฬาลงกรณ์มหาวิทยาลัย
ปีการศึกษา 2558

CHARACTERISTICS OF VEIN RELATED TO HIGH GRADE GOLD MINERALIZATION FROM EASTERN A PIT OF THE CHATREE GOLD DEPOSIT, CHANGWAT PHICHIT AND PHETCHABUN, THAILAND

Miss Phinyaphat Rongkhapimonpong

A Thesis Submitted in Partial Fulfillment of the Requirements
for the Degree of Master of Science Program in Geology
Department of Geology
Faculty of Science
Chulalongkorn University
Academic Year 2015

Thesis Title	CHARACTERISTICS OF VEIN RELATED TO HIGH GRADE GOLD MINERALIZATION FROM EASTERN A PIT OF THE CHATREE GOLD DEPOSIT, CHANGWAT PHICHIT AND PHETCHABUN, THAILAND
By	Miss Phinyaphat Rongkhapimonpong
Field of Study	Geology
Thesis Advisor	Associate Professor Chakkaphan Sutthirat, Ph.D.
Thesis Co-Advisor	Weerasak Lunwongsa, M.Sc.

Accepted by the Faculty of Science, Chulalongkorn University in Partial Fulfillment of the Requirements for the Master's Degree

.....Dean of the Faculty of Science
(Associate Professor Polkit Sangvanich, Ph.D.)

THESIS COMMITTEE

.....Chairman
(Assistant Professor Pitsanupong Kanjanapayont, Dr.rer.nat.)

.....Thesis Advisor
(Associate Professor Chakkaphan Sutthirat, Ph.D.)

.....Thesis Co-Advisor
(Weerasak Lunwongsa, M.Sc.)

.....Examiner
(Associate Professor Visut Pisutha-Arnond, Ph.D.)

.....External Examiner
(Somboon Khositanont, Ph.D.)

ภิญญาพัชญ์ รงคะพิมลพงศ์ : ลักษณะเฉพาะของสายแร่ที่สัมพันธ์กับการเกิดแร่ทองคำความสมบูรณ์สูงจากบ่อเอตะวันออกของแหล่งทองคำชาตรี จังหวัดพิจิตรและเพชรบูรณ์ ประเทศไทย (CHARACTERISTICS OF VEIN RELATED TO HIGH GRADE GOLD MINERALIZATION FROM EASTERN A PIT OF THE CHATREE GOLD DEPOSIT, CHANGWAT PHICHIT AND PHETCHABUN, THAILAND) อ.ที่ปรึกษาวิทยานิพนธ์หลัก: รศ. ดร.จักรพันธ์ สุทธิรัตน์, อ.ที่ปรึกษาวิทยานิพนธ์ร่วม: วีระศักดิ์ ลันวงษา, 127 หน้า.

เหมืองแร่ทองคำชาตรีเป็นแหล่งแร่ทองคำ-เงิน-อิพิเทอร์มอลล์ใหญ่ที่สุดในประเทศไทย แหล่งแร่ประกอบด้วยสายแร่ ที่มักประกอบด้วยแร่ควอตซ์, คาร์บอเนต คลอไรต์ อะดูลาเรีย ไพไรต์ และสายแร่เนื้อกรวดเหลี่ยมตัดเข้ามาในชุดหินตะกอนภูเขาไฟและหินกรวดเหลี่ยมแอนดีไซต์ เหมืองชาตรีมีหลายบ่อเหมือง ในการศึกษาครั้งนี้จะเน้นศึกษาในบ่อเอตะวันออก ทางตอนเหนือของแหล่งทองคำชาตรี พบทองคำเกิดในสายแร่ ควอตซ์และหินกรวดเหลี่ยมจากน้ำแร่ร้อน ในชุดหินตะกอนและตะกอนภูเขาไฟดังกล่าว

การศึกษาสายแร่ทองคำความสมบูรณ์สูง พบลักษณะเฉพาะขององค์ประกอบสายแร่ ควอตซ์ คาร์บอเนต ไพไรต์ ในสายแร่ลำดับที่สอง ที่แสดงลักษณะแถบริ้วแถบ และโครงร่างตาข่าย การศึกษาลักษณะทางศิลาวรรณาและเนื้อแร่ควอตซ์พบทองคำและอิเล็กตรัม เกิดเป็นมลทินขนาดเล็กมาก ส่วนใหญ่เกิดในผลึกแร่ไพไรต์ ทองคำยังพบเป็นมลทินร่วมกับแร่อะดูลาเรียในผลึกแร่ไพไรต์ จากการศึกษาธรณีเคมีตัวอย่างสายแร่ทองคำความสมบูรณ์สูงพบสัมพันธ์กับปริมาณ Te ซึ่งพบเป็นองค์ประกอบร่วมอยู่กับอิเล็กตรัม เนื้อของแร่ควอตซ์จะประกอบไปด้วย ลักษณะเป็นแถบริ้ว, แบบพู่ขนนก, แบบซี่หวี-ริ้วขนานการเติบโตของผลึก, แบบรัศมีวงกลมคล้ายพืชมอสส์หรือผลึกมุมมืดแบบรัศมี และแบบผลึกเนื้อน้ำตาล แผนภูมิความน่าจะเป็นดูความผิดปกติและการกระจายตัวของข้อมูลของธาตุร่องรอย สามารถบ่งชี้ธาตุร่องรอยที่บ่งชี้แร่ทองคำความสมบูรณ์สูงได้แก่ Ag, As, Cu, Pb, Zn, Sb และ Te ซึ่งเมื่อวิเคราะห์โดยใช้แผนภูมิกล่อง เปรียบเทียบความสัมพันธ์ของธาตุร่องรอยในแต่ละกลุ่ม กับเนื้อแร่ ควอตซ์ และ วิเคราะห์เปรียบเทียบธาตุร่องรอยในแต่ละกลุ่มขององค์ประกอบแร่ แสดงให้เห็นว่าธาตุร่องรอยที่เป็นตัวบ่งชี้การเกิดแร่ทองคำดีที่สุดได้แก่ Au, Ag, Te และ Zn

ภาควิชา ธรณีวิทยา	ลายมือชื่อนิสิต .....
สาขาวิชา ธรณีวิทยา	ลายมือชื่อ อ.ที่ปรึกษาหลัก .....
ปีการศึกษา 2558	ลายมือชื่อ อ.ที่ปรึกษาร่วม .....

5472247323 : MAJOR GEOLOGY
KEYWORDS: QUARTZ TEXTURE / PATHFINDER / HIGH GRADE GOLD MINERALIZATION / CHATREE GOLD DEPOSIT

PHINYAPHAT RONGKHAPIMONPONG: CHARACTERISTICS OF VEIN RELATED TO HIGH GRADE GOLD MINERALIZATION FROM EASTERN A PIT OF THE CHATREE GOLD DEPOSIT, CHANGWAT PHICHIT AND PHETCHABUN, THAILAND. ADVISOR: ASSOC. PROF. CHAKKAPHAN SUTTHIRAT, Ph.D., CO-ADVISOR: WEERASAK LUNWONGSA, M.Sc., 127 pp.

Chatree gold mine is the largest gold-silver epithermal deposit in Thailand. This deposit is characterized by quartz-carbonate-chlorite-adularia-pyrite veins and breccias vein cross-cutting into volcaniclastic sedimentary rock and andesitic volcanic breccia. Several mining pits have been operated at the Chatree deposit. This study area is focused on the Eastern A pit which is located in the northern part of the deposit in which gold mainly occurs in quartz veins and hydrothermal breccias hosted by volcanogenic sedimentary rock.

High grade gold veins were investigated in mineralogical characteristics related to the main gold mineralization, particularly in the second stage vein of quartz-carbonate-pyrite (sulfide-base metal) band or stockwork. Based on quartz textural and petrological analyses gold and electrum usually form as fine inclusions significantly in pyrite host. Moreover, adularia may occur with gold forming multiple-phase inclusions in pyrite host. Geochemical investigation indicates that high grade vein samples are related to higher Te content and Te appears to enrich in electrum grains. Various textures of quartz in these veins were recognized includes band, plumose, comb-zonal, moss, ghost-sphere and saccharoidal texture. Among them, banded and plumose quartz textures appear to be closely associated with high grade gold and both textures are mostly common found in vein samples under this studies. The significant pattern of trace elements in probability diagram were determined for possible pathfinder of gold which they are Ag, As, Cu, Pb, Zn, Sb and Te. In addition, box diagram of trace elements was correlated with quartz texture and sulfide assemblage in the main gold mineralized vein; consequently, the significant pathfinder of gold deposit were indicated including Au, Ag, Te and Zn.

Department:	Geology	Student's Signature	.....
Field of Study:	Geology	Advisor's Signature	.....
Academic Year:	2015	Co-Advisor's Signature	.....

ACKNOWLEDGEMENTS

The author would like to thank Issara Mining Ltd., for financial and technical support. Special thank is send to Ron James, Genesio Circosta, Fiona Davidson and Brendan Badley.

The author would like to thank her thesis advisor Associate Professor Dr. Chakkaphan Sutthirat and co-advisor Mr. Weerasak Lunwongsa for their advice, reviewing and comment throughout this work.

Saranya Nuanla-ong was supervising in sampling and study of vein paragenesis. Phuriwit Sangsiri was teaching in microscopic and textural investigation. Alongkot Funka and Sopit Pumpuang assisted in EPMA analysis and logistical support. Many staffs of Issara Mining who were helping in sample collection. Natthee Rongkhapimonpong helped to produce figures and also gave encouragement and support.

Special thank is sent to Jensarin Vivatpinyo and Suphansa Toaree for encouragement and suggestion during my study. The author also thanks Dr. Abhisit Salam, Department of Geology, Chulalongkorn University for comment and suggestion in petrographic and geochemical interpretation.

Great encouragement and support from my parents are the most crucial driving force for this success.

CONTENTS

Page

Page

List of Tables

List of Figures

CHAPTER 1
Introduction

1.1 General Statement

"Gold" is a precious metal which has been highly demanded since ancient times. Gold is also used in coinage, exchange reserves under the gold standard, jewelry, electronics, telecommunications, medical profession and dentistry. Gold most often occurs as a native metal, typically in a metal solid solution with silver. Such alloys usually have a silver content of 8–10%. Electrum is an elemental gold with more than 20% silver. Electrum's color varies from golden-silvery to silvery, depending upon the silver content. Sometimes, gold occurs combined with tellurium as the minerals calaverite, krennerite, nagyagite, petzite and sylvanite and as the rare bismuthide maldonite (Au_2Bi) and antimonide aurostibite ($AuSb_2$), and also occurs in rare alloys with copper, lead, and mercury. Thailand is one of the great potential and has been discovered with many of gold occurrence suitable for mining over the past years , ((Amstutz et al., 2012); Cooke (1982); Christie and Brathwaite (2011)).

Chatree gold mine is one of the largest epithermal gold-silver deposit in the central Thailand which was green field discovered in 1995 and subsequently developed to operation in 2000. It is located on the eastern edge of the Tertiary Chao Phraya Basin (Diemar and Diemar, 1999), 280 km north of Bangkok in Phichit province, (see Figure 1.1). This gold mineralization occurs in the central part of the Loei Phetchabun Permo-Triassic volcanic belt, which extend from Lao, through Central Thailand southeastward into Cambodia. Currently, the Chatree mine has defined pits and prospects, including Q, A, C, H, D, K, J, P, S pits and B, N and V prospects (see Figure 1.3). The ore production of Chatree in 2014 was approximately 3.84 million ounces of gold (181.3 Mt) at an average grade of 0.66 g/t Au and 6.46 g/t Ag (Jame et al., 2014).

According to an intersected broad zone of high grade gold mineralization in A pit, results include an intersection of 49.4 metres at 4.3g/t gold (from 227 metres), including a high grade interval of 29.8 metres at 6.25g/t gold (from 246 metres), from diamond drill hole of the year 2013. The high grade mineralization confirms the additional exploration drill holes in order to evaluate the potential of the deposit towards the east part of A pit (B. Branden, personal communication, 2013). Resource

development drilling has identified targeting extensions and deeper gold mineralization in Eastern A pit and required the vein characteristic related to high grade Au. The characteristics of vein which related to high grade gold have been considered to define the ore body boundary, continuity of the deposit and increase the gold reserves in prospective of high grade potential zone, Braund (2006). The relatively high gold grade occurrences hosted in quartz veins were identified on the A east lode ore body which is currently being mined as an open pit and located in Chatree north. Vein samples in this study were collected from lower to higher gold grades for examination. This study is aimed to define the vein characteristics in term of texture, and to examine the geochemical tools for targeting high grade gold mineralization. The results of this study, geochemical indicators, can be used to identify the pathfinder element for gold.

Figure 1.1 Index map of Thailand showing location of Chatree Mine (reference map of Thailand: Nations Online Project).

1.2 Location and Accessibility

The Chatree gold mine is located on the boundary between Thap Klo District, Phichit Province and Wang Pong District, Phetchabun Province, (see Figure 1.2). It is

about 280 km north of Bangkok (latitude 16° 18′ and longitude 100° 40′) and approximately 27 km north of Khao Sai Town.

The study area is defined as Eastern A pit which is in the northern part of Chatree deposit (Figure 1.3). This Eastern A pit covers approximately 0.45 sq km in which the study area between vertical UTM grid lines from 676670 m E - 676710 m E and horizontal UTM grid lines from 1803465 m N - 1803610 m N. The main accessibility is using the Highway No.1 from Bangkok passing through Pathum Thani, Saraburi, Lopburi Provinces before turning right to Highway No. 11 from Tak Fa District, Tak Province to Thap Klo District, Pichit Province. The alternative routes are taking train to Taphan Hin station of Phichit Province, or by taking airplane to Phitsanulok Province, then taking car to follow Highway no. 11 to Thap Klo District. The study area can be accessed using road No.1301 (Ban Nong Khanak), to about 6 km from Khaosai Junction, then turning right to Chatree mine.

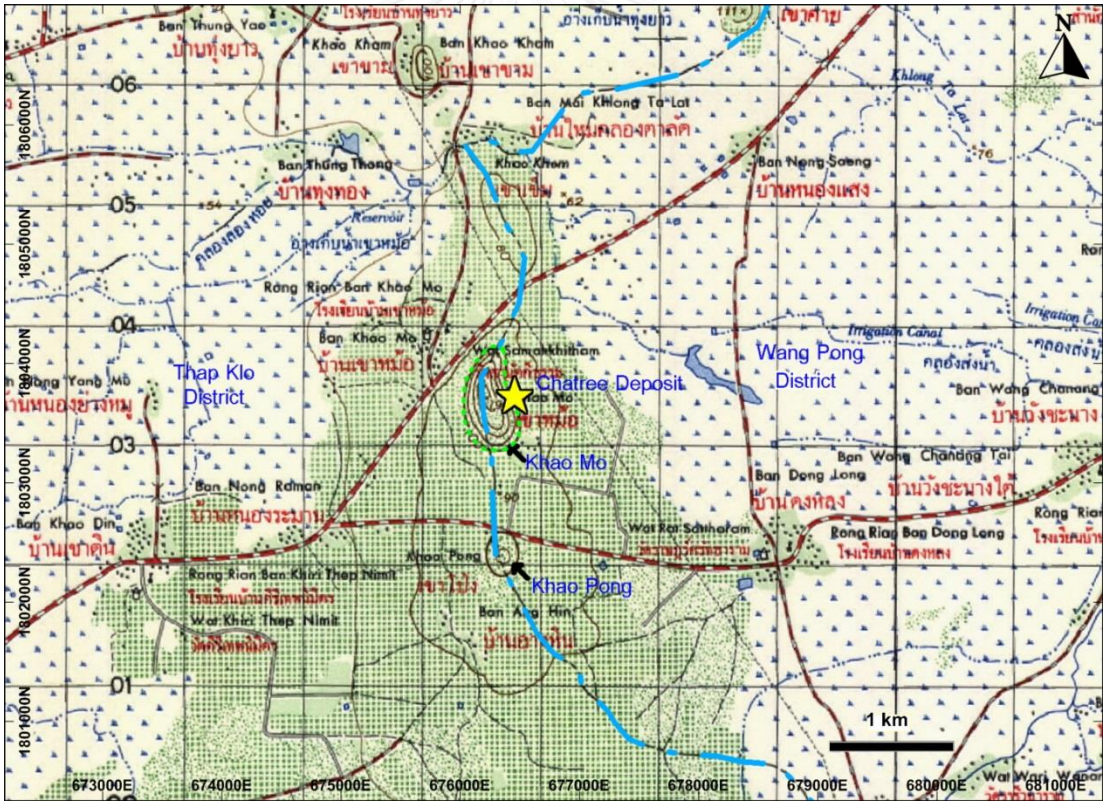

Figure 1.2 Topographic map of the Chatree deposit, located between Thap Klo District of Phichit Province and Wang Pong District of Phetchabun Province. (Topographic map sheet Phaenthi Phumiprathet, published by The Royal Thai Survey Department, Bangkok, Thailand).

Figure 1.3 Aerial photo showing the study area at the Eastern A pit (AE) of the Chatree Mine.

1.3 Objectives

The main objectives of this study are to investigate petrography and geochemistry of mineralization from Eastern A pit of the Chatree gold deposit and to determine the characteristics of veins related to high grade gold mineralization.

1) To describe the mineralized characteristics in term of mineralized texture, paragenesis, mineralized composition.

2) To interpret the geochemical data to determine the pathfinder element for gold mineralization.

1.4 Previous works

Several researches (as reported by Cumming et al. (2006)) have investigated gold mineralization in Chatree mine; in which is located in the central part of the Loei-Petchabun-Prachinburi-Chantaburi Permo-Triassic volcanic belt (LPC). The LPC extends from western Lao PDR along the western edge of Khorat plateau passing through the Cambodian central plain. Geologically, it contains calc-alkaline intrusives, volcanic rocks and sedimentary rocks.

Corbett (2002) classified Chatree gold deposit as epithermal low sulfidation system in term of "rift low sulfidation" that is typically confined by rifts system within magmatic arcs or back arc environments. The Rift Low Sulphidation deposit is indicated by adularia-sericite epithermal gold-silver occurred as banded fissure veins, local vein and breccias which comprise predominantly colloform banded quartz, adularia, quartz pseudomorphing carbonate, and dark sulphidic material termed as ginguro bands. Gangue minerals contain chalcedony, adularia, quartz pseudomorphing platy carbonate. It locally displays carbonate-basements and quartz-sulfide gold styles.

Cumming (2004); Cumming et al. (2008); Salam et al. (2014) studied lithological components of the Chatree deposit. The Chatree district-scale units of volcanic succession are subdivided into four main units. The last updated lithological components of Salam et al. (2014) contains seven major geological units around the Chatree mine from the oldest to youngest: (i) Carboniferous volcanogenic sedimentary rocks and Lower Permian limestone; (ii) Late Permian plagioclase–hornblende-phyric basaltic andesite; (iii) Late Permian polymictic mafic–intermediate breccia; (iv) Upper Permian to Lower Triassic volcanogenic sedimentary unit; (v) Late Permian to Early Triassic fiamme breccia; (vi) Middle Triassic diorite and post-mineralization dykes and (vii) Upper Triassic and Jurassic Khorat Group.

Salam (2011) also studied the lithology and mineralization of Chatree mine. This study suggested that the volcanic breccia such as polymictic mafic-intermediate breccia facies (unit 3), volcanogenic sedimentary facies association (unit 2) and monomictic plagioclase-phyric andesite breccia facies (unit 4), are the most abundant gold mineralization. The minor mineralization is rarely found in a coherent plagioclase-hornblende-phyric andesite facies. The fiamme breccia facies appears to be a good cap-rock for mineralization of A and H pits.

The main gold-silver mineralization is closely associated with Stage 4 (Salam, 2011) which is characterized by colloform-crustiform banded quartz ± carbonate ± chlorite ± adularia-sulfide-electrum vein (Corbett (2002); Salam (2011); Salam et al. (2014)). Most of the gold is present as native gold and electrum (combined Au and Ag) which they form inclusions crucially in pyrite (Kromkhun, 2005); (Cumming et al., 2008); (Tangwattananukul et al., 2009); (Salam et al., 2014).

Higher Au grade is confined by sulfide-rich assemblage and associated with quartz veins and banded vein (Salam, 2011). The majority of mineralized vein trends N-S to NNW-SSE with about 60° to 85° dipping to the west (gentle west dipping in the western part of the A Pit and steeper dipping in A pit to A east pit). The main gold mineralization of A pit includes mainly colloform-crustiform banded and breccia of quartz ± carbonate ± chlorite-sulfide-electrum, massive vein and stockwork vein of quartz-carbonate±adularia- sulfide-electrum (Sangsiri, 2010).

Tangwattananukul (2012), studied the vein characteristics in Q prospect of the Chatree mine which this work presented the gold-bearing quartz vein composing mainly of quartz, adularia, chlorite, calcite and sulfide. They are related to microcrystalline-quartz and quartz-calcite stockwork vein with high concentrations of base-metals.

There are various examples of epithermal vein deposit, such as Kencana (Gosowong gold field, Indonesia), Cracow, Pajingo (Australia), La Josefina (Argentina), Hishikari and Kushikino (Japan), Karangahake and Waihi (New Zealand) and Lebong Donok (Indonesia).

Kencana gold deposit is a low sulfidation epithermal Au/Ag and is a part of Gosowong Gold field that is similar to Chatree in mineralization and alteration style. Richards et al. (2005) studied mineralized assemblage which is formed by multistage mineralization, with four different types, namely, 1) crystalline quartz vein in massive to banded texture, bladed textures in calcite pseudomorphs and electrum with some base metal sulfide (<5 g/t gold grades); 2) quartz-adularia vein forming as crustiform-colloform banded quartz with dark chlorite interlayer (10-50 g/t gold grade); 3) quartz-

chlorite vein and banded quartz-chlorite having brecciated pre-existing vein, with bonanza 10-100 g/t Au grade Au grade; 4) silica-sulfide including hydraulic reactivation of mineralized faults with brecciation. The mineralization zone is presented by quartz-illite-chlorite alteration. High grade quartz-adularia is associated with the bonanza gold grades in quartz-chlorite within distinctive illite-chlorite alteration halo at Gosowong.
Pinder (2006) studied mineralization and geochemical evaluation of the Vera Nancy system, Pajingo. This work reported that mineralization in Pajingo Epithermal is low sulfidation, quartz-adularia type, with bonanza Au and Ag. The whole results of rock geochemistry are referred as pathfinder for gold mineralization. At the upper level, Ag, As, Sb, Tl, Cd and Hg are high value and decreasing against depth. As and Sb are depleted in the main Au-Ag zone. Textural features of quartz was also recognized in the Pajingo. The best indicator of mineralized quartz vein is banded texture that hosts significant Au grade (>100ppm) with electrum, Au, Ag, Te and tetrahedrite (sulfosalt group). Milky chalcedony hosts moderately high Au grades (<100ppm) with electrum and moderate amounts of Ag minerals and sulfosalt.

The most complex textures of low sulphidation epithermal in the Cracow gold field are generally correlated to the highest gold grade (> 10 g/t). Colloform, moss, pseudo acicular-acicular in both quartz and adularia within central vein and or overprinted by hydrothermal breccias channel which are coincident with high gold grade. Braund (2006) studied geochemical vectoring of Cracow deposit and consequently defined a key elemental distribution; Au is associated with Ag and dominated in the upper level. At deeper level, Au associated with Te is more significant than Au-Ag assemblage. Variation of Pb sulfide species are composed of galena, altaite (PbTe) and another Pb sulfosalt varieties with no direct relation to dept. Variation of Cu sulfide species contain chalcopyrite, bornite and tetrahedrite also without direct relation to dept. Ag is greater than Au at halo and intercept above Bonanza shoot (approximately 1:3 of Ag: Au). Ag-Te anomaly is located just below bonanza Au zone. Ag-Te and As-Sb can apply to elemental proximity halo to Au shoot.

For geochemical indicator of La Josefina low epithermal Au-Ag deposit studied by Palomera et al. (2012), geochemical vectoring is concentrated in hydrothermal vein and breccias indicating hydrothermal alteration and representing in four vertical cross sections. At the deposit scale, it shows high concentrations of As, V, Co, Mn, FeO, Au, Pb, Cu, Hg, Cr, Ni, P, MgO and Zn (high value of carbonate-chlorite-pyrite), and low

concentration of Ba, Be and CaO. These can be geochemical indicators of the mineralized zone or proximal to Au rich vein. In detailed-scale, P, Au, Cu, Pb, Hg, Ba and MgO show the strongest compositional drifts those can be the best geochemical indicators.

1.5 Methodology

1.5.1 Fieldwork and Sample Collection

Geological setting, rock distribution and mineralization and cross-cutting relationship of vein paragenesis were firstly investigate using the previous researches of Cumming et al. (2006) and Salam (2011). The later work reported the detailed mineral paragenesis and rock unit classification.

Revising extremely high gold grade interval of diamond-drill core samples by mineralization logging was carried out prior to samples collection. Logging of samples in the main lode ore of A east pit was focused on hydrothermal breccias and quartz vein zones in detailed textural characteristics, mineral compositions, distinctive physical properties, sulfide species and vein paragenesis. Forty vein samples were then collected to represent vein types including stockwork vein, breccia vein and banded vein in volcaniclastic sedimentary host from the A east ore zone. The selected vein samples were re-analyzed for Au grade at Chatree laboratory. This study was focused on the gold grades greater than 8 g/t Au; presenting a grade of gold ranging from 1-73 g/t Au (relatively higher Au grade) and also selected small amount of samples containing the lowest gold grade between 0.1-0.9 g/t.

All 40 vein samples taken from 23 drill holes along north to south between sections 19625 to 19775N in the part of M01 mineralized zone were picked up because they show good continuity of gold grade and the best intersections of gold mineralized veins. The high grade gold mineralization in A pit can be divided into 6 major lodes which are M01 to M04, E01 and E02, and sub-lodes 01 to 03 (Nuanla-ong, 2012) (see Figure 1.4).

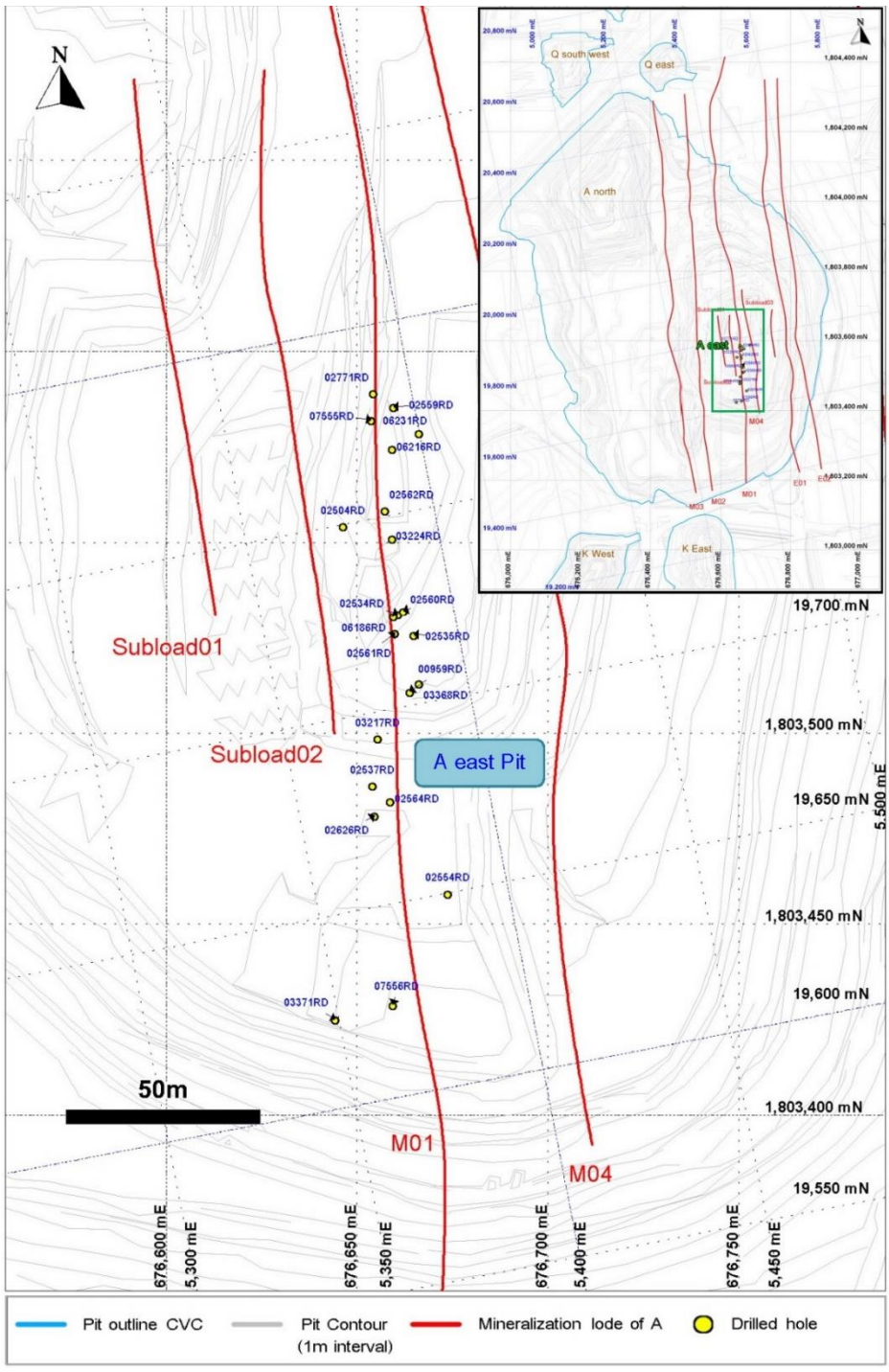

Figure 1.4 Location of A east area, a part of the Chatree gold mine showing drilled-holes location along M01 mineralization lodes, the selected ore zone for this study.

1.5.2 Laboratory Works

1.5.2.1 Petrographic Description

All forty vein samples were prepared as 46 thin sections and 37 polished sections for petrographic study. The polished thin sections were usually prepared at about 50 μm thick before polishing with 12, 6, 3, and 1 μm diamond pastes, respectively. The petrographic description and ore microscopic investigation were aimed to identify relationship of mineral phases under a polarizing microscope. These descriptions include vein texture, crystal shape, mineral assemblage, replacement and intergrowth, especially in quartz, carbonate, sulfide and adularia.

1.5.2.2 Mineral Chemistry

Ten polished sections are selected for electron-probe micro-analysis (EPMA) using wavelength-dispersive (WDS) spectroscope for composition of sulfide minerals related to gold mineralization. They were prepared from representative high gold grade vein samples including A001 (16 g/t Au), A002 (73 g/t Au), A010 (11.95 g/t Au), A011 (21.1 g/t Au), A012 (14.5 g/t Au), A013 (11.1 g/t Au), A017 (16.7 g/t Au), A024 (8.8 g/t Au), A032 (14.3 g/t Au) and A038 (8.8 g/t Au). They are the highest gold grade samples (analysed from the Chatree laboratory); these samples also contain high concentration of sulfide. A JEOL JXA-8100 EPMA based at Geology Department, Faculty of Science, Chulalongkorn University was used for these mineral chemical analyses. Accelerating voltage of 15kV and probe current of about 24 nA were set to produce an electron beam with a diameter smaller than 1 μm for surface analysis of selective mineral grains. The selected points under microscope for EPMA analysis were focused on the mineral phases accumulated with gold. The EPMA results can clearly determine compositions of sulfide minerals appeared in gold mineralization. Moreover, determination of Au and Ag concentrations in these sulfides (e.g., pyrite, sulfosalt, sphalerite and chalcopyrite) were also carried out. Quantitative analyses are reported as element weight percent. Elements under this consideration are Al, Mg, Au, Cu, Ag, Te, Si, Ca, Fe, Sb, Th, Na, Cr, Mn, S, Tl, As, Pb, Ni, Mo, Se, Zn, K and Sr. The reference standards used for electron microprobe are pure metals (i.e., Au, Cu and Ag), pure oxides (i.e., Al_2O_3 for Al, MgO for Mg, SiO_2 for Si, Cr_2O_3 for Cr, MnO_2 for Mn, $BaSo_4$ for Ba, Ni_2O_3 for Ni, PbO for Pb, MoO_2 for Mo, $SrBaNb_2O_6$ for Sr), mineral standards (i.e., wollastonite ($CaSiO_3$ for Ca), fayalite (Fe_2SiO_4 for Fe), jadeite ($NaAlSi_2O_6$ for Na), zinc oxide (ZnO for Zn), pottasium oxide (K_2O for K), and internal standards for Te, Sb, Th, As and Se. These standards were summarized in Table 1.1.

Table 1.1 Summary of standard materials used for EPMA analysis

Type of Standard	Name of Standrd	Element	Concentration	Type of Standard	Name of Standrd	Element	Concentration
Mineral Standard	Potassium	K_2O	23.80	Oxide Standard	Corundum	Al_2O_3	99.99
	Titanium	TiO_2	46.33		Periclase	MgO	99.99
	Phosonate	P_2O_5	35.87		Eskolalite	Cr_2O_3	99.99
	Barite	BaO	65.12		Manganosite	Mn_2O	99.9
		SrO	0.68		Lead Vanadium Germanium Oxide	PbO	79.29
		SO_3	34.10			GeO_2	7.42
	Zinc oxide	ZnO	99.80			V_2O	12.88
		SiO_2	0.13			SiO_2	0.38
		Al_2O_3	0.20	Pure Metal Standard	Gold	Au	99.99
	Fayalite	FeO	70.15		Silver	Ag	99.99
		SiO_2	29.49		Copper	Cu	99.99
	Wallastonite	MgO	0.15		Cadmium	Cd	99.9
		SiO_2	50.94	Sulphide Standard	Stibnite	Sb	71.48
		CaO	48.00			S	28.44
		MnO	0.09	Internal Standard	Arsenic	As	-
		FeO	0.11		Molybdenum	Mo	-
	Jadeite	Na_2O	15.10		Tellurium	Te	-
		MgO	0.10		Thallium	Th	-
		Al_2O_3	25.10				
		SiO_2	59.40				
		FeO	0.13				

1.5.2.3 Whole-Rock Geochemistry

Whole-rock trace element analyses of all forty vein samples were carried out using combination method of ICP-MS and ICP-AES at the Australian Laboratory Service (ALS). In order to report the widest possible concentration range, this method uses both ICP-MS (Inductively Coupled Plasma-Mass Spectrometer) and ICP-AES (Inductively Coupled Plasma Atomic Emission Spectrometer). They provided multi-element package useful for exploration which analyses included Ag, Cu, Hg, Pb, Zn, Rb, Se, As, Bi, Sb, Te, Tl, Cd, Mo, Fe, Mg and S. Prior to both ICP-MS and ICP-AES analytical techniques, minimum 1 g of milled samples were digested using the Aqua Regia Method. Then these solutions were analyzed by both techniques with ultra-low detection limits. Aqua Regia digestion is suitable for the determination of gold and related elements in rock, soil and stream sediment samples as determined by ALS Chemex laboratories.

Finally, interpretation, discussion and conclusion were performed. All results are then reported in thesis report. Moreover, presentation and a draft of manuscript for an international journal are also preparing. All steps of methodology are summarized as schematic diagram in Figure 1.5.

This thesis report contains 5 chapters. This chapter is introduction of research background, objectives and analytical methods. Chapter 2 reports an overview of tectonic evolution of Thailand, particularly focused on the Loei fold belt, geologic

setting of Chatree deposit and stratigraphic sequences. Chapter 3 describes the vein characteristic as textural features, compositions, assemblage and sequences of gold mineralization. Chapter 4 presents whole-rock geochemistry and ore mineral chemistry with interpretation of these data. Eventually, discussion and conclusion of all results are made for the specific aspects in Chapter 5.

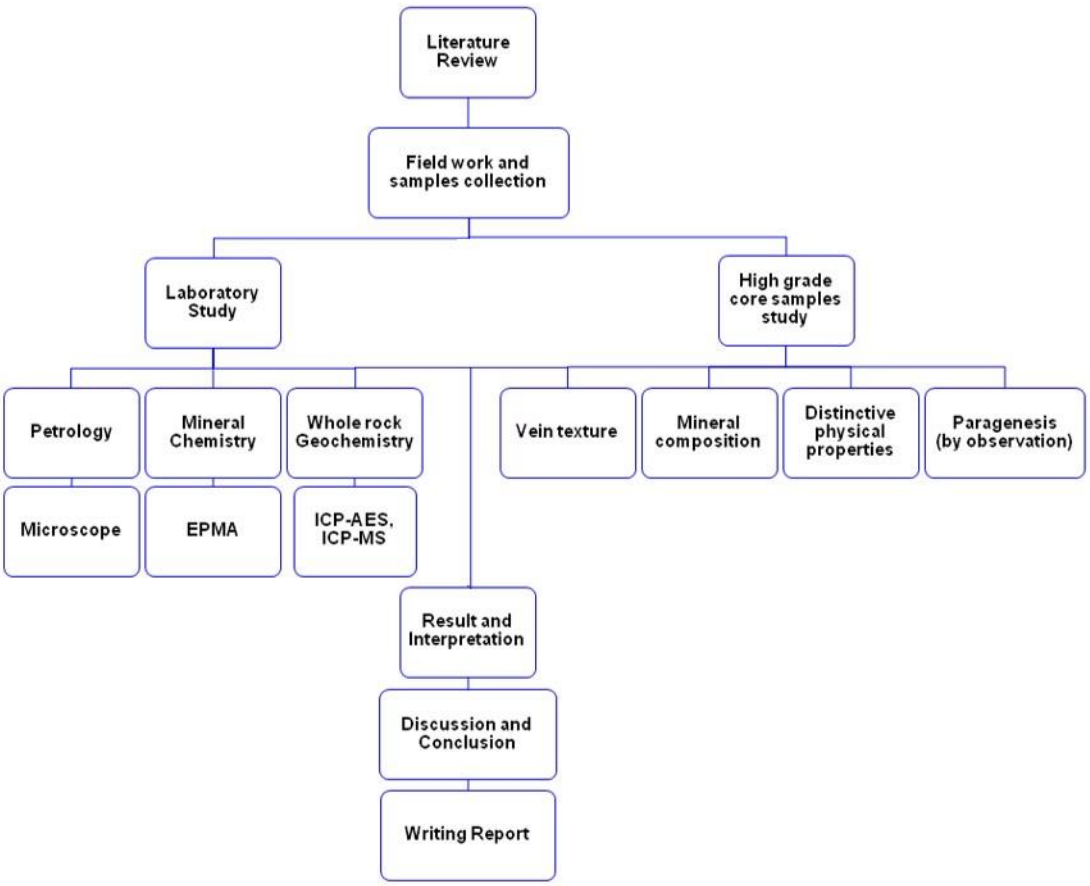

Figure 1.5 Schematic diagram showing sequences of work under this study.

CHAPTER 2
Geological Setting

2.1 Tectonic Evolution of Thailand

Based on tectonic setting, Thailand is part of Mainland Southeast Asia which comprises three major terranes, i.e., Western Burma, Shan-Thai and Indochina (see Figure 2.1) ((Burrett et al., 1990); (Hutchison, 1975); (Gatinsky et al., 1978); (Bunopas, 1981); (Burrett et al., 1990); (Barber and Crow, 2003); (Metcalfe, 2006). Bunopas (1981) and Hada et al. (1999) reported that eastern Thailand consists of two major continental plates: namely Shan Thai to the west, and Indochina to the east. Both continents were parts of Gondwanaland and they attached to the Australian continent (Bunopas, 1981). The Shan-Thai terrane has been drifted northwestwards in the early Permian ((Bunopas and Vella, 1983); (Gatinsky et al., 1984); (Metcalfe, 1988); (Hutchison, 1989); (Bunopas, 1991); (Barber and Crow, 2011)). The Indochina terranes formed as a part of north-eastern Gondwana in the Early Palaeozoic ((Audley-Charles, 1988); (Burrett et al., 1990); (Metcalfe, 1991)) before it was drifted apart in the Silurian or Devonian (Hutchison, 1989).

Salyapongse (1992) suggested that the Shan-Thai terrane is occupied by an inferred Precambrian amphibolite facies which formed as the oldest crystalline basement rock. The younger rocks possibly formed as Early Paleozoic metaclastic-marine non-clastic sedimentary rocks and Middle Paleozoic marine sedimentary rocks that unconformably overlie the inferred Precambrian rock. The Indochina terrane is an elongated block with a NNW-SSE trend which almost deviates to east-west direction in the north. The oldest rock of the Indochina terrane are the Middle Paleozoic deformed sequences of the older arc setting (Salyapongse et al., 1997). The Late Paleozoic to Early Mesozoic igneous rock is composed of felsic-intermediate plutonic rock, basaltic breccia and hyaloclastite, and rhyolitic to andesitic volcanics.

The Lampang-Chiang Rai and Nakhon Thai blocks, lie along the western and eastern parts of the Shan-Thai and Indochina blocks, respectively. Sukhothai Fold-Belt (SFB) is part of the Lampang-Chiang Rai block whereas the Loei Fold-Belt (LFB) is part

of the Nakhon Thai blocks ((Tulyatid and Charusiri, 1999); (Charusiri et al., 2002)). Both SFB and LFB occurred as subduction-related Permo-Triassic magmatism (Zaw et al., 2007). (Singharajwarapan and Berry, 2000) assumed that the structural and volcanic relationships in the Loei Fold Belt may be related to an Early Triassic collision within parts of the Indochina terrane. Collision between the Lampang-Chiang Rai and Nakhon Thai blocks should yield more than one suture (Charusiri et al., 2002).

Metcalfe (2013) revealed that many authors have used Sibumasu and Shan-Thai interchangeably, but these are actually not the same terrane. The Shan-Thai Terrane includes eastern Burma, western Thailand and northwestern Malay Peninsula and excludes any part of Sumatra or western China (Bunopas, 1981). The Sibumasu terrane includes more plates of the Shan States of Burma, Northwest Thailand, Peninsular Burma and Thailand, western Malaya and Sumatra and extending northwards into western China and Tibet (Metcalfe, 1984).

Sone and Metcalfe (2008) studied Tethyan sutures in mainland SE Asia and suggested that Shan-Thai (part of Sibumasu) collided with Indochina after prolonged subduction of the Devonian–Triassic Palaeo-Tethys Ocean. They recognized two sub-parallel suture zones along the belt of convergence between Sibumasu and Indochina; a wide suture zone represents an extensive accretionary complex of the Palaeo-Tethys (Changning–Menglian and Inthanon sutures), and a narrow suture zone represents a closed back-arc basin (Jinghong, Nan and Sra Kaeo sutures). Several workers have agreed on paired subduction in which subduction occurred on the both side of Palaeo-Tethys Ocean underneath Shan-Thai and Indochina Terranes (Gatinsky et al., 1978); (Bunopas, 1981); (Hutchison, 1989); (Intasopa, 1993); (Charusiri, 1989).

The Sra Kaeo Suture Zone was interpreted as a significant collision zone between the Shan-Thai (or Sibumasu) and Indochina blocks (Bunopas and Vella, 1978); (Hada et al., 1997); (Metcalfe, 1999). Sone and Metcalfe (2008) considered that the Sra Kaeo Suture is a continuation of back-arc basin (Sukhothai back-arc) suture. Magmatism in Loei Fold Belt were formed due to crustal thickening which yielded granitiod rocks of S-type affinity. The S-type granitoids was generated from partial melting of the Sibumasu crust subducted beneath the Palaeo-Tethys accretionary complex (Sone and Metcalfe, 2008).

The term Chiang Mai Suture used by Metcalfe (2006) is equivalent to the Inthanon Suture which contains various rock types, including Permian basaltic volcanics, Carboniferous–Permian limestones, Devonian–Triassic radiolarian cherts, Triassic S-type granitoids, and mylonitic/migmatitic gneisses. The Permian Chiang Mai Volcanics appear to have generated in a back-arc rift setting within the Shan-Thai Terrane (Barr et al., 2006). Early Carboniferous to Late Permian, abundant micro-fossils of warm-water Tethyan type have been discovered in limestones of this period. These limestones are regarded as seamount caps formed within the Palaeo-Tethys Ocean. Wakita and Metcalfe (2005) suggested that the Palaeo-Tethys Ocean is represented by a progression of suture extending southwards from Lancangjiang and Changning-Menglian zones in Yunnan through Chiang Rai-Chiang Mai Volcanic Belt in the northern Thailand, to the Sra Kaeo in the eastern Thailand and Bentong Raub Suture in the peninsular Malaysia.

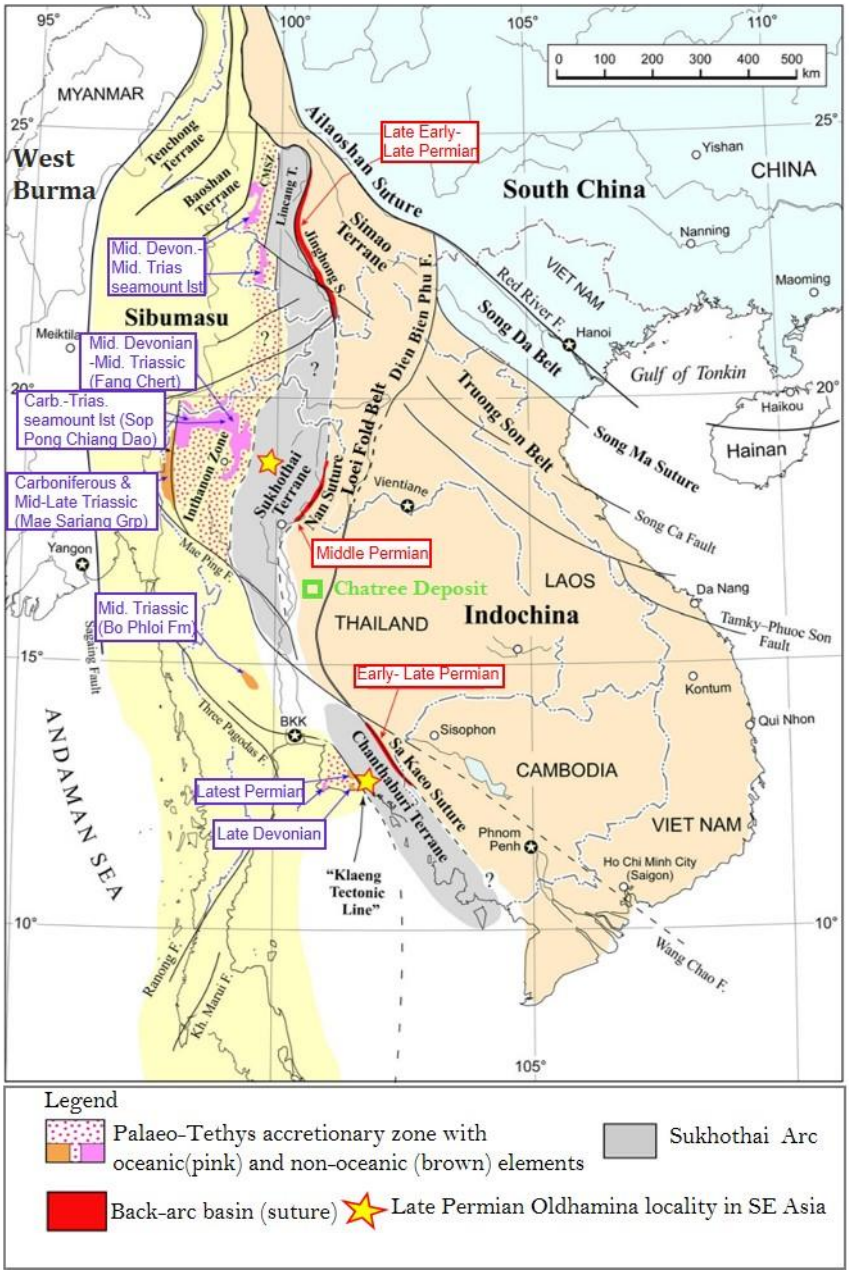

Figure 2.1 Tectonic map of the mainland SE Asia (Modified from (Ueno and Hisada, 1999); (Sone and Metcalfe, 2008); (Hara et al., 2010); (Sone et al., 2012)), showing the main tectonic terranes, suture zones of Permo-Triassic sequences, and Sukhothai Arc resulted from Carboniferous–Triassic subduction of the main Palaeo-Tethys beneath Indochina Terrane.

2.2 Pre-Jurassic volcanic rocks in Thailand

The pre-Jurassic volcano-plutonic rocks in Thailand have been identified into three belt, namely Chiang Rai-Chiang Mai, Chiang Khong-Lampang-Tak and Loei-Phetchabun-Nakhon Nayok belts, (Figure 2.2) ((Jungyusuk and Khositanont, 1992); (Panjasawatwong et al., 1997); (Barr and Charusiri, 2011)).

Chiang Mai-Chiang Rai volcanic belt is composed of basics lavas, hyaloclastic and pillow breccias (Panjasawatwong et al., 1997). Chemical characteristics of the San Kamphang basic volcanic rocks relate to tholeiitic and transitional alkaline in composition. The Chiang Rai - Chiang Mai mafic volcanic rocks are chemically interpreted to be subduction related rocks by Barr and Macdonald (1987). The Chiang Rai - Chiang Mai volcanic belt extends southwards from the Changning-Menglian suture in China (Wu et al., 1995); (Yang et al., 1994); (Tulyatid and Charusiri, 1999); (Ueno and Hisada, 1999); (Barr et al., 2000); (Metcalfe, 2002); (Ueno, 2002); (Feng et al., 2005). Ages of these volcanic rocks range from Late Carboniferous to Late Permian and Mid Permian to Permo-Triassic (Chuaviroj et al., 1980); (Bunopas, 1981); (Bunopas and Vella, 1983); (Panjasawatwong et al., 1997).

Chiang Khong- Tak volcanic belt is the most abundant volcanic rocks which comprise felsic to mafic volcanic rocks, including rhyolite, dacite, andesite and pyroclastic rock. Stratigraphic correlation (Piyasin, 1972; Piyasin, 1975); (Charoenpravat et al., 1987) indicated that these volcanic rocks occurred in Permo-Triassic and possible Late Triassic to Early Jurassic. The Chiang Khong –Tak volcanic belt is the southern extension of Lincang – Jinghong volcanic belt in China (Yang et al., 1994); (Barr et al., 2006). It can also be extending southwards to the Sra Kaew – Chanthaburi volcanic belt in the eastern Thailand.

Loei-Phetchabun-Nakhon Nayok Volcanic Belt

The Loei-Phetchabun-Nakhon Nayok volcanics belt (Panjasawatwong et al., 1997) and Loei-Phetchabun-Ko Chang volcanic belt (Jungyusuk and Khositanont, 1992) are now called as Loei Fold Belt (LFB). This belt occurs along the NNE-SSW trend from Loei Province in the north through Phetchabun and NW-SE trend from Nakhon Sawan to Saraburi, Prachinburi and Sra Kaeo Provinces. The LFB may may have formed during Permo-Triassic and Cenozoic age, related to subduction, oceanic island arc, (Intasopa

and Dunn, 1994); (Panjasawatwong et al., 1997); (Panjasawatwong et al., 2006). Predominant andesite and rhyolite with subordinate basaltic rock were described by Intasopa (1993). These LFB volcanic rocks had occurred under multiple volcanic events during arc formation, based on Rb-Sr isochron ages. They comprises three main periods of volcanism, including Devonian to Early Carboniferous, Middle Triassic and Tertiary. Rhyolite is the oldest volcanic rock occurred in Devonian (374 Ma) which is found in the eastern LFB (Jungyusuk and Khositanont, 1992). Rhyolite from eastern Pakchom district yielded a Rb/Sr isochron age of 374±33 Ma with an initial 87Sr/86Sr ratio of 0.706 whereas spilitic basalt (located 16 km south of Pakchom) gave a Rb/Sr isochron age of 361± 11 Ma with an initial ratio of 0.70455 (Intasopa, 1993). Both ages were confirmed by stratigraphic correlation in the peroid of Upper Middle Devonian to Late Devonian (Jungyusuk and Khositanont, 1992). Late Devonian age related to ocean floor tholeiites which derived at a spreading centre between the Shan-Thai and Indochina Terranes prior to closing of Palaeo-Tethys. (Panjasawatwong et al., 2006) classified basalts in this area as transitional tholeiitic basalt, tholeiitic microgabbro and calc-alkalic basalt/andesite and the first two groups were interpreted as MORB and the third one was interpreted as oceanic island arc lavas which are composed mainly of fine-grained andesite porphyry and andesitic breccia with subordinate rhyolite and rhyolitic tuff (Jungyusuk and Khositanont, 1992). These rocks yielded $^{40}Ar/^{39}Ar$ age of 242 Ma (Intasopa et al., 1990).

Chatree epithermal Au-Ag deposit is located in the Late Paleozoic to Early Mesozoic Loei-Petchabun volcanic belt extending from north to south of central Thailand (Jungyusuk and Khositanont, 1992); (Charusiri et al., 2002). The Loei-Phetchabun Volcanic belt appears to have originated during northward subduction of a large ocean basin (Paleo-Thethys) beneath the Indochina Terrane during Late Permian and Triassic (Intasopa, 1993); (Metcalfe, 1996). The closure of this ocean basin may have been responsible for the northward drift of the Shan Thai terrane and eventually collided to Indochina (Metcalfe, 2006). Salam et al. (2014) investigated the volcanic sequence in detailed field mapping, U–Pb zircon dating, geochemistry and stratigraphy; consequently, they suggested that this volcanic sequence can be subdivided into two volcanic suites. The Late Permian Suite 1 (overlying Suite 2)

volcanic units are sourced from a more depleted mantle and composed of basalt, andesite and dacite with very low LREE composition. The Late Permian Suite 1 probably formed immediately after the beginning of subduction and creation of a new island arc. The less depleted Early Triassic Suite 2 had erupted during active subduction; they contain andesite to dacite compositions with slightly higher contents of Ti, Zr, Y, Ce, P and LREE. The Chatree deposit may have occurred by a mixed volcano-plutonic magmatism at the Late Permian-Early Triassic (260-240 Ma, based on Laser Ablation ICP-MS analyses of U-Pb zircon techniques reported by Salam et al. (2014).

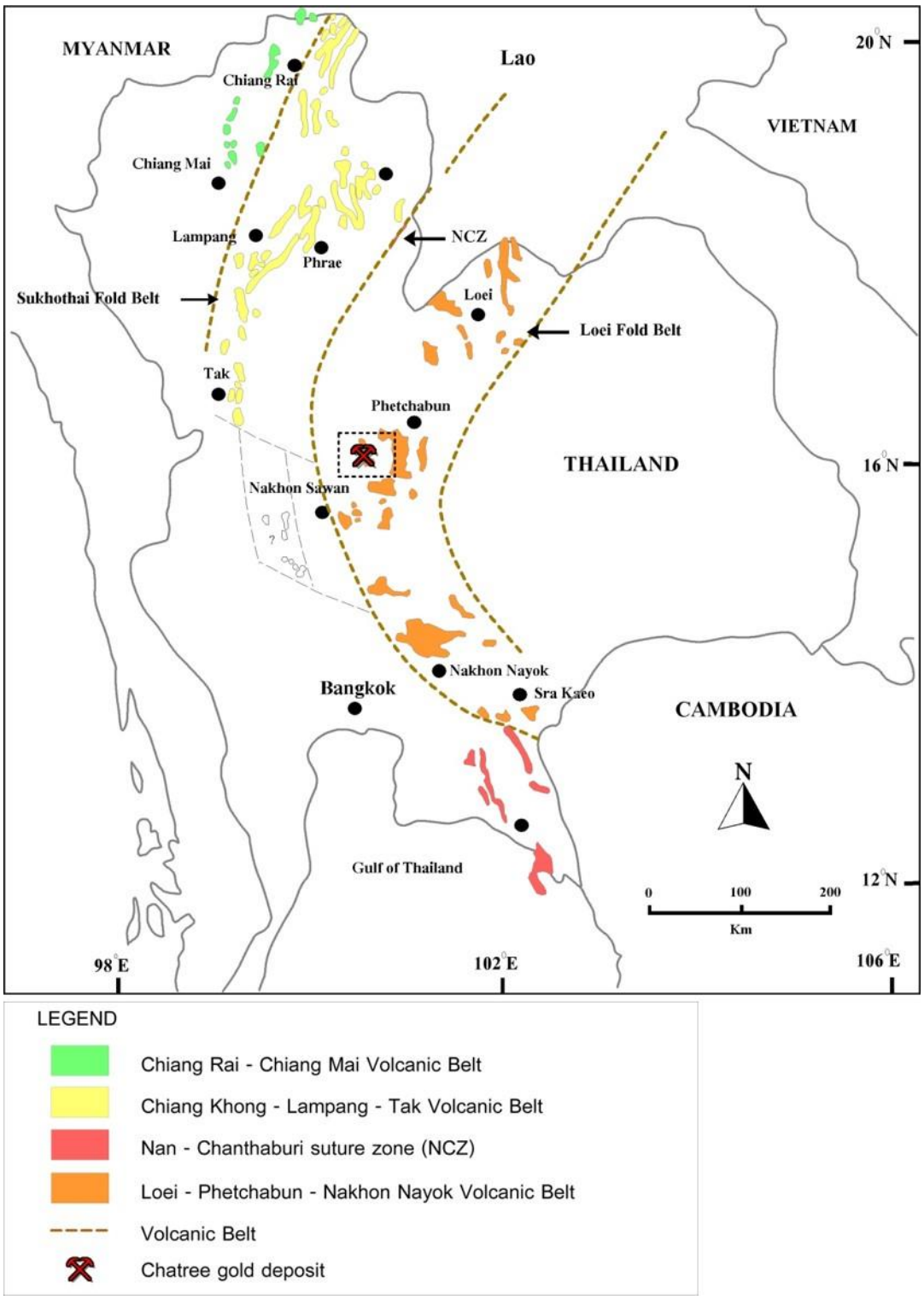

Figure 2.2 Distribution of the Pre-Jurassic volcanic rocks in Thailand and the Chatree deposit in the Loei Fold Belt (modified from Panjasawatwong et al. (1997)).

2.3 Regional Geology

Geological map modified by Salam et al. (2014) (Figure 2.3) was carried out using new field mapping data and core logging study for revising the stratigraphic divisions, in combination with district-scale units. This study area is located on the boundary between Thap Klo District (Phichit Province) and Wang Pong District (Petchabun Province). Carboniferous to Early Permian sedimentary rocks and igneous rocks are unconformably overlain by Late Triassic to Cretaceous-Tertiary sedimentary rocks of the Khorat Group in the uppermost unit (e.g. (Racey et al., 1994); (Meesook et al., 1995); (Buffetaut et al., 1997)). Geological units of Chatree deposit can be complied using data from previous studies of Salam (2006); Cumming et al. (2008); Salam (2011); (Salam et al., 2014) (Figure 2.4). They identified and interpreted these rock units, based on detailed mapping, mineralogical and textural observation, drill core logging and thin section examination. These rock units are described from the oldest to the youngest as below.

2.3.1 Carboniferous volcanogenic sedimentary rocks and Lower Permian limestone

The Carboniferous volcanogenic sedimentary rocks, parts of the Dan Lan Hoi formation mainly consist of conglomerate, sandstone, shale, slate and chert. The lower Permian limestone, based on the Department of Mineral Resources (DMR) (1976) is also grouped in this rock unit. Carboniferous to Early Permian rocks of this unit have northwest-southeast striking from Dong Khui to Wang Pong Districts. They show moderately folding on outcrop as well as on the regional map scale with steeply-dipping beds. However, their beds exposed in the Chatree area are moderately gently folded. Rhyolite and rhyolitic breccia are also associated with the Carboniferous volcanogenic sedimentary rocks. These rhyolite were dated and yield at 323 ± 5 Ma from Khao Sai sample and 321 ± 5 Ma from Wang Yai sample, (Zaw et al., 2007). Both Carboniferous volcanogenic sedimentary rocks and Lower Permian limestones are unconformably overlain by the Middle Permian to Early Triassic volcanic succession, significantly exposed in the Chatree deposit. The Middle Permian limestone were named as "Saraburi Group" (Bunopas, 1981) and composed of massive to thick bedded, fossiliferous limestone interbeded with thin shale, siltstone and chert (Crossing, 2004).

2.3.2 Late Permian plagioclase–hornblende-phyric basaltic andesite (unit 4)

The lower stratigraphic unit (Figure 2.4) of the Chatree Volcanic Complex is characterized by andesitic to basaltic compositions, particularly grouped as porphyritic andesite (unit 4) which can be named as plagioclase–hornblende-phyric basaltic andesite, plagioclase-phyric andesite, mono/polymictic andesitic breccia, mudstone-matrix monomictic andesitic breccia and fiamme breccia. The unit 4 unconformably overlies the Permian limestone of the Saraburi Group. This unit is distributed crucially in the Chatree south to Khao-Sai District.

2.3.3 Late Permian polymictic mafic–intermediate breccia (unit 3)

The Late Permian polymictic mafic–intermediate breccia is characterized by polymictic mafic-intermediate breccia (unit3 in succession of the Chatree deposit). This unit is mainly composed of polymictic mafic–intermediate breccia interbedded or intercalated with thin beds of monomictic plagioclase-phyric and/or plagioclase–hornblende-phyric basaltic andesite breccia. This unit is well exposed in the Chatree mine, southeast of Khao Sai Township, as well as west of the Chatree mine where it is composed of polymictic mafic–intermediate breccia and minor monomictic plagioclase-phyric and/or plagioclase–hornblende-phyric basaltic andesite breccia. In A pit, a thick sequence (~150 m) of polymictic mafic-intermediate breccia underlies the volcanogenic sedimentary facies.

2.3.4 Upper Permian to Lower Triassic volcanogenic sedimentary unit (unit 2)

The volcanogenic sedimentary rocks (unit 2) are composed of laminated siltstone, carbonaceous mudstone, sandstone, quartz-rich fiamme breccia, sand-matrix polymictic breccia and feldspar-phyric rhyolite. The true thickness of this volcanogenic sedimentary unit of Chatree varies from 30 m in H Pit and may reach 150 m thick in A pit. The sand matrix polymictic breccia mainly occurs at the lower part of this succession, overlying the mafic–intermediate polymictic breccia (unit3). Sandstone occurs in the upper part of unit 2 and commonly contains fiamme breccia intercalation. In the western and southern part of Chatree, this unit also includes plagioclase-phyric basalt, plagioclase-phyric andesite and monomictic andesitic breccia overlain by volcanogenic sedimentary facies. These rocks of unit 2 are overlain by fiamme breccia (unit 1).

2.3.5 Late Permian to Early Triassic fiamme breccia (unit 1)

The uppermost unit consists of lithic-rich fiamme breccia interbedded with fiamme-rich sandstone and thin beds of accretionary lapilli-rich siltstone and polymictic mud-matrix breccia (Figure 2.5). At H and D pits, this unit overlies the polymictic mafic–intermediate breccia (unit 3). The original true thickness of the unit 1 is unknown because their top has never been identified in the Chatree area. However, the preserved thickness is estimated at about 100 to 150 m. At A pit, the lithic-rich fiamme breccia generally overlies the laminated siltstone and carbonaceous mudstone facies.

2.3.6 Middle Triassic diorite and post-mineralization dykes

The post-mineralization dykes of the Chatree deposit including xenolithic basaltic, basaltic andesite, porphyritic andesite and andesite dykes. The post-mineralization basaltic dyke is also present at C pit which is cross-cut by Au–Ag bearing quartz–carbonate veins. Most dykes are confined by ore zones in sub-parallel trending. Basaltic dyke at D pit contains xenoliths of Middle Triassic diorite. The Middle Triassic diorite is associated with the NW-SE trending in southeast and northwest of Khao Sai Township.

2.3.7. Upper Triassic and Jurassic Khorat Group

The Upper Permian and Lower Triassic rocks are overlain by the Upper Triassic to Cretaceous–Tertiary sedimentary rocks belonging to the Khorat Group (Racey et al., 1994); (Meesook et al., 1995); (Buffetaut et al., 1997). The Khorat Group is composed of non-marine clastic sedimentary rocks such as siltstone, sandstone, shale and conglomerate. Huai Hin Lat Formation (the lowest part of the Khorat Group) exposed in the south-eastern part of Chon Daen district where the rocks are known to be unconformity and underlain by rocks of Middle to Late Permian Saraburi Group and Late Permian volcanic rocks. This unconformity is also marked change in the orientation of bedding with gentle (5° to 10°) dips in the sedimentary rocks of the Khorat Group to much steeper dips in the Middle Permian limestone of Saraburi Group (Crossing, 2004). The Khorat Group mainly covers the northeastern and southeastern parts of the area. The regional geological maps and field observation in the area suggest

that one or more unconformities existing between the Khorat Group and the Chatree volcanic succession (Meesook and Saengsrichan, 2011).

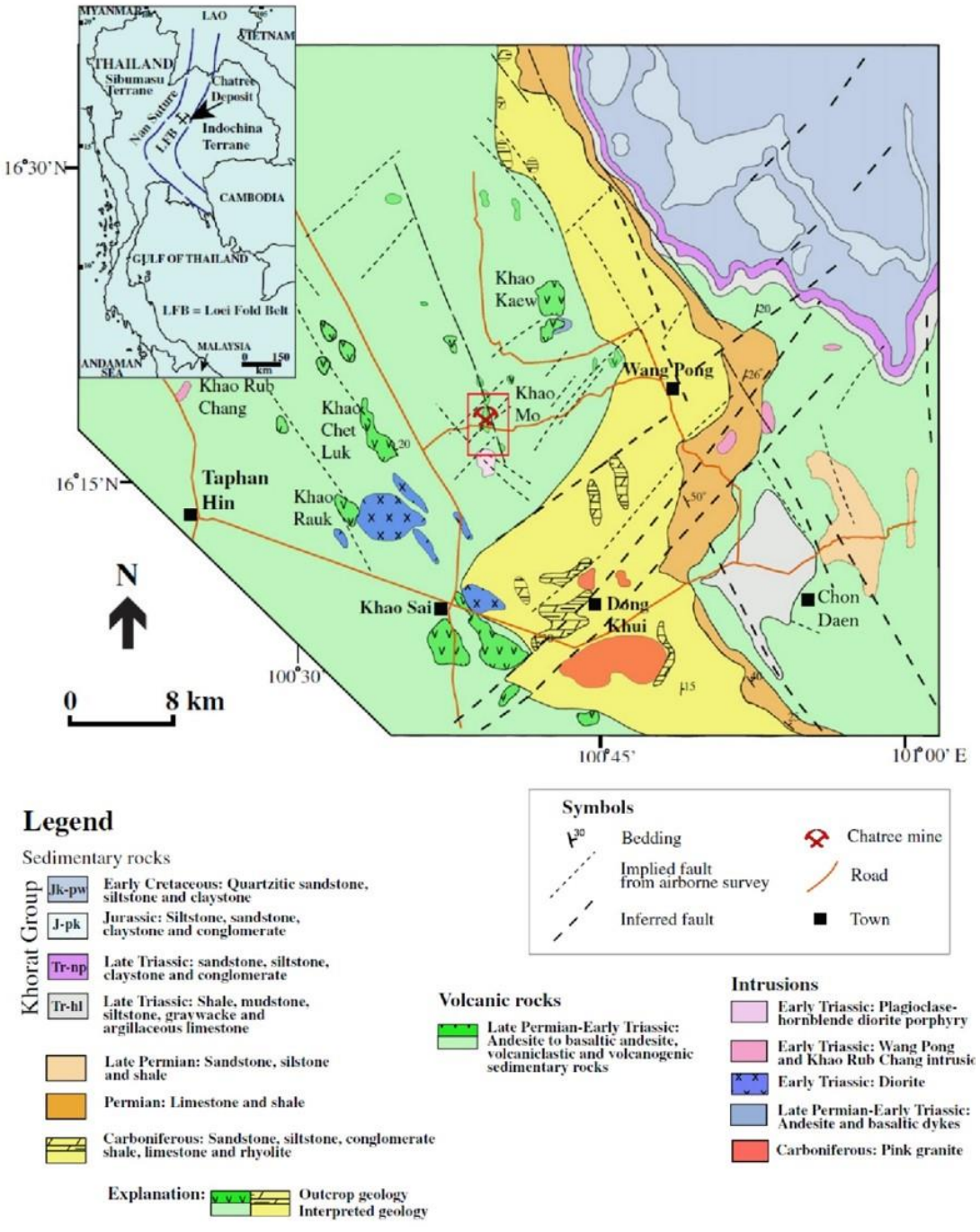

Figure 2.3 Geological map showing detailed geology of the Chatree area, central Thailand (modified from (Salam et al., 2014), based on map scale 1:250000 of Royal Thai Department of Mineral Resources, 1976).

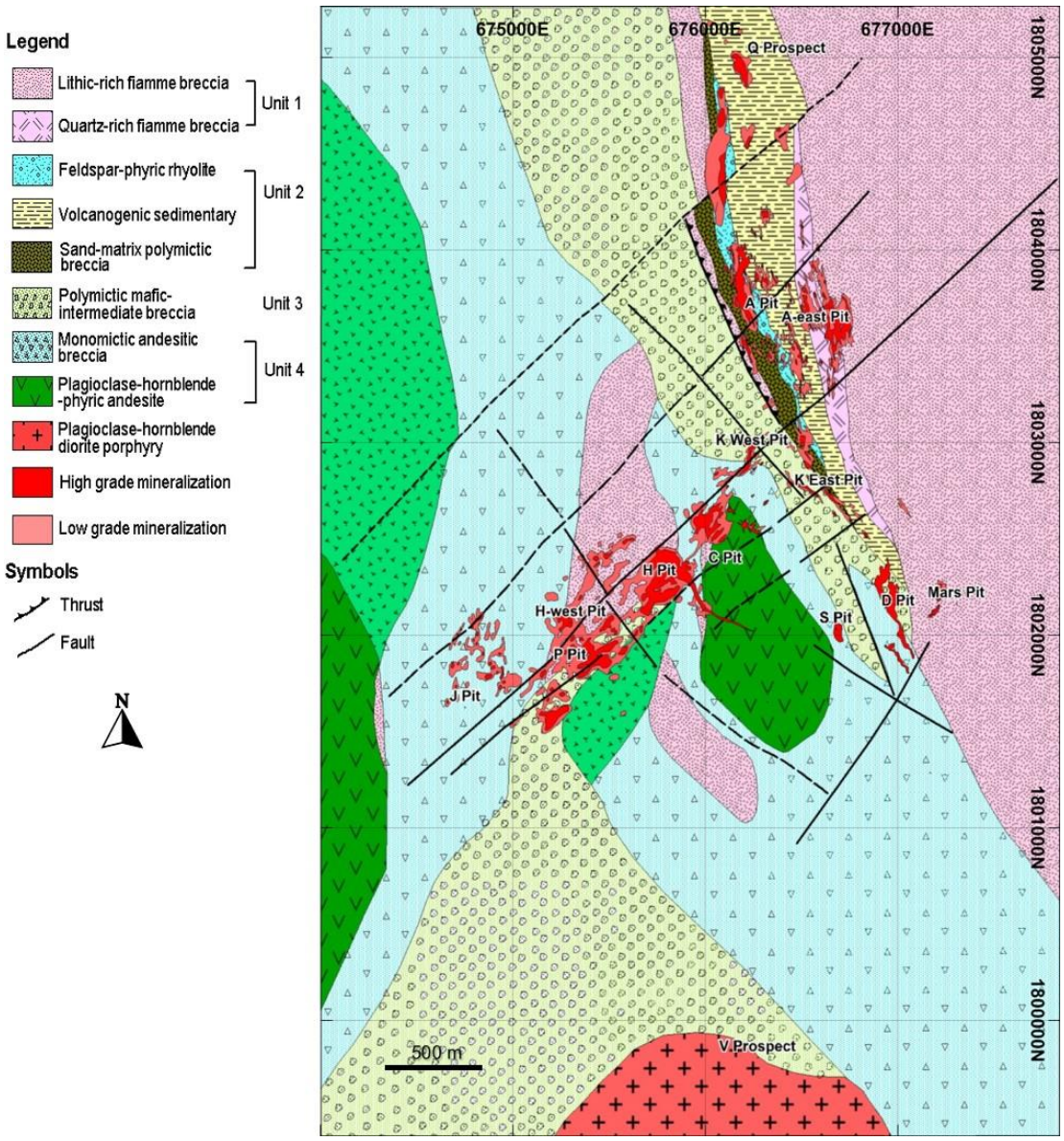

Figure 2.4 Geological map of the Chatree deposit showing the volcanic units and mineralization (modified after Salam (2011)).

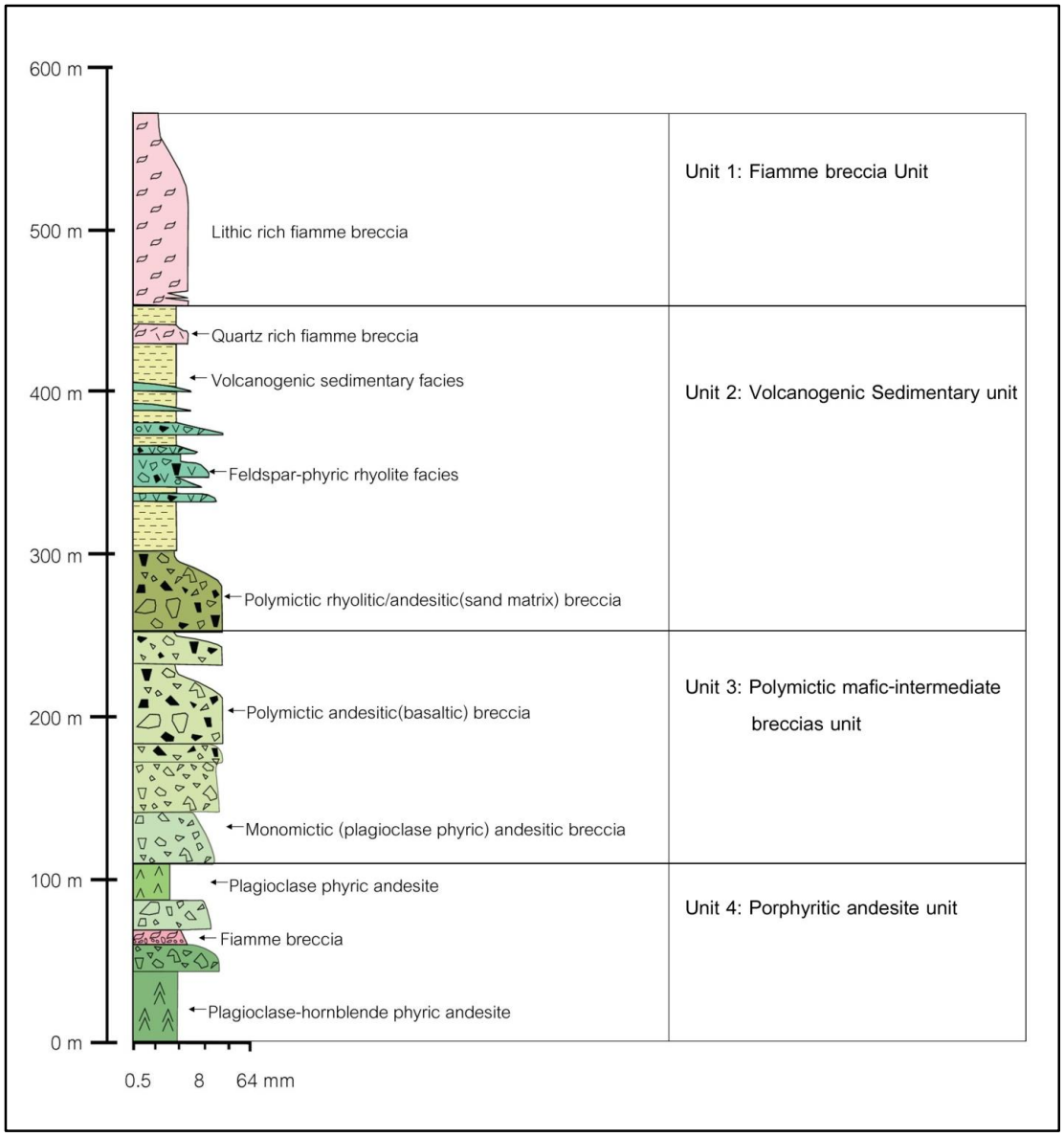

Figure 2.5 Stratigraphic units of Chatree Deposit (modified after Salam (2011)).

2.4 District Geology

Based on geologic map of Department of Mineral Resources (2004) (DMR) (2004), the oldest rock, Carboniferous, in the area has exposed at Chon Daen. This Carboniferous unit comprises siltstone, sandstone and conglomerate with thin limestone beds. Crossing (2004) described this rock unit as Wang San sediments. This sequence is capped by a thick limestone unit probably belonging to Middle Permian. The volcano-sedimentary rocks are predominant in this area; however, some of them were mapped as Quaternary sediments in geologic map of (DMR) (2004). Intasopa

(1993) dated volcanic rocks samples from Chon Dan using $^{40}Ar/^{39}Ar$ method and reported age of 238 ± 4 Ma (Permo-Triassic age). Upper Triassic sedimentary rocks of Huai Hin Lat Formation at Chon Daen (Intasopa, 1993) overlie these volcanic rocks.

The volcano-sedimentary sequence around the Chatree deposit contains several andesitic volcanic rocks and a couple of rhyolite rocks. Large and well-exposed andesitic volcanic rocks are at Ban Mai Wang Takhian, Chatreee mine, Khao Phanompha (Crossing, 2004). Proximal to andesitic volcanic edifices are intercalated lavas, pyroclastic and volcaniclastic sedimentary rocks displaying significant lateral facies variation and complex interfingering to the adjacent volcanic centers. Thick andesite lava flows interbedded with andesitic autobreccias, and these interbedded with lithic tuffs mixed provenance sedimentary rocks. Crystal and ash fall tuffs are less volumetrically important (Crossing, 2004). The rhyolitic volcanic centers at Khao Khieo was formed by a very thick rhyolitic crystal tuff with occasional lithic fragments, which distally interbedded with andesite units. It contains some thin interbeds of tuffaceous sediments and appears to overlay the adjacent andesitic lithologies. At Ban Nikhom flow banded rhyolite, rhyolitic tuff and pumiceous perlite are exposed in several shallow dams. These volcanic units may be interlayered by thick well-bedded sequences of fine-grained volcaniclastics and epiclastic siltstone and shale, massive tuffaceous mudstone and more distally epiclastic siltstone and shale. These units are well-exposed at Wang Pong. Various intrusives ranging in composition from felsic to mafic intruded into the volcanic sequences; they are mostly small- to medium-sized stocks and dykes. Volumetrically most important unit is mafic intrusive dominated by diorite but ranging in composition from granodiorite to diorite, and texturally from fine-grained, equigranular to porphyritic. Crossing (2004) reported that granitic intrusions occur as stocks and dykes, one to the north of the Chatree gold mine around Ban Wang Phlap, and the other to the south (Ban Lang Du). They appear to be spatially associated with northeast and southeast structural trends. (Kamvong et al., 2006) studied plutonic rock at Wang Pong district (about 50 km from Chatree mine) and they were consequently described as small stocks. They range in composition from granite to diorite. Kamvong also grouped these rocks into two types, namely biotite granite and granodiorite. The former one is fine-, to medium-grained and the later one is

medium-grained inequigranular texture. Petrochemical study suggested that they, however, fall within the same A-type granite (Kamvong et al., 2006). Diorite (?) porphyry has also been encountered in the drill holes at N-prospect and V-prospect.

2.5 Mineralization at Chatree deposit

Geology of Chatree gold deposits in Q, A, K, D, S, C, H, J, N, P and V zones was complied, based on geological map of Crossing (2006), volcanic facies studied by Cumming (2004) and detailed pit mapping and mineralization data reported by Salam (2011). These results and crucial information are summarized and reported below.

Q pit is located the north of Chatree. It is composed mainly of quartz-rich fiamme breccia (interbeded with polymictic mud matrix breccia), epiclastic and fine volcaniclastic sediment and mono/polymictic andesitic breccia in descending order, respectively (Cumming et al., 2006). The gold-bearing quartz veins are mainly composed of quartz, adularia, chlorite, calcite and sulfide minerals which are hosted in volcanic-sedimentary and andesitic volcanic-clastic rocks (Tangwattananukul et al., 2009). The mineralization veins are orientated along NW-SE, NE-SW and N-S directions with moderate to steep dipping. They also occur between strata of volcanic - sedimentary and andesitic volcanic-clastic rocks.

A pit and A east pit are composed of mono-polymictic andesitic breccia and hornblend phyric andesite at the lower sequence underlying volcaniclastic rocks which include polymictic andesitic/rhyolitic sedimentary breccia (with sand-silt matrix), laminated sandstone, laminated siltstone, sandstone to pebbly sandstone and sedimentary breccia. The uppermost unit is lithic-rich fiamme breccia (Cumming et al., 2006). The host rocks proximal to the mineralized zones are involved by silicification, quartz-adularia alteration; subsequently, they were cut by veins of carbonates and Fe-sulfide – Fe-Ti-oxide – sphene/leucoxene assemblages, respectively. The host rocks distal from the mineralized zones are dominated by propylitic alteration assemblages such as chlorite/serpentine and/or Fe-Ti oxides (Sangsiri and Pisutha-Arnond, 2008). Mineralization of A pit is mainly hosted in volcanogenic sedimentary rock. The high gold grade in the large ore zone is favorably hosted in volcanogenic sandstone and laminated with pervasive silica. The majority of mineralized veins trend N-S to NNW-SSE with dips of 60° to 85° to the west; gentle west dipping is in the western part of the A Pit and steeper dipping is in A pit to A east pit (based on field data of Salam (2011)

C pit: C-north pit is composed of massive veins toward the hanging wall and stockwork veins toward the footwall. The mineralization is mainly hosted by volcanic breccia (monomictic, polymictic sandstone and breccia). The plagioclase-hornblende-phyric andesite in the footwall of C Pit is rarely mineralized. The crustiform-colloform banding of alternating grey silica, quartz-carbonate-sulphides and quartz-carbonate-chlorite also occur in C ore body. The C south mineralization occurs as massive veins with minor breccia vein of quartz-carbonate-pyrite assemblage with subordinate quartz-carbonate-chlorite assemblage. The high-grade zone known as "Honey Pot" is located at the C-south and this high-grade zone is separated by the northeast-southwest trending fault. The "Honey Pot" is located below the oxidized zone. The stockwork vein was founded at C-central near the surface area. The strike of mineralization is in N-S trend with dipping to the west in average 40°. The grey silica breccia is characterized by angular clasts of mainly porphyritic andesite, minor fine-grained sedimentary rocks and fiamme breccia; they are confined to the footwall at C-south and C-north. Multiple stage breccia is also founded overprinting the grey breccia stage (based on Salam (2011)).

H pit: H ore body includes two mineralization zones as H north and H south. The H north is associated in NE-SW striking with NW dipping about 30-40 degrees extending into ore body of H south in the SW direction. Both ore zones are possibly merged together at the deeper level. The H ore body is hosted by polymictic andesitic lithic breccia and matrix-rich polymictic andesitic lithic breccia with sharp contrast to the hanging wall fiamme breccia undertaken hydrothermal alteration. Colloform-crustiform banding also occurs in H pit and tends to confine the massive veins. The mineralization styles are complicated including quartz-sulphide (stage 3-assemlage 1) at the H-central and H-south. Quartz-carbonate-pyrite (stage 3-assemblage 2) is widely distributed through the pit; quartz-carbonate-chlorite (stage 3-assemblage 3) and quartz-carbonate-chlorite-sulphide are identified mainly confined to the area of H-central and H-north. The latter two stages usually carry high gold grade (Salam, 2006).

K pit: K west pit is composed of lower-fiamme breccia, polymictic andesitic lithic breccia and matrix rich polymictic andesitic lithic breccia which are the host of mineralization and associated with quartz-carbonate-sulfide veins with minor quartz-

carbonate-chlorite veins. Bands of fine-grained white to pale grey quartz and fine-grained chlorite and coarse-grained sulfide with steeply west dipping are found in K west extended from C north ore body. The gold-bearing vein cross-cut grey silica vein which may form as vein, veinlet and breccia matrix. The hydrothermal, phyllic and propylitic alteration have been observed in the K pit (Salam, 2006). Mineralization in K east extended from D pit with the same detail as described below.

D pit is mainly composed of polymictic andesitic lithic breccia at the western pit wall (hanging wall). Thin beds of fiamme breccia occur at the footwall along with coherent andesite or crystal-rich coherent andesite (Dedenczuk, 1998). Mineralization of D pit tends to have steep dipping slightly to the west to vertical dipping with 350° (NNW-SSE) strike; it extends northwards to the K-East pit. Massive vein, colloform-crustiform band, sheeted vein and stockwork vein of predominant quartz - carbonate - sulphide – gold assemblage with minor quartz - carbonate - chlorite - sulphide – gold assemblage have been observed in D pit. Massive carbonate veins are common and cross-cutting the gold-bearing veins which may in turn dilute the gold grade in these mineralized veins. Massive quartz veins related to the higher gold grade were discovered particularly in the southern part of D pit. Xenolithic basalt, feldspar-porphyritic dacite and andesite dyke (Dedenczuk, 1998) have been found in the D pit. The xenolitic dyke is sub-parallel to the mineralization and this dyke also extends to K-East.

S pit: Mineralization took place near the contact between coherent porphyritic andesite and monomictic andesitic breccia; however, it is preferentially hosted in the coherent porphyritic andesite with sigmoidal-shaped vein. Mineralization of S lens is characterized by quartz ± carbonate ± adularia- sulphide with high contents of base metal. It commonly occurs as veins and veinlets or stockworks near the surface and commonly forms as breccia filling matrix at the deeper level. This ore len has NNW-SSE strike with steeply dipping to the west at about 80°. It appears to be parallel to the D lens. The vein geometry of the S ore lens is similar to the C and D lens with a greater width near the surface.

J prospect is composed of plagioclase-hornblende-phyric andesite as basement overlain by a fiamme breccia (10-20m thick) unit containing limestone with

a few meters thick. This sequence is overlain by monomictic andesitic breccia on the top. These rocks dip eastwards presumably on the eastern side of another andesite dome-like structure. Mineralization occurs as several narrow zones within NE striking and steeply dipping to the NW. The veins are mostly hosted by monomictic andesitic breccia.

P pit: the ore zone is hosted at the contact between polymictic mafic-intermediate breccia and plagioclase-phyric andesite. Stockworks are also observed at the footwall with less abundance. The ore zone is located on the NE-SW structure, a continuation from the H-south, truncated and offset to the east by an EW trending fault. The ore zone shows NE-SW strikes with a moderate dip (45°) to the NW. It comprises major vein (about 4 m wide) parallel to a few small veins (<1 m wide). Both major and small veins show well-banded textures characterized by alternating quartz-rich and carbonate-rich bands similar to the D ore lens. The supergene ore zone is located at the top 35 to 40 m near main vein which is considered as the major ore grade and tonnage for the P Pit.

N prospect shows typical features of porphyry Mo-Cu-Au deposits such as multiphase intrusions, alteration and vein deposition which low grade Cu mineralization and insignificant gold content have been identified. A coarse-grained diorite with feldspar phenocrysts (up to 3 mm long) continues from surface to the finer-grained diorite at the lower part with probably younger intrusion (Corbett, 2004). Alteration is found as early stage of potassic alteration whereas the later halos of silica-sericite-pyrite (phyllic) alteration is also recognized. The mineralization contains very low Au grades and Cu content is in the order of 0.16 % both in the RC and diamond drill cores. Corbett (2004) also reported that isolate higher Au, Cu and Zn grades around the margins of the magnetic anomaly might be associated with polymetallic veins marginal to the porphyry system.

Marhotorn et al. (2008) reveals that felsic porphyry and aphanitic mafic rocks were cross cut by subsequent alteration and mineralization. Two types of alteration were recognized as pervasive and selective patterns. The pervasive style was dominated by replacement of biotite, chlorite, sericite and K-feldspar. The selective style of alteration was observed as veins and veinlets. The felsic rocks in the N zone

bear similar microporphyritic toporphyritic and phaneritic textures and they are classified as porphyritic fine-grained granodiorite. Aphanitic intermediate-mafic rocks bear similar porphyritic andesite. Granodiorite contains plagioclase (An_{30}) with zoned texture, anhedral and vermicular quartz and relict hornblende.

V prospect: Marhotorn et al. (2008) studied rocks from the V zone. They are mainly composed of porphyritic aphanitic intermediate to mafic rocks with abundances of green minerals (e.g., chlorite and epidote) and minor vein minerals. Rock is dominated by altered porphyritic andesite, relic plagioclase and hornblende. Groundmass of plagioclase, sericite and opaque minerals with glassy mineral exhibit prominent flow textures. Alteration mineralogy is characterized by epidote replacing plagioclase, chlorite-replacing plagioclase, and sericite replacing plagioclase and devitrified glass. Geochemically, they were classified as island-arc tholeiites and volcanic arc basalt (Marhotorn et al., 2008).

Salam (2011) classified seven stages of mineralization vein as following.

Stage 1: microcrystalline quartz + pyrite veins/veinlets and breccia are found in C and A pits. Characteristics of stage 1, early breccia zone could be observed in C pit whereas vein/veinlet and stockwork with minor breccia could be found in A pit.

Stage 2 contains quartz-chlorite-sericite-pyrite vein/vein breccia and (stage 2A) and quartz-sericite ± chlorite-chalcopyrite-pyrite-sphalerite ± galena breccia filling and vein (stage 2B). The stage 2A is hydrothermal vein breccia which characterized by jigsaw-fit texture occurring in Q, A, H, J and LD areas. The stage 2B cross- cut stage 2A which can be identified by microscopic study. But stage 2B has high amounts of chalcopyrite and sphalerite- rich veins with comb quartz at the vein margin. They are usually observed in H-central, H-south and P pits.

Stage 3: quartz-carbonate-(K-feldspar) ± carbonate ± sulfide occurs as veins/veinlets and breccia with the colloform-crustiform texture. The major composition contains quartz, carbonate and K-feldspar which are hosted in plagioclase-hornblende-phyric andesite. The majority of vein has been observed at the H-north pit whereas the infill breccia may be observed at C, H and K west pits and small vein can be observed at K-west. Salam (2011) also suggested that vein stage 3 occurs as the post-dated to stage 2A.

Stage 4 comprises 3 sub-stages including quartz-chlorite ± carbonate ± adularia-sulphide-electrum (Stage 4A), quartz ± carbonate-adularia-sulfide-electrum (Stage 4B) and carbonate ± quartz-adularia-sulfide-electrum-argentite-tetrahedrite (Stage 4C). The stage 4 is interpreted to be the main gold-silver mineralization of the Chatree deposit by Salam (2011). All three sub-stages are formed as crustiform and colloform textures with chlorite- quartz- carbonate-rich bands. The stage 4B cross-cut into stage 4A whereas the stage 4B is cross cut by stage 4C. Enrichment of gold and silver is in the late stage 4C which is the most abundant electrum and acanthite.

Stage 5 is characterized by quartz ± carbonate veins. This stage formed as comb quartz, crustiform-colloform band open-space filling textures veins and breccia matrix. The massive vein is characterized by crystalline quartz (comb quartz), microcrystalline quartz (chalcedony), carbonate and rhodochrosite. The vein stage 5 was not related to the gold mineralization but it influenced in ore grade by diluting due to mixture of waste ore.

Stage 6 contains quartz ± carbonate veins/veinlets. The stage 6 is composed of quartz, chalcedonic and carbonate without sulfide mineral.

Stage 7 is composed of quartz-zeolite-carbonate vein which is the post mineralization or perhaps the latest vein stage.

In summary, the main gold-silver mineralization is closely associated with vein stage 4 (Salam, 2011) which is characterized by colloform-crustiform banded quartz ± carbonate ± chlorite ± adularia-sulfide-electrum vein (Corbett (2002); (Salam, 2011); (Salam et al., 2014)).

CHAPTER 3

Stages of Gold Mineralization and Quartz Textures

3.1 Introduction

The Eastern A pit in Chatree epithermal Au-Ag deposit is locally situated in volcanogenic sedimentary rock units that have been cut by variety of vein types including stockwork vein, brecciated vein, banded vein and massive to minor vein. The major gangue minerals in the Eastern A pit are characterized by quartz, pyrite, base metals, carbonate, chlorite, adularia and sericite. The vein generally trends N-S to NNW-SSE with west dipping (65-85°) (Salam, 2011). At the Eastern A pit, veins contact mainly to volcaniclastic rocks including polymictic andesitic/rhyolitic sedimentary breccia (with sand-silt matrix), laminated sandstone, laminated siltstone, sandstone to pebbly sandstone and sedimentary breccia. These host rocks may develop silica flooding by replacement process related to microcrystalline quartz (chalcedony). The volcanogenic sedimentary rocks are underlain by mono-polymictic andesitic breccia and hornblende phyric andesite whereas the uppermost unit consists of lithic-rich fiamme breccia, (see Figure 3.1). In ascending order of facies, the polymictic andesitic breccia is mainly cross -cut by wall rock brecciated vein at elevation below -200m (msl). Sulfide dissemination and narrow vein ranging from a few centimeters to 50 centimeters thick also occur in andesitic host which is identified as possible feeder zone to the mineralization. The volcanogenic sedimentary unit is located between +5 and -200m msl; it is composed of stockwork, breccia vein, banded vein, massive to minor vein. The massive vein is rarely observed in the Eastern A pit whereas the stockwork and breccia veins are abundant. These veins have thickness ranging from a few mm to 10 m and show colloform banded quartz vein overprinting in brecciated host. The banded veins also cross-cut sandstone and pebbly sandstone and may occur as the earliest vein. The large mineralization zones in the Eastern A pit are hosted mainly by volcanogenic sedimentary unit yielding the large quantity of high grade Au. The high grade Au frequently occurs within favorable sedimentary storage. The uppermost fiamme breccia above +5m msl, which is part of volcaniclastic facies appearing to be a trap of mineralization, Salam (2011). Cumming et al. (2006) suggested

that over 100 meters thick of fiamme breccia with intercalated laminated, fine sandstone are mineralogically characterized by microcrystalline quartz.

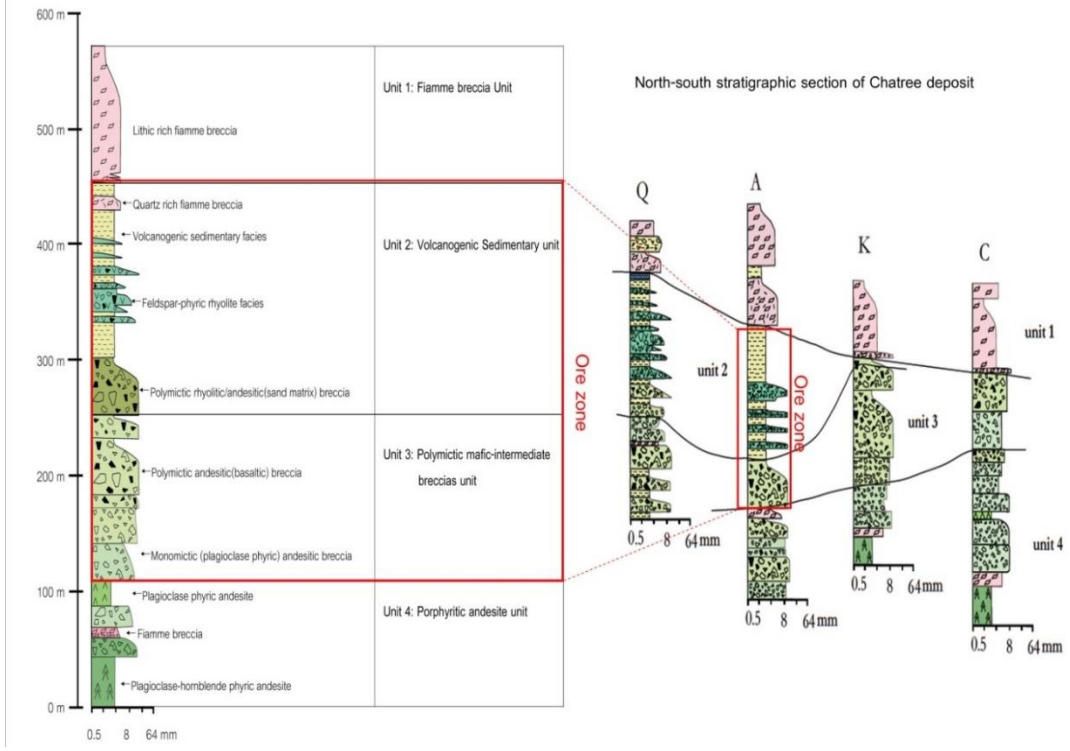

Figure 3.1 Stratigraphic correlation of the Chatree deposit (modified from Salam, 2011), showing the volcanogenic sedimentary facies (unit 2) which host most stages of mineralization. They comprise laminated siltstone, sandstone and polymictic andesitic/rhyolitic sedimentary breccia (with sand-silt matrix). Polymictic andesitic breccia (unit 3) is also associated with the ore zone.

The paragenetic sequence of mineralization in the Eastern A pit was examined before the study of high grade vein. The paragenesis of vein in 5 assemblages was then identified by 441 drilled core samples on the basis of cross-cutting relationship and core logging as well as data from previous researches (e.g., Salam, 2011; Cumming et al., 2006; 2008). The study of high gold grade veins from 40 drilled core samples is focused on the vein stage of the main gold mineralization, including: quartz-carbonate-pyrite (sulfide-base metal) banded-stock work vein of stage 2 which is a good vein stage of gold deposition, especially in volcaniclastic sedimentary host. Quartz+carbonate+chlorite+sulfide banded-stockwork vein of stage 3 also has high to

very high gold content. Similarly, the main gold-silver mineralization stage 4 Salam (2011) is composed of quartz-carbonate- chlorite-adularia-sulfide-electrum.

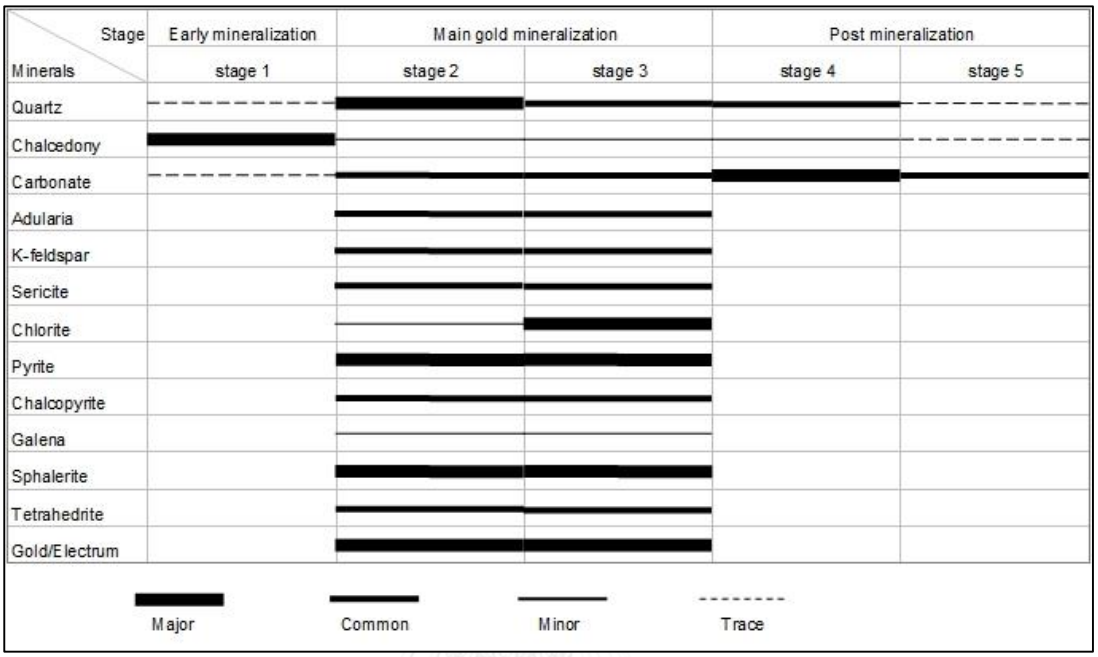

Figure 3.2 Paragenetic sequence of mineralization in the Eastern A pit (modified after Salam, 2011).

3.2 Mineralization stage 1 (Grey quartz+chalcedony±sulfide)-rich microcrystalline quartz

Mineralized vein contains mainly fine-grained silica-rich microcrystalline quartz which formed at low temperatures conditions. This stage normally occurs as banded vein, vein breccias, andesitic breccia with grey silica cement and pervasive grey silica vein. These veins mainly cross cut into polymictic andesitic breccia that is a part of volcaniclastic sedimentary host. Stage 1 has been considered as a base preparation step or pre-gold mineralization which contains quite low gold grade.

3.3 Mineralization stage 2 (Quartz + carbonate+pyrite ±sulfide±sericite ±chalcedonic)

Mineralization stage 2 is related to the gold mineralization. It is represented significantly by quartz, carbonate and pyrite. The sulfide forms as dissemination layer for which contains majority of pyrite and the other sulfide minerals such as

chalcopyrite, galena and sphalerite. Sericite also occurs patchy tiny grains associated with fine-grained quartz and sulfide. This vein stage 2 is often observed and contains high grade gold. It mainly occurs as band, stockwork vein infilled matrix or infilled open space in volcaniclastic sedimentary host rocks. These veins of stage 2 are sometimes cross-cut by the mineralized vein of stage 3.

Based on mineral composition, especially sulfide minerals stage 2 vein samples from the Eastern A pit can be classified from forty drilled core samples into four majors groups, assemblage, groups I to IV (Salam, 2011).

3.3.1 Assemblage group I: Quartz-grey silica-carbonate vein breccia-trace sulfide.

This mineralization assemblage contains silica-chalcedonic (microcrystalline quartz) and grey silica matrix of mineralization stage 1 with partly replaced by quartz-carbonate veins of mineralization stage 2, (see Figure 3.3). Traces of pyrite, chalcopyrite, galena and sphalerite have also been disseminated in this assemblage. This assemblage normally occurs as vein breccia and vein/veinlet in volcanic sedimentary breccia host and some massive carbonate veins without sulfide concentration. Quartz-carbonate vein breccia contains low grade gold with an average lower than 1 g/t which is the lowest range of selected vein samples.

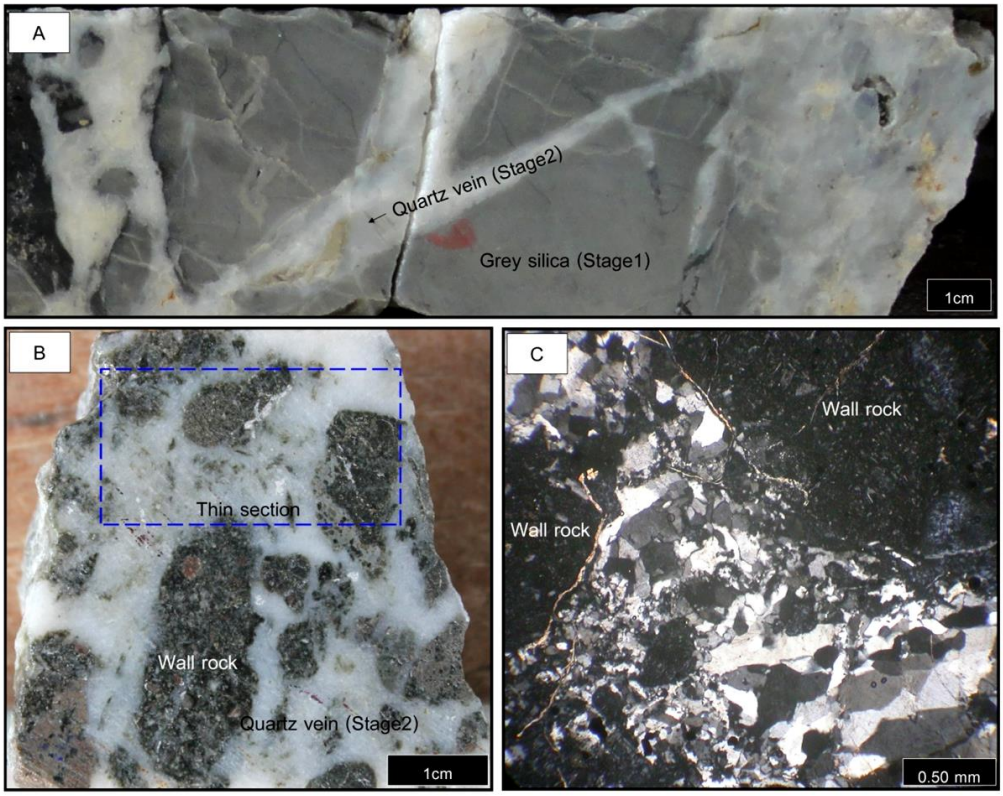

Figure 3.3 Assemblage group I: A) Specimen (sample A04 of core 6231RD-194.30) showing grey silica stage 1 cross-cut by quartz vein stage 2 in assemblage group I; B) Specimen (sample A42 of core 7556RD) of quartz vein breccia matrix in stage 2 hosted by polymictic andesitic sedimentary breccia; C) Photomicrograph showing coarse gained crystalline quartz and trace of sulfide.

3.3.2 Assemblage group II: Quartz-carbonate-pyrite±chlorite±feldspar and minor sulfide (±chalcopyrite, sphalerite, galena and tetrahedrite/tennantite).

Quartz, carbonate, pyrite, chlorite, feldspar and minor sulfide are generally observed in assemblage group II which are similar to the group I. However, this group II has additional composition of chlorite, feldspar and dominantly pyrite with higher gold content (0.5-6.5 g/t). This assemblage group II occurs as vein breccia hosted in volcanic clastic to sedimentary breccia. Some selective samples under this study are listed below.

- Quartz-carbonate-feldspar-chlorite-pyrite (with sphalerite-tetrahedrite/tennantite and ±galena±chalcopyrite) vein breccia (sample HG39, see Figures 3.4A and 3.4B)

- Quartz-carbonate-chlorite-pyrite and small inclusions of sphalerite-tetrahedrite/tennantite and electrum (sample HG33, see Figures 3.4C, 3.4D, 3.4E, 3.4F)
- Quartz-chalcedonic-carbonate-chlorite-pyrite and sulfide (rare chalcopyrite, galena, sphalerite) vein breccia (sample HG14)
- Quartz-chlorite-feldspar-pyrite vein to vein breccia with ±chalcedonic±grey silica±sphalerite (sample HG21)
- Quartz-chalcedonic-grey silica-(10%) pyrite and trace sphalerite (sample HG31)

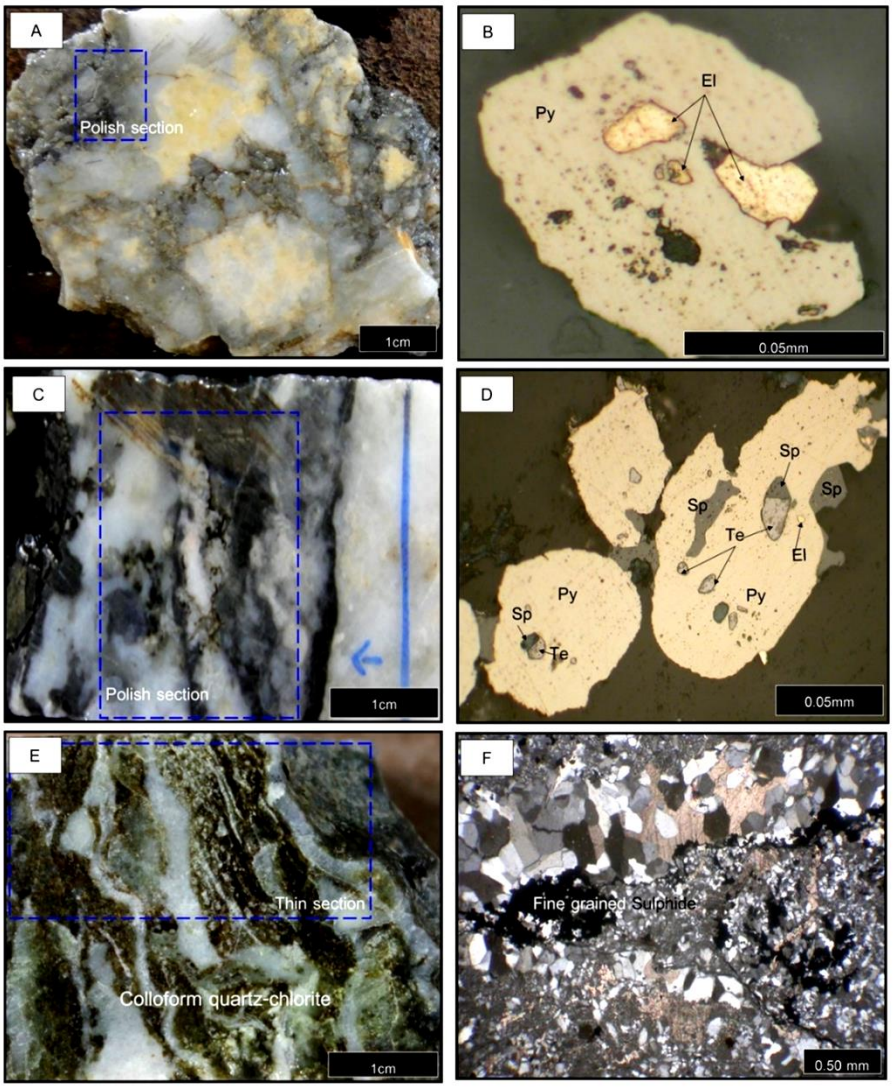

Figure 3.4 Some selective samples of Assemblage group II: A) Clast-supported breccia specimen (sample no. A039 of core 7555RD-267.70) showing angular and subrounded quartz in various clast sizes, with dark sulfide dissemination and late stage replacement of cream carbonate; B) Photomicrograph of the same samples showing electrum (El) grains associated with corroded pyrite (Py) crystal; C) Specimen (sample no. A033 of core 3224RD-222.30) showing quartz vein with layers of fine black sulfide layering and its photomicrograph D) showing tiny inclusion of multiphase inclusion of tetrahedrite (Te) and sphalerite (Sp) in corroded pyrite host; E) Specimen (sample no. A033 of core 3224RD-217.5) showing colloform quartz; and green chlorite band with disseminated pyrite, and its photomicrograph F) showing coarse-grained quartz (upper) infilled by calcite, fine-grained sulfide disseminated as layers along coarse-grained quartz band.

3.3.3 Assemblage group III: Quartz-carbonate-sericite-feldspar (±adularia)±chlorite-sulfide-sulfosalt (tetrahedrite/tennantite)

Assemblage group III is predominantly characterized by quartz-carbonate-sericite or quartz-(±sericite)-feldspar with pyrite, chalcopyrite, sphalerite, galena±tetrahedrite/tennantite and ±chlorite. Tetrahedrite/tennantite adularia and chlorite occur with minor amount in assemblage group III. This assemblage group III contains higher gold grade with average of 3.7-9.8 g/t which usually occurs as vein breccia and banded vein, such as quartz-carbonate-pyrite-feldspar-adularia (sample HG41), quartz-sericite-feldspar-grey silica-carbonate-pyrite-chalcopyrite-galena-sphalerite-tetrahedrite (sample HG27), quartz-sericite-feldspar-grey silica-pyrite (sample HG19, Figure 3.5) and quartz- (colloform chlorite)-feldspar- (adularia)-grey silica-carbonate-pyrite-chalcopyrite-sphalerite (sample HG7).

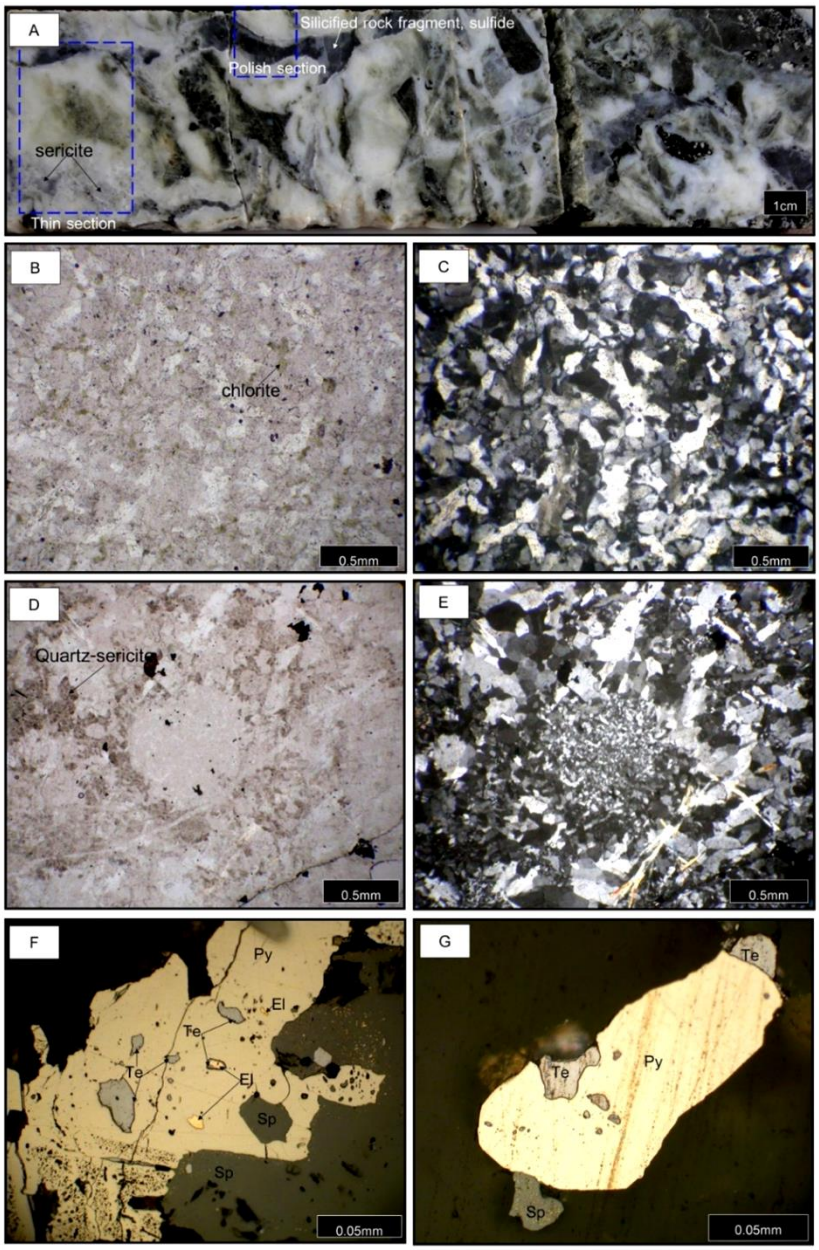

Figure 3.5 Some selective samples of Assemblage group III: A) Specimen (sample no.A019 of core 2771RD-222.05) of quartz-sericite vein breccia in stage 2 with replacement of dark sulfide in silicified rock fragment; B) and C) Photomicrographs showing crystalline quartz, pale green chlorite and sulfide disseminated; D) and E) Photomicrograph showing crystalline quartz, dark brown sericite and disseminated sulfide; F) Electrum (El) and tetrahedrite (Te) inclusions and their multiphase inclusion in pyrite host overgrowth with sphalerite (Sp); G) Tetrahedrite (Te) corroded pyrite crystal associated with sphalerite (Sp).

3.3.4 Assemblage group IV: Quartz-carbonate-pyrite-chlorite-feldspar (+adularia)-electrum-sulfide (chalcopyrite, sphalerite, ±galena, ±argenthite - sulfosalt)

Assemblage group IV comprises quartz, chlorite, feldspar (+adularia), pyrite, electrum, sulfide (chalcopyrite, sphalerite, galena, ±argenthite) and sulfosalt (tetrahedrite/tennantite). The assemblage group IV has dominant chlorite, feldspar, adularia and sulfide (mainly pyrite, chalcopyrite, sphalerite, tetrahedrite/tennantite) with relatively high gold (in the form of electrum) contents ranging from 3.8 g/t to 73 g/t Au with an average of 16 g/t Au.

The assemblage group IV is usually characterized by crustiform-colloform band to vein breccia and multi-phases of vein breccia which are exemplified below.

- Quartz (±grey silica±chalcedonic)-carbonate-chlorite-K-feldspar pyrite-chalcopyrite-galena-sphalerite-tetrahedrite/tennantite-electrum (samples A001 in Figure 3.6, A002 in Figure 3.7, A009 in Figure 3.8, A018 in Figures 3.9-3.10, A010 and A024).
- Quartz (±grey silica±chalcedonic)-carbonate-chlorite-strong sulfide (pyrite-chalcopyrite-galena-sphalerite-tetrahedrite/tennantite-electrum) (samples A011 and A012).
- Quartz (±greysilica)-adularia-sulfide (pyrite-arsenopyrite-sphalerite-tetrahedrite/tennantite)-electrum-late stage carbonate (sample A013 in Figures 3.8 D to G).
- Quartz (±grey silica)-chlorite-K-feldspar (+adularia)-pyrite-chalcopyrite-sphalerite-tetrahedrite/tennantite-electrum (sample A017).
- Quartz (±grey silica)-adularia-sulfide (pyrite-chalcopyrite-galena-sphalerite-tetrahedrite/tennantite) -electrum-late carbonate (sample A032 in Figures 3.11 A to C).
- Quartz (±grey silica)-sulfide (pyrite-arsenopyrite-sphalerite-tetrahedrite)-electrum-late carbonate (sample A038 in Figures 3.11 D to F).

The characteristic features of assemblage group IV show in Figures 3.6-3.11.

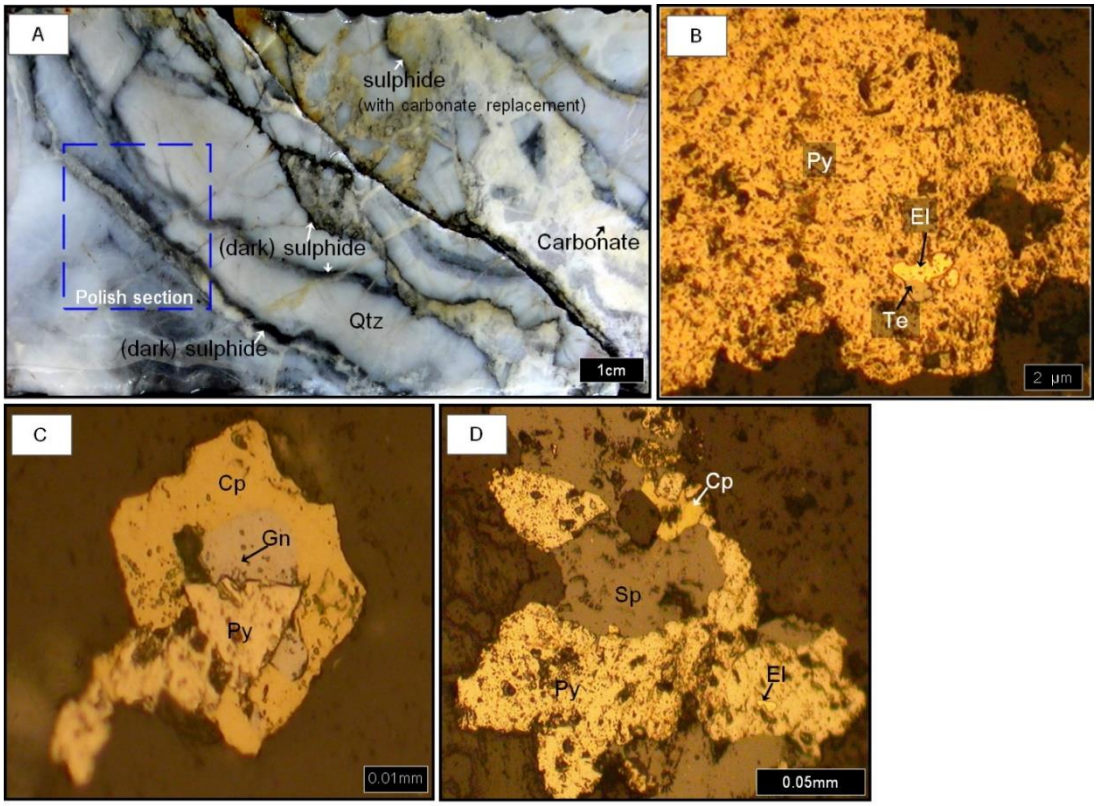

Figure 3.6 Some selective samples of Assemblage group IV: A) Specimen (sample A001 of core 3371RD-215.5) showing brecciated vein containing fine-grained crystalline quartz to chalcedony, dark and yellow sulfide bands and replaced carbonate; B) Photomicrograph showing multi-phase inclusion of tetrahedrite (Te)and electrum (El) in pyrite crystal; C) Pyrite (Py) is mutually intergrowth with chalcopyrite (Cp) and galena (Gn); D) Spongy anhedral pyrite grains with electrum (El) inclusion intergrowth with sphalerite (Sp) and chalcopyrite (Cp).

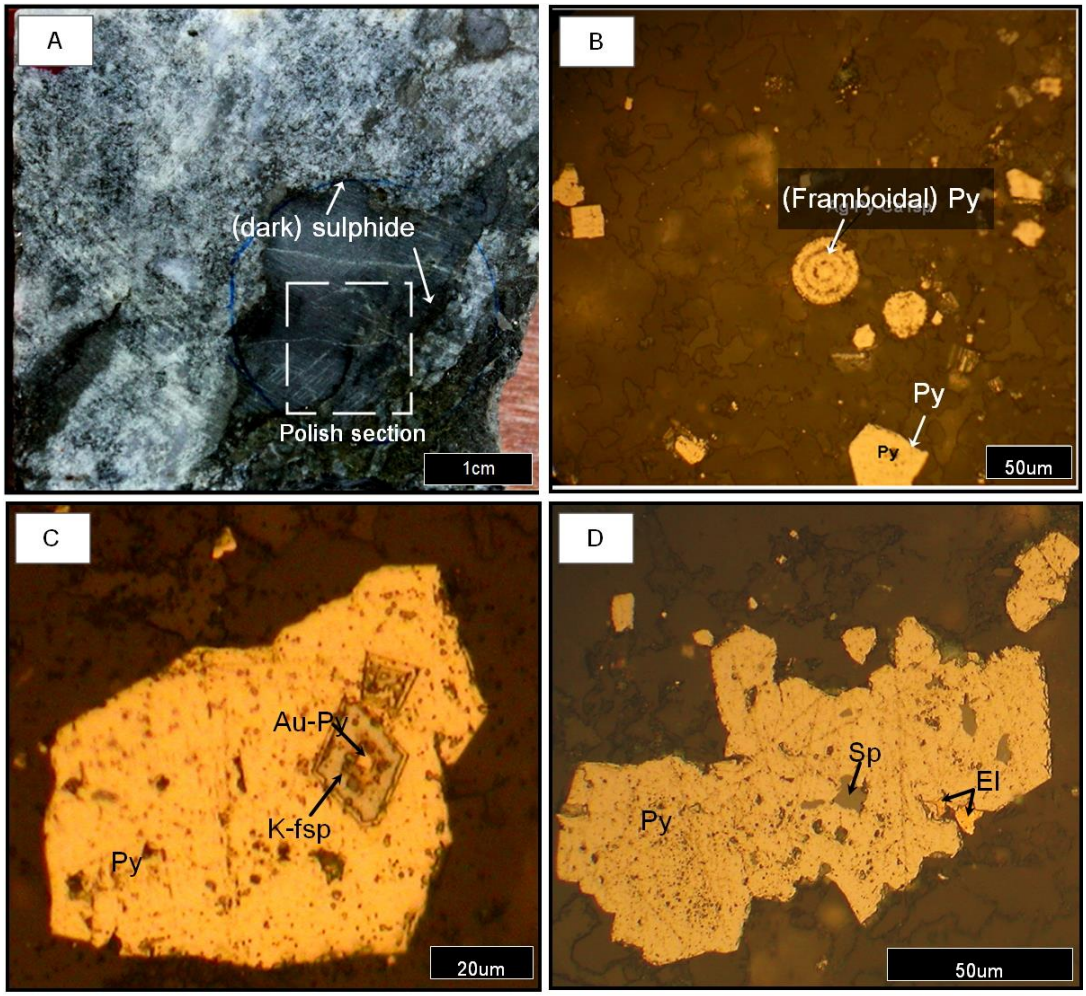

Figure 3.7 A) Specimen (sample no. A02 of core 3371RD-216.50) showing quartz-carbonate vein stage 2 in assemblage group IV with dark sulfide layer and disseminated fine-grained sulfide; B) Spherical or framboidal form of pyrite (Py) with calcium feldspar rich grain; C) Multiple phases inclusion of gold (Au)-pyrite(Py) in rhombic K-feldspar crystal (adularia habit); D) Electrum (El) and sphalerite (Sp) inclusions in pyrite (Py).

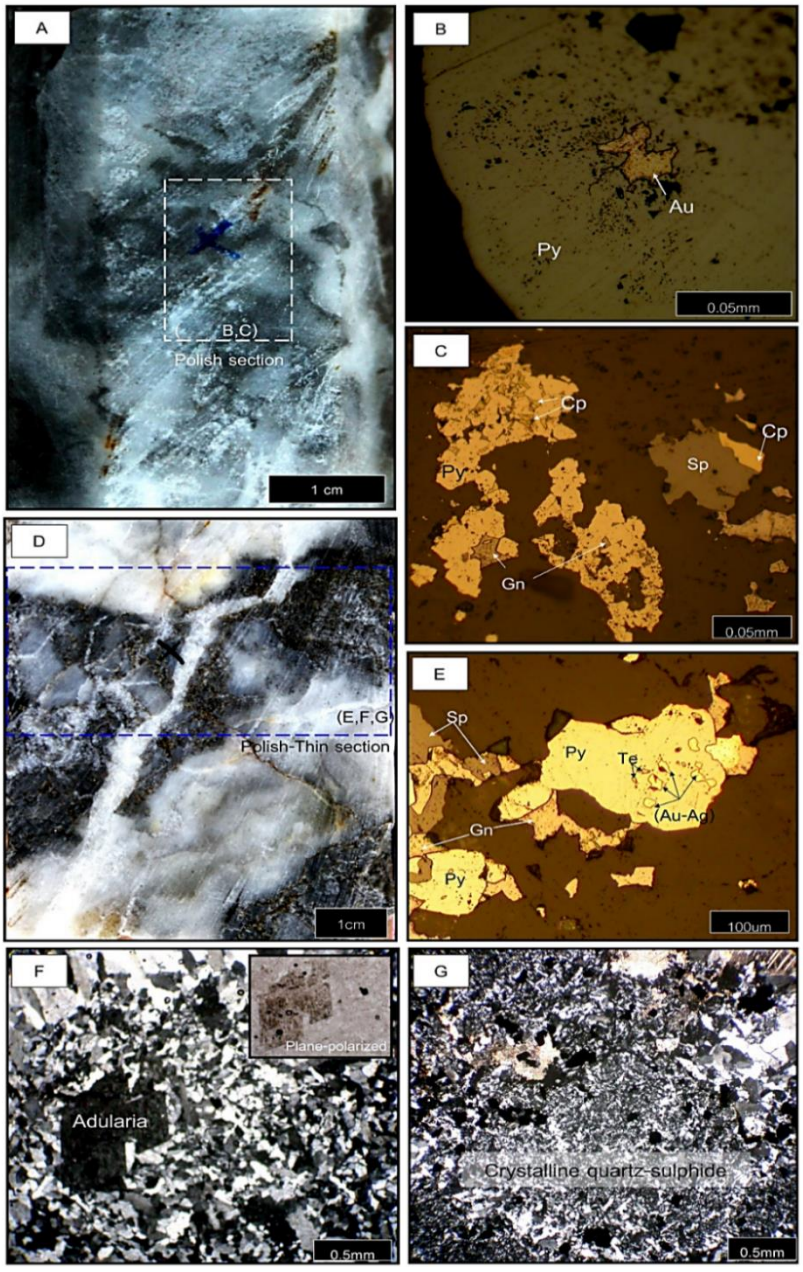

Figure 3.8 A) Specimen (sample A09 of core 2561RD-213.7) showing crystalline quartz and colloform quartz-sulfide cross-cut by late stage carbonate vein breccia; Photomicrographs B) and C) showing gold inclusions occurred in pyrite host crystal; C) Galena (Gn) and chalcopyrite (Cp) formed as inclusion in pyrite (Py) and chalcopyrite intergrowth with sphalerite (Sp); D) Specimen (sample no. A013 of core 6231RD-195.8) showing opalline-crystalline quartz vein breccia with minor grey silica with strong sulfide dissemination and late stage carbonate cross-cut other phases; E) Gold (Au) inclusion occurred in pyrite (Py) crystal and pyrite (Py) intergrowth with galena (Gn) and sphalerite (Sp); F) Coarse-grained crystalline quartz intergrowth with subhedral grains rhombic adularia; G) Coarse- to fine-grained crystalline quartz containing disseminated sulfide.

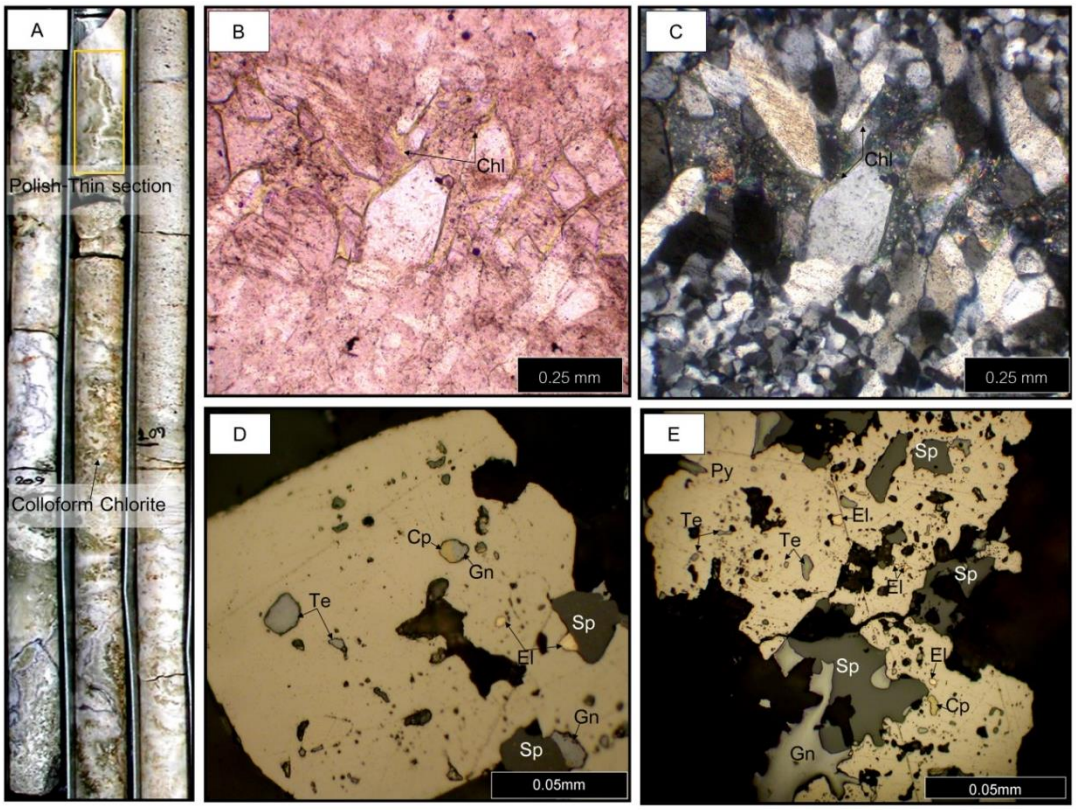

Figure 3.9 A) Drilled core sample (sample A018 of core 2771RD-207) showing colloform quartz-chlorite banded vein; B) and C) Photomicrographs showing chlorite (Chl) and coarse crystalline quartz (chlorite filled fracture); D) Multiphase inclusions of galena (Gn) and chalcopyrite (Cp), tetrahedrite (Te) and electrum (El) inclusion in pyrite (Py) crystal intergrowth with sphalerite (Sp) and galena (Gn); E) Many inclusions of electrum (El) and tetrahedrite (Te) and some chalcopyrite (Cp) inclusions in pyrite (Py) crystal associated with galena and sphalerite.

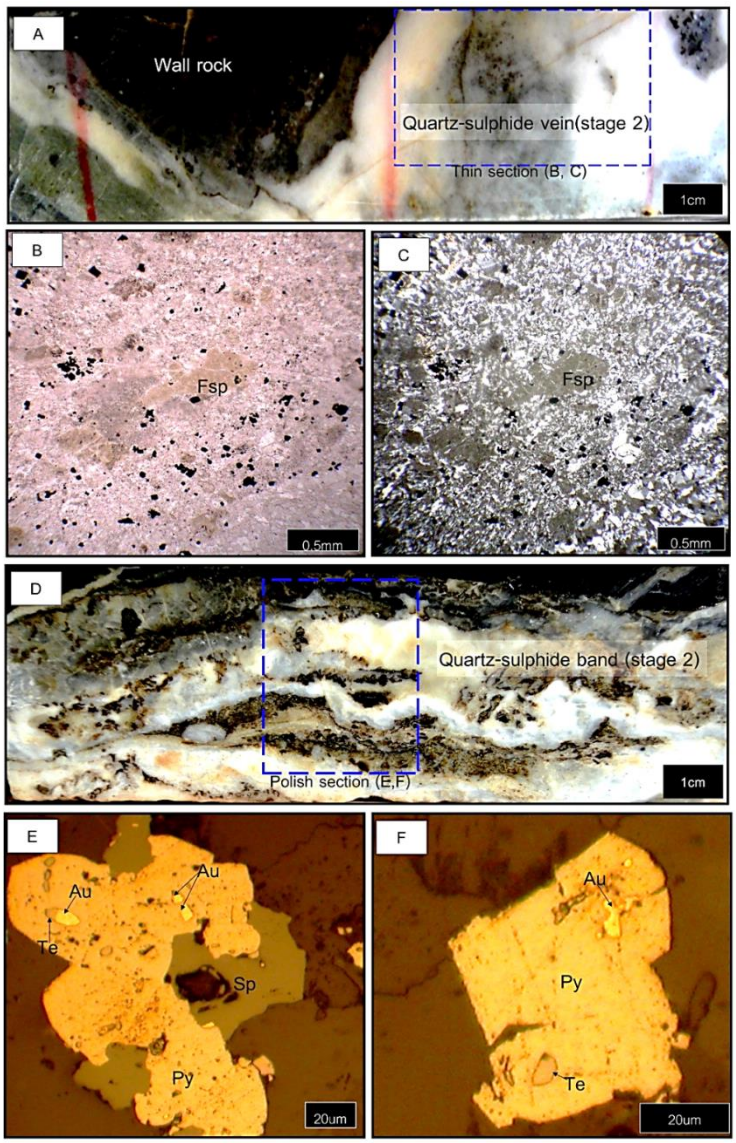

Figure 3.10 A) Specimen (sample no. A018 of core 2771RD-216.5) showing quartz and disseminated sulfide vein (stage 2) cross-cut into sandstone wall rock; B) and C) Photomicrographs showing coarse to fine crystalline quartz-feldspar and disseminated sulfide. The subhedral feldspar show brown colored under plane polarized in B; D) Specimen (sample no. A024 of core 00959RD-142.40) showing colloform quartz-sulfide vein and late stage of brown carbonate; E) Gold (Au) inclusions and multiphase inclusion of gold and tetrahedrite (Te) in pyrite (Py) crystal intergrowth with sphalerite (Sp); F) Inclusions of gold and tetrahedrite in pyrite crystal.

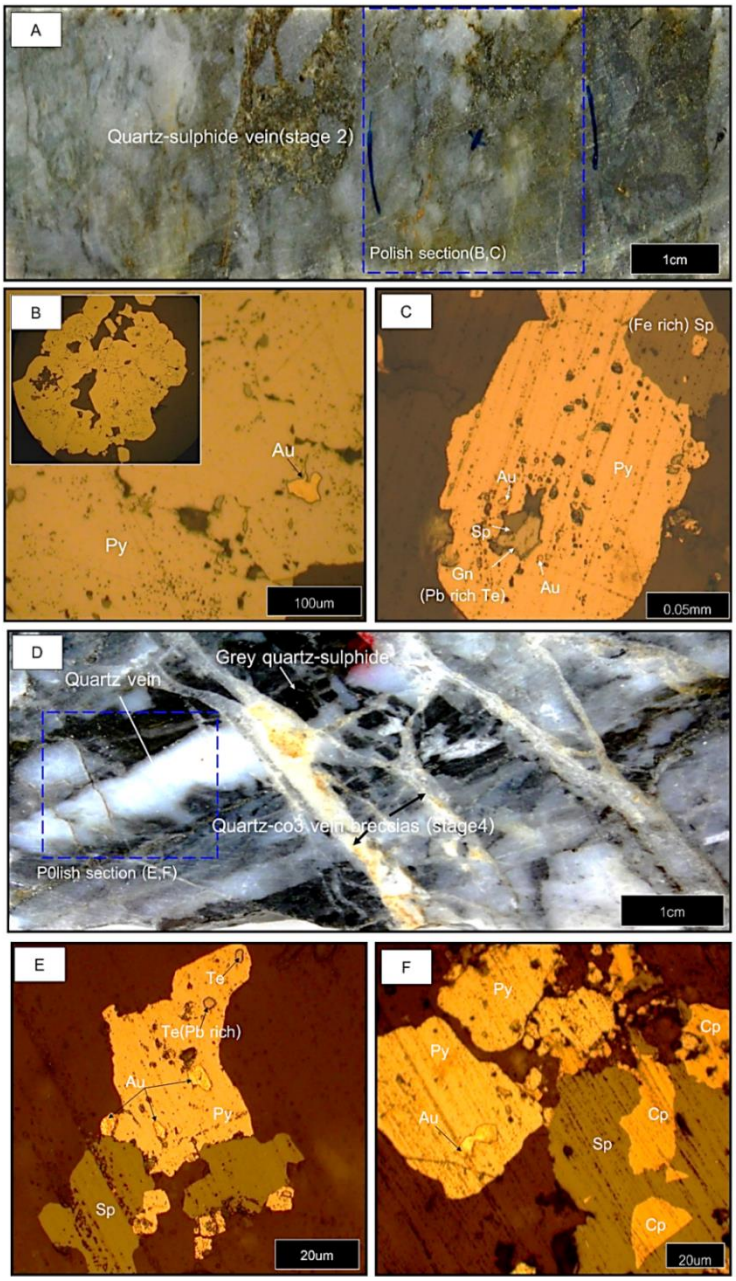

Figure 3.11 A) Specimen (Sample no. A032 of core 02562RD-244.2) showing quartz-sulfide brecciated vein. Sulfide formed as stringer vein, disseminated and filled fracture; Photomicrograph B) showing gold (Au) inclusion in pyrite; C) Galena (Gn) enclosing sphalerite (Sp) grain and small gold (Au) inclusions in pyrite (Py) associated with dark sphalerite (Sp); D) Specimen (sample no. A038 of core 7554RD-208.85) showing opaline-grey quartz (stage1) and crystalline white quartz vein (stage 2), cross-cut by quartz-carbonate vein breccia (stage 4) with disseminated dark sulfide in grey quartz and sulfide stringer vein.; E) Inclusions of gold (Au) and tetrahedrite (Te) in corroded pyrite (Py) with sphalerite (Sp); F) Gold (Au) inclusion in pyrite (Py) associated with chalcopyrite (Cp) and sphalerite (Sp).

3.4 Mineralization stage 3 (Quartz±carbonate+chlorite+pyrite±sulfide±sericite ±chalcedonic)

Mineralization vein stage 3 predominantly formed as chlorite-pyrite stockwork and banded vein. These veins are represented by dark green to green chlorite vein commonly disseminated by sulfide. Gold crucially forms as electrum which is relatively high abundant in sulfide-rich chlorite band. This quartz-chlorite-carbonate-sulfide assemblage appears rarely, but it often gives high gold grade veins.

3.5 Mineralization stage 4 (Quartz-chalcedonic-carbonate-sulfide vein breccia) (brecciated zone)

The mineralization vein stage 4 is recorded in clasts of early stage 1 and/or stage 2 which are accumulated in breccia vein. Quartz-carbonate, quartz-grey silica-carbonate -pyrite and quartz- carbonate -pyrite that occur as matrix in breccia vein. Gold grades of this stage vary from place to place, depending on overprinted vein, styles of clast-matrix and sulfide mineralization. Quartz-carbonate-chlorite-sulfide band appears to have yielded higher gold content.

3.6 Mineralization vein stage 5 (Post gold mineralization)

The post gold mineralization is defined as the latest vein stage without sulfide and gold occurrences. Mineralization vein stage 5 is characterized by carbonate, carbonate-laumontite, quartz-carbonate-zeolite and comb quartz.

Examples of mineral paragenesis of A – Eastern A pit containing in stages 1 to 5 is also shown in Figure 3.12.

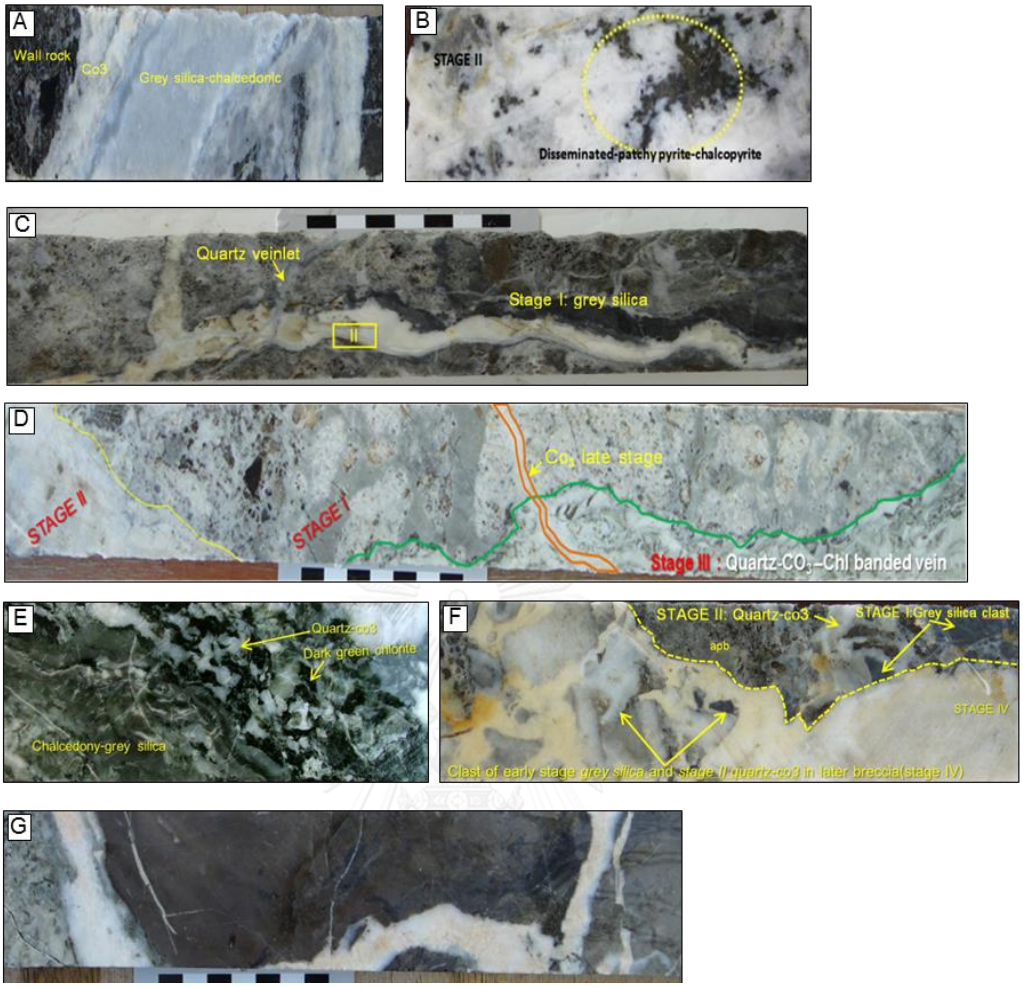

Figure 3.12 Examples of mineral paragenesis of A – Eastern A pit containing in stages 1 to 5: A) Specimen (core 5007RD-112.0) of banded grey silica-chalcedonic vein, narrow late stage, brown carbonate vein, andesitic sedimentary breccia host rock; B) Specimen (core 3379RD-202.7) of massive quartz-carbonate-disseminated and pyrite-chalcopyrite hosted by polymictic andesitic-sedimentary breccia; C) Specimen (core 2603RD-125.0) of dark grey, grey silica vein (stage I), quart-carbonate vein breccia (stage II) cross-cut by late stage quartz veinlet; D) Specimen (core 00836RD-117.0) of grey silica (stage I) vein breccia, quartz-carbonate vein (stage II), band of quartz-carbonate-chlorite vein (stage III) cross-cut by the late stage carbonate-laumontite vein; E) Specimen (core 00937RD-195.0) of chalcedonic and grey silica vein (stage I), sub-angular quartz-carbonate vein breccia (stage II), dark green coarse chlorite and disseminated sulfide infilled open space (stage III); F) Specimen (core 00876RD-146.0) of quartz-(cream-white) carbonate vein breccia (stage IV) hosted by polymictic andesitic breccia with strong silicified; G) Specimen (core 3302RD-359.0) of late stage (white-cream) carbonate vein cross-cut quartz-carbonate vein breccias (stage2) hosted by sandstone wall-rock.

3.7 Quartz Textures Related to Gold Mineralization

Quartz textures of mineralization vein stage II, the highest grade of gold mineralization, in Eastern A pit, are defined on the basis of mutual geometrical relations among individual crystal, crystal aggregates and the internal features of individual grains as suggested by Dong et al. (1995). Quartz textures can be described by three main texture types including primary growth, recrystallization and replacement textures. (Dong et al., 1995) also considered genetic point of view in these three major textures. The crustiform/colloform, moss, massive, comb and zonal are considered as primary growth texture that relate to amorphous silica deposit during crystal growing. The plumose, ghost sphere and mosaic are product of recrystallization texture. The saccharoidal is classified as replacement texture that may be replaced by fine-grained aggregates of anhedral quartz.

Quartz texture observed in core samples can be divided into five groups. They include (Q1) saccharoidal texture, (Q2) moss/ghost-sphere texture, (Q3) comb and zonal texture, (Q4) plumose (feathery/flamboyant) texture and (Q5) banding (colloform/crustiform) texture. They can be described from relatively lower to higher gold grade as following.

Q1: Saccharoidal texture

Saccharoidal texture displays in opaline quartz or crypto-crystalline quartz and usually associates with rhombic calcite (see Figure 3.13). This saccharoidal texture appears to be involved by carbonate solution with decreasing temperature in the early precipitation before replacement of silica minerals as suggested by Dong et al. (1995). Rhombic calcite occurs as a late-stage filling or cross-cutting to form breccia matrix. They are typically associated with low gold concentration. Microscopically, homogeneous texture is referred to massive quartz vein without banding or other features. Massive quartz is also observed in hand specimens of massive carbonate vein with gold grade of 1 g/t. The massive texture is an original growth feature during slow precipitation as suggested by Moncada et al. (2012). In general saccharoidal quartz with rhombic calcite yield low gold grade between 0.1-1 g/t. Small amounts of electrum and sulfide can be observed under microscope.

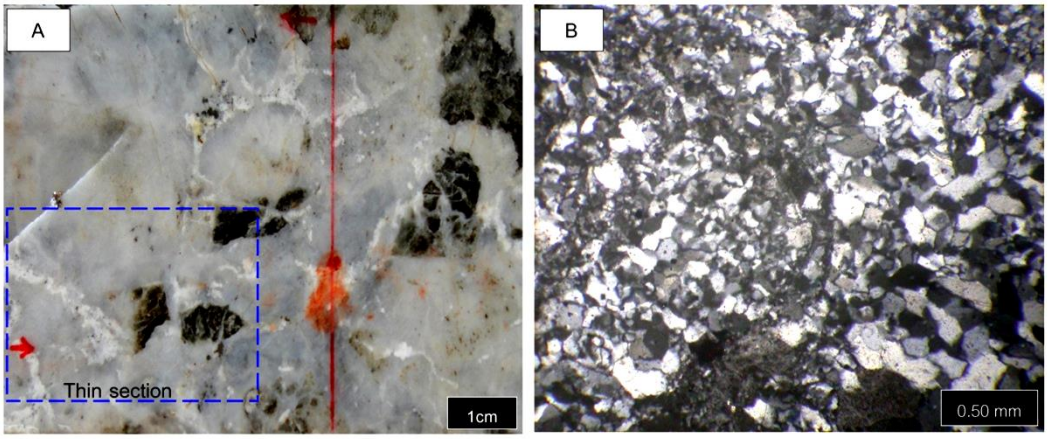

Figure 3.13 A) Specimen (sample no. A023 of core 2626RD-261.9) showing opaline quartz-sericite vein breccia hosted by pebbly sandstone which appears to have undertaken silicification; B) Saccharoidal, subhedral quartz crystals and opaline quartz distributed randomly in this section.

Q2: Moss/ghost sphere texture

Moss texture shown as sphere ranges from 0.1-1.0 mm in size. This texture is formed by aggregation of tiny quartz crystals observable under microscope (see Figure 3.14). Ghost sphere is referred to special moss texture formed by amorphous silica or chalcedonic-quartz (notified by Dong et al., 1995). Ghost sphere texture shows microscopically radiated extinction that may be caused by silica gel crystalline to flamboyant texture. The moss (ghost-sphere) texture displays in the early stage vein and may be precipitated during or immediately after banded quartz texture as suggested by Ovenden et al. (2005). The moss/ghost sphere usually contains low gold concentration ranging between 0.8-2.7 g/t. It is also associated with chlorite, feldspar, tetrahedrite/tennantite, electrum and sulfides with dominant pyrite and perhaps chalcopyrite, sphalerite and galena.

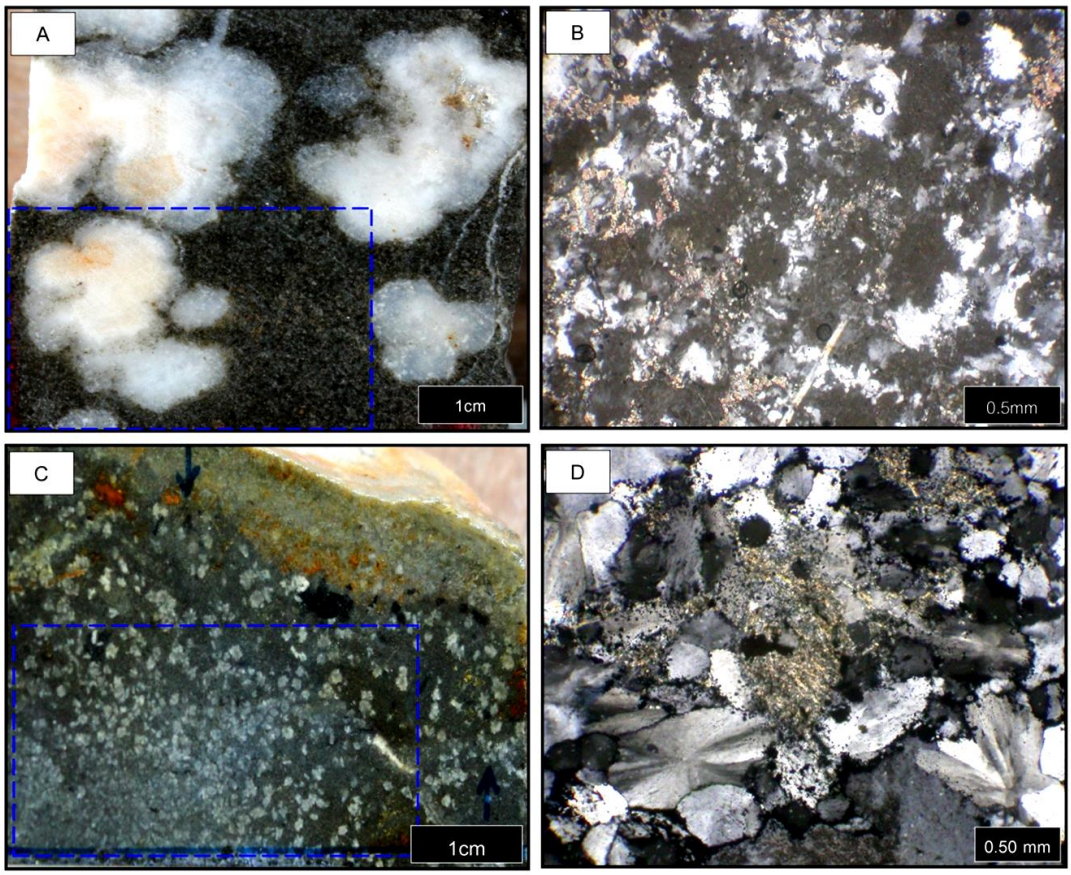

Figure 3.14 A) Specimen (sample no. A030 of core 6186RD-120.20) showing recrystallization of quartz formed as spherulites texture in sandstone; B) Photomicrograph showing spherical distribution of fine to coarse crystal quartz and defined in term of moss texture; C) Specimen showing white quartz and plagioclase-feldspar in form of radiate crystals (lower than 1-2 mm. in size) with strong disseminated pyrite in sandstone; D) Photomicrograph showing spherulitic texture of crystalline quartz associated with strong dissemination of sulfide and alteration of K-feldspar to yellow sericite.

Q3: Comb/zonal texture

Comb texture is observed in a few samples. Comb texture with prismatic euhedral growth zone appears to have developed parallel orientation (see Figure 3.15). Zonal quartz texture can also be observed in these samples which show individual euhedral quartz crystal. The Q3 texture contains moderate gold grade (5.9-6.6 g/t). These Q3 is associated with quartz, carbonate, sericite, pyrite, chalcopyrite, sphalerite, galena and tennantite.

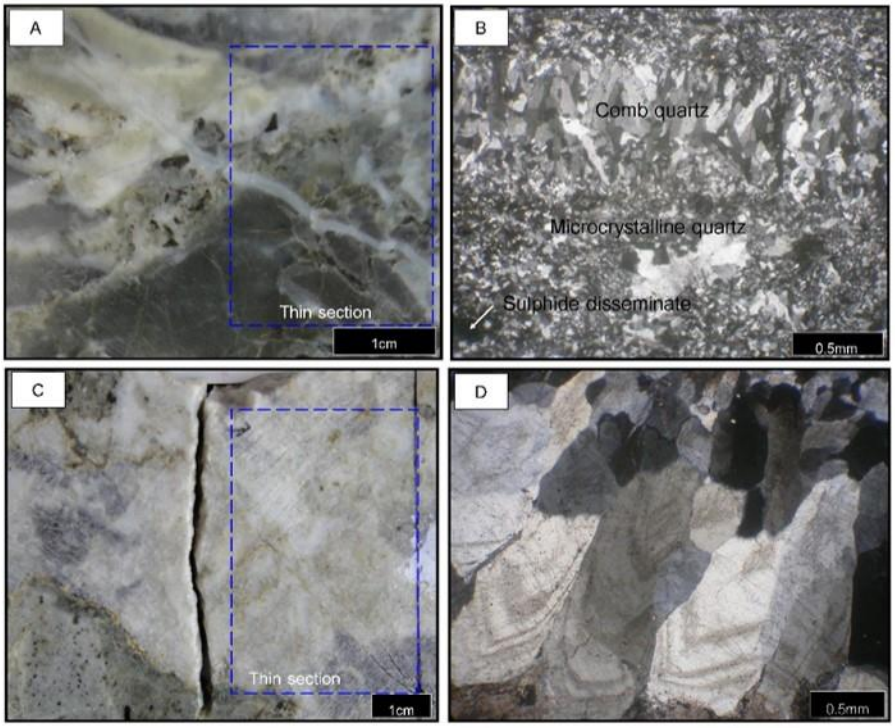

Figure 3.15 A) Specimen (sample no. A016 of core 6216RD-221.08) of grey silica and quartz vein breccia; B) Photomicrograph showing microcrystalline quartz and disseminated sulfide cross-cut by coarse-grained comb quartz texture; C) Specimen (sample A026 of core 3217RD-326.26) showing quartz with replacement of carbonate vein breccia hosted by sand matrix andesitic breccia; D) Photomicrograph showing coarse crystalline quartz intergrowth with fine crystalline quartz. The individual euhedral, coarse grained quartz is characterized by zonal texture.

Q4: Plumose (feathery-flamboyant) texture

Plumose quartz texture is the most abundant texture in these studied samples (see Figures 3.16 and 3.17). This quartz texture has been defined as feathery which is similar to plumose as suggested by Adam (1920) and (Sander and Black, 1988). The feathery texture is recrystallized amorphous silica and chalcedonic quartz. The feathery displays patches extinction throughout quartz crystal (see Figure 3.16C). The term of flamboyant is also similar to the feathery texture. The flamboyant is determined by radiated extinctions of rounded quartz crystals (see Figure 3.16E). The plumose texture vein has a range of gold content from 3.0 up to 14.5 g/t. This Q4 texture is associated with adularia and other feldspars, sericite, ±chlorite±carbonate, sulfide (i.e., pyrite, chalcopyrite, sphalerite and galena), tennantite and electrum. Feathery quartz may be up to 1mm in size and overgrowth by saccharoidal quartz.

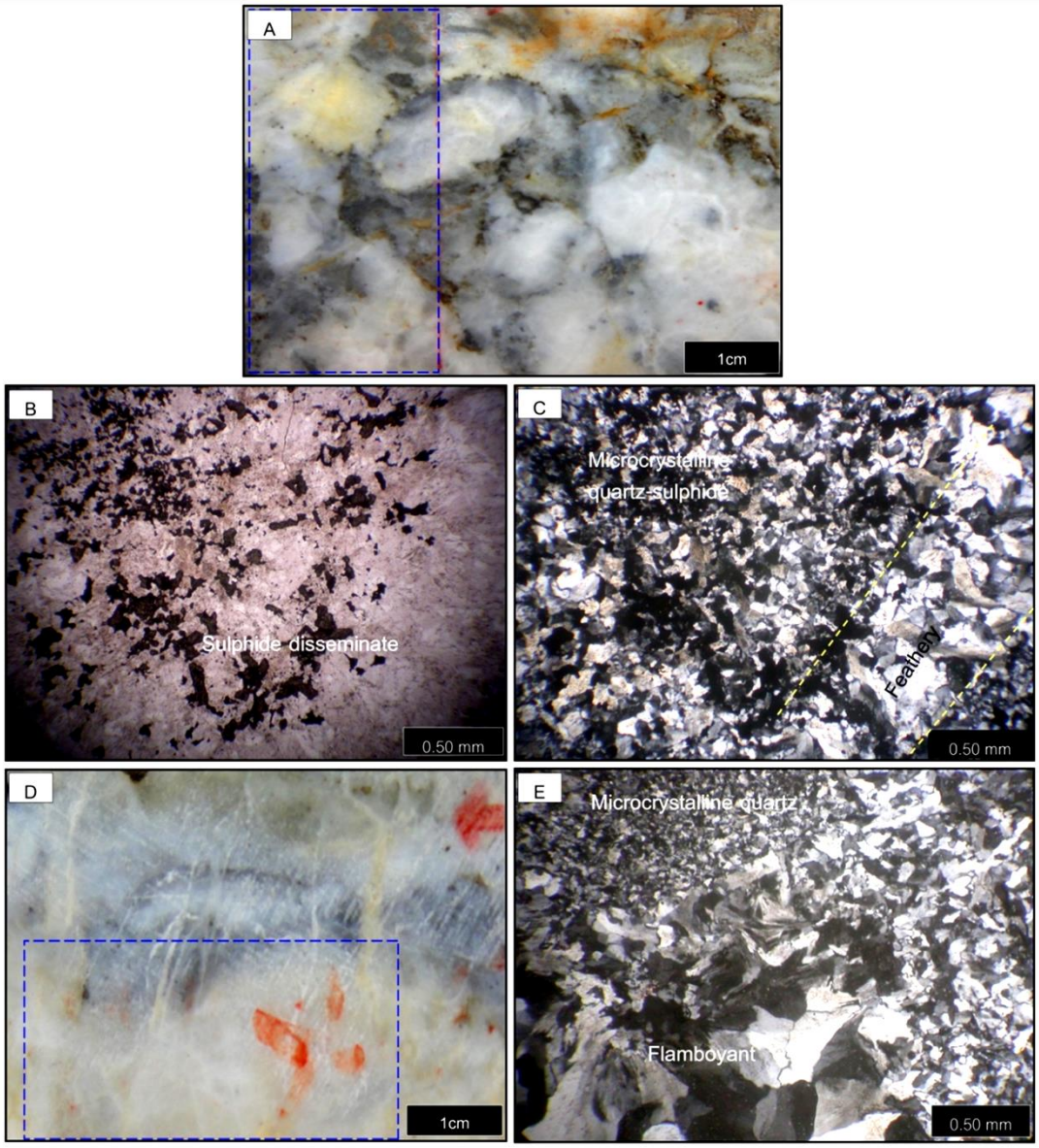

Figure 3.16 A) specimen (sample A017 of core 6216RD-229.5) of crystalline quartz with disseminated pyrite (stage 2) and its photomicrographs under plane polarized light (B) and cross polarized light (C) showing fine crystalline quartz-sulfide (center) intergrowth with coarse crystalline, feathery quartz texture; D) Specimen (sample no. A021 of 2537RD-160.3) showing quartz-sulfide vein cross-cut by late stage cream carbonate; photomicrograph under cross polarized light (E) showing microcystalline quartz and disseminated sulfide intergrowth with coarse crystalline, flamboyant texture and extinctions of quartz.

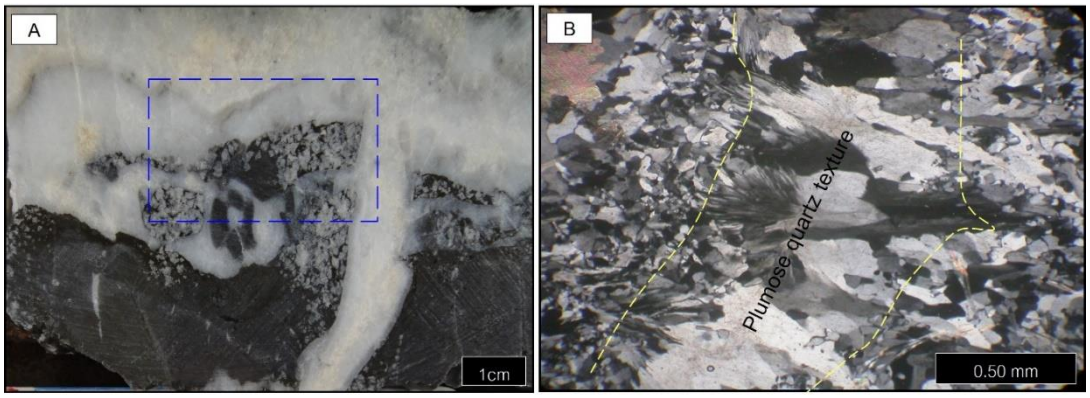

Figure 3.17 A) Specimen (sample A041 of core 7556RD-180.0) of crystalline quartz vein cross-cut into siliceous sandstone, and recrystallized quartz occurs as radius fragment; B) Photomicrograph showing microcrystalline quartz cross-cut by coarse-grained plumose quartz texture.

Q5: Banded (crustiform-colloform) texture

Banded features are characterized by crustiform and colloform texture with some layering and slight brecciation. The term crustiform band is characterized by narrow (up to a few centimeters), sub-parallel band. Fine banding of microcrystalline and comb quartz were developed from both walls. Colloform occured as concentric curve which under microscope shows fine-grained and coarse-grained quartz overgrowth texture (see Figure 3.18). The banded texture which can be observed in hand specimens. Both crustiform and colloform are founded in association with mono-polymictic rhyolitic breccias and volcaniclastic sedimentary unit, pebbly sediment to polymictic andesitic sedimentary breccias in the uppermost part of sedimentary unit. They are the second most common quartz texture which is usually composed of quartz-carbonate-sulfide, quartz-carbonate-chlorite-sulfide in banded vein. Chlorite, feldspar, adularia and sulfide (mainly pyrite, chalcopyrite, sphalerite and tennantite) are often found in association with this Q5 texture. The Q5 banded texture presents the highest gold grade that ranges between 3.8-73 g/t. Sulfide and electrum tend to be enriched in the quartz-chlorite rich band with subordinate enrichment in the carbonate band. The sulfide-rich chlorite-quartz band tends to have a high gold grade by petrographic study of Salam (2011).

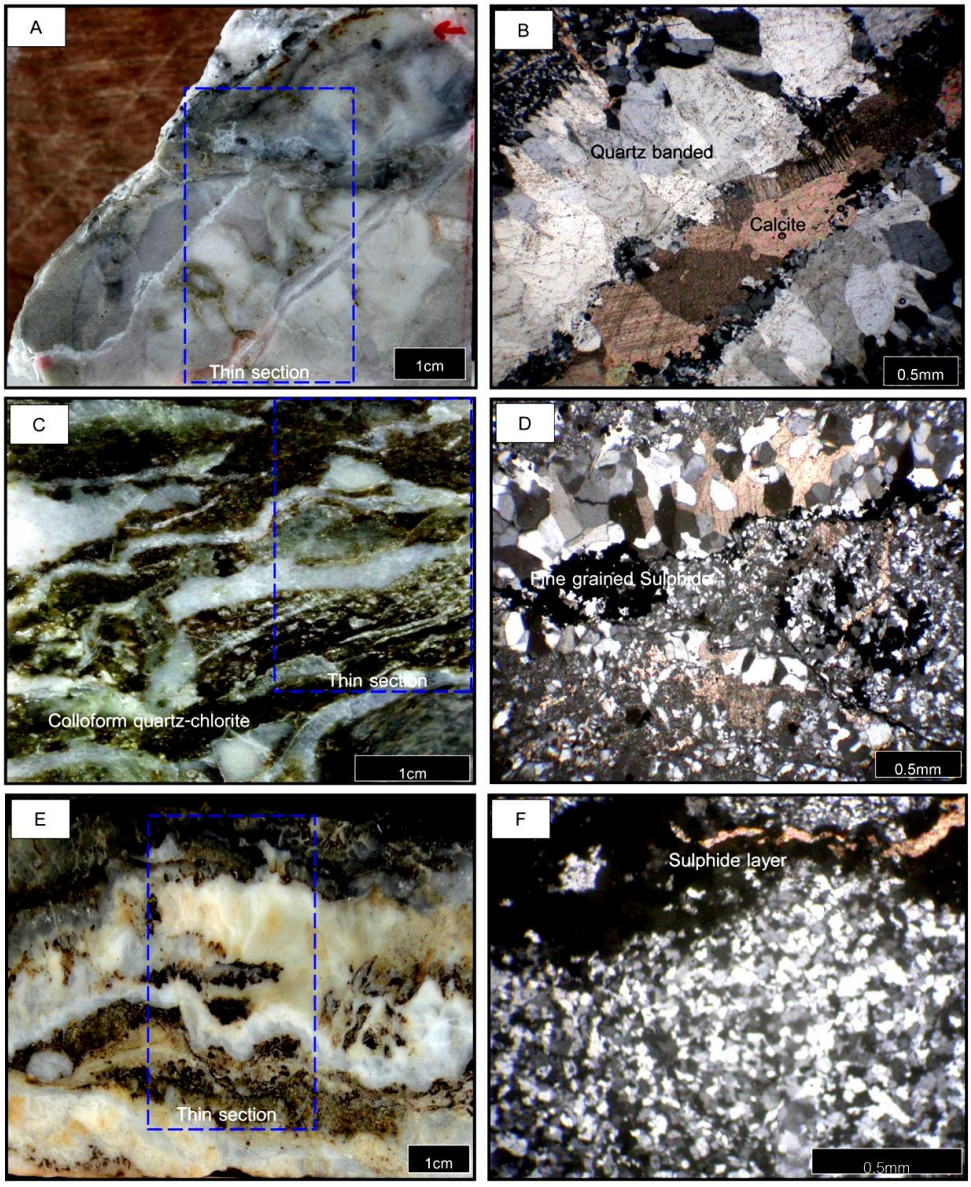

Figure 3.18 A) Specimen (sample no. A001 of core 3371RD-215.3) showing quartz-chalcedonic band and vein breccia with disseminated layer of sulfide; B) Photomicrograph showing fine-grained crystalline quartz matrix with coarse-grained quartz overgrowth within banded vein and late stage carbonate infilled open space; C) and D) Photomicrographs (sample no. A033 of core 3224RD-217.5) showing colloform quartz-chlorite vein containing sulfide layer with coarse crystalline quartz and late stage carbonate-infilled fracture; E) and F) Photomicrographs (sample A024 of core 0959RD-142.4) showing colloform quartz - sulfide vein with sulfide layer in crystalline quartz.

CHAPTER 4
Mineral Chemistry and Whole-Rock Geochemistry

4.1 Introduction

Trace geochemistry of epithermal Au-Ag deposit are usually used for identification of geochemical indicator of the gold mineralization zones. For examples, elemental analyses, distribution of high gold grade veins and gold-correlation matrix were suggested by Braund (2006); trace element patterns of pre-gold and main-gold mineralization stages were also introduced by Salam et al. (2014). The ICP whole-rock analyses were used to characterize pathfinder of gold mineralization. This research project was focused on ore chemistry in correlation with gold concentration and geochemical indication. This chapter will report: (1) ore chemistry related to high grade gold mineralization; (2) whole-rock trace geochemistry; (3) statistical correlation coefficient of whole-rock geochemical data.

The high grade gold mineralization is locally associated with brecciated quartz veins with colloform banding texture. Gold presents very fine grains ranging from less than 1 to 10 μm. A few irregular shapes may be up to 30 μm. The most common gold present in high grade gold mineralization from Eastern A pit usually occurs as electrum (combined Au and Ag) in pyrite (see Figure 4.1 A). Electrum is composed of Ag-rich composition presenting pale yellow color whereas Au-rich grain is golden yellow color. They usually form as inclusions particularly in pyrite and perhaps invisible gold composition in sphalerite (see Figure 4.1 B). Electrum also occurs along with tennantite as multi-stage inclusions in pyrite host (see Figure 4.1C) particularly in the colloform quartz-chlorite vein. The fine individual grains of gold and electrum may occur in medium- to coarse-grained quartz-adularia veins, fine- to coarse-grained quartz-sericite veins and fine-grained quartz-chlorite veins. K-feldspar with adularia habit is also associated with pyrite crystal (see Figure 4.1D). It is also associated with quartz and carbonate vein.

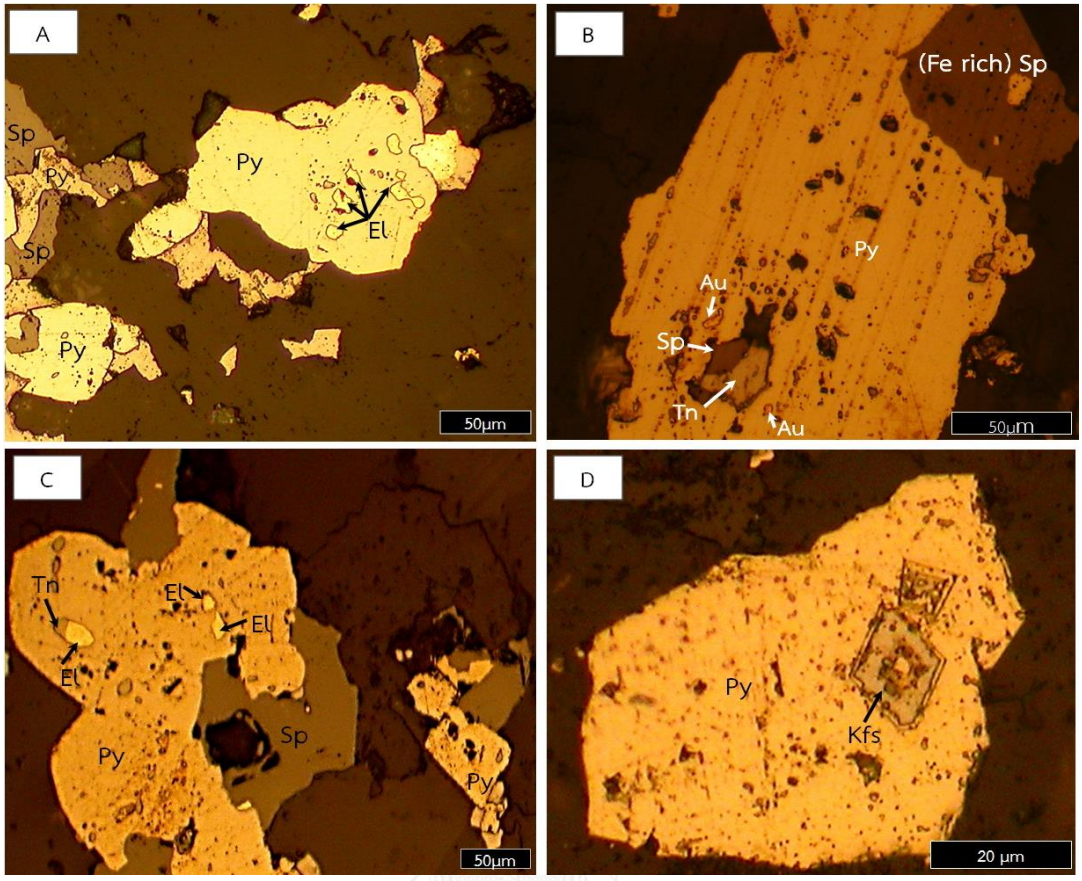

Figure 4.1 A) Electrum (El) inclusions in pyrite (Py); B) Iron-rich sphalerite with invisible gold concentration (see mineral chemical analyses in Table 4.2.2); C) Electrum (El) attached to tennantite (Tn) inclusion (left) in corroded pyrite (Py) intergrowth with sphalerite (Sp); D) Rhombic K-feldspar (Kfs) (adularia habit) in pyrite (Py) host (all micrographs were taken under cross-polarized reflected light).

4.2 Mineral Chemistry

Microscopic observation of sulfide minerals and spot chemical analysis using Electron Probe Micro-Analyzer (EPMA) were performed on the selected ore minerals from the banded and plumose quartz textures of mineral assemblage IV (quartz-chlorite-feldspar (+adularia)-electrum-tennantite-pyrite-sphalerite) of mineralization stage II which is closely related to high gold grade. It also contains higher abundance of sulfide. Ten polished section are prepared from ten representative vein samples including A001 (16 g/t Au), A002 (73 g/t Au), A010 (11.95 g/t Au), A011 (21.1 g/t Au), A012 (14.5 g/t Au), A013 (11.1 g/t Au), A017 (16.7 g/t Au), A024 (8.8 g/t Au), A032 (14.3

g/t Au) and A038 (8.8 g/t Au) which are the top gold grade samples (reported by Chatree laboratory).

However, gold occurrence in some samples could not be observed under 50X microscope. EPMA was then used to analyze the chemical compositions. Sulfide minerals including pyrite, sphalerite, tennantite, and some gangue minerals, particularly feldspar were analyzed. Electrum and associated ore minerals are described below.

4.2.1 Pyrite

Pyrite (FeS_2) is commonly found as individual grains with porous masses (spongy network with size of 50-200 μm). Pyrite predominately comprises about 40-50 wt. % of total sulfide with the molybdenite (Mo) up to 0.75 wt. %. The EPMA results (see Table 4.1) of electrum inclusions in pyrite crystals are composed of 19.01-42.75 %S, 11.14-29.11 %Fe, 12.06-35.42 %Au and 10.64-41.96 %Ag (see Table 4.2.1). The results of invisible gold-silver composition in pyrite crystal may contain 7.52 %Au and 9.01 %Ag. This indicate pyrite composition of $Fe_{0.74}S_2$ with $Au_{0.04}$ and $Ag_{0.08}$.

In addition, tellurium (Te) occurs invisibly in electrum inclusions with content up to 0.23 %Te. Tennantite ($Cu_{12}As_4S_{13}$) also distributed as small inclusions in pyrite. It may occur in association with electrum as multiphase inclusions (with size of 0.01-0.02mm). Electrum occurs in association with tennantite in the main gold-bearing stage of Chatree deposit as reported by Salam (2011).

Some smaller electrums and other sulfide grains are unable to be analyzed by EPMA due to limitation of beam diameter and grain size.

Table 4.1 Representative EPMA analyses of electrum inclusions and invisible Au-Ag composition in pyrite.

Mineral	Pyrite	Electrum						
Sample point	A10_Au1	A12_Au1	A13_Au1	A24_El1	A24_El4	A38_El1	A38_El2	A38_El4
Analysis (wt.%)								
Au	7.52	18.60	14.26	17.78	34.61	35.42	12.06	17.09
Ag	9.01	18.63	10.64	18.36	33.61	34.03	41.96	13.00
As	-	0.01	-	0.08	-	0.02	-	0.04
Mo	0.60	0.60	0.75	0.44	0.24	0.24	0.15	0.47
Zn	0.07	-	0.07	0.41	0.09	-	0.27	0.31
Cu	0.03	0.12	0.13	0.00	0.13	0.13	0.07	-
Te	0.22	-	0.15	0.23	0.18	0.00	0.04	0.10
Fe	32.22	24.21	29.11	25.23	11.80	11.14	12.16	27.94
S	50.24	37.89	42.75	37.43	19.29	19.01	24.48	41.04
Al	0.06	-	-	0.04	0.06	0.05	0.09	0.03
Si	0.01	-	-	-	-	0.01	8.73	0.01
Se	-	-	-	0.00	0.05	-	-	-
Na	0.04	-	-	0.02	-	-	-	-
Tl	-	-	0.35	-	-	-	-	-
K	0.04	-	-	-	-	-	-	-
Total	100.05	100.06	98.20	100.01	100.06	100.04	100.01	100.03

- Concentration below detection limit

4.2.2 Sphalerite

Sphalerite (ZnS) is a main mineral of the studied samples. It is a common mineral found at the second most inferior to pyrite. The sphalerite displays irregular and filamentous texture in size of 0.05 to 0.2 mm. The grey sphalerite forms as almost pure sphalerite (ZnS) with Fe content ranging from 1.47-2.53 % (3-4 mol% FeS) without gold composition. In general,

EPMA analyses of sphalerites are composed of 53.25-56.25 %Zn and 36.23-38.66 %S (see Table 4.2). The grey-black color of iron-rich sphalerite (ZnFeS) is observed in quartz-adularia-sericite-black sulfide vein. It contains Fe content reaching to 26.06 % (46 mol% FeS), up to 0.44 %Au and up to 1.24 %Ag.

Table 4.2 Representative EPMA analyses of sphalerite.

Mineral	Sphalerite				Fe-rich Sphalerite
Sample point	A17_Sp1	A38_Sp1	A38_Sp2	A38_Sp3	A32_Sp1
Analysis (wt.%)					
Au	-	-	-	-	0.44
Ag	-	-	-	-	1.24
As	-	0.04	-	0.01	0.06
Mo	0.53	0.48	0.52	0.51	0.64
Zn	56.25	55.08	53.25	53.99	20.00
Cu	0.68	0.29	0.84	0.78	0.07
Te	0.10	-	0.07	-	-
Fe	2.53	1.52	1.47	1.66	26.06
S	36.23	38.39	38.66	38.50	50.09
Na	2.38	2.47	2.47	2.47	0.83
Al	0.08	-	-	0.01	0.44
Tl	0.21	0.05	-	0.31	-
Mn	0.09	0.08	0.09	0.07	-
K	-	0.07	0.05	0.06	-
Total	99.07	98.41	97.36	98.30	99.86

- Concentration below detection limit

4.2.3 K-feldspar (Adularia)

The high-grade vein samples also contain potassium feldspar. It usually occurs as rhombic shape with an average size of about 20 μm in pyrite (see Figure 4.1D). This assemblage is associated with quartz-carbonate-sulfide banded vein undertaken silicification.

Only two EPMA analyses (A02_Kfs1 and Kfs2) of alkali feldspar are availably composed of 67.75-67.25 %SiO_2, 8.69-16.74 %Al_2O_3, 0.13-1.69 %FeO, up to 0.40 %MnO, up to 0.77 %MgO, 0.12-0.84 %CaO, 13.19-13.26 %K_2O and 0.15-0.16 %Na_2O. These analyses are recalculated, based on 8 oxygens as shown in Table 4.3. However, both analyses are poor quality due to highly altered grains but they are qualitatively comparable to composition of K-rich feldspar.

Table 4.3 The EPMA analyses of K-feldspar.

Mineral	Alkali feldspar	
Oxides(wt.%)	A02_Kfs1	A02_Kfs2
SiO_2	67.25	67.75
Al_2O_3	16.74	8.69
FeO	0.13	1.69
MnO	0.04	0.00
MgO	0.00	0.77
CaO	0.12	0.84
Na_2O	0.15	0.16
K_2O	13.26	13.19
Total	97.69	93.08
Formula 8(O)		
Si	3.11	3.33
Al	0.91	0.50
Fe^{2+}	0.00	0.07
Mn	0.00	0.00
Mg	0.00	0.06
Ca	0.01	0.04
Na	0.01	0.02
K	0.78	0.83
Total (S)	4.83	4.84
Atomic %		
An	0.76	4.97
Ab	1.68	1.71
Or	97.56	93.32

4.3 Whole-rock trace analyses

Trace element analyses of forty vein samples were obtained by combination between ICP-MS and ICP-AES techniques. The results are summarized in Table 4.4. The representative trace analyses of Au, Ag, As, Cd, Cr, Cu, Hg, Mo, Pb, Rb, S Sb, Se, Te, and Zn are selected for interpretation. All 40 vein samples are described in individual assemblage groups (I, II, III and IV). Assemblage group I contains microcrystalline quartz and trace sulfide. Assemblage group II contains predominantly

quartz and pyrite with minor sulfide. Assemblage group III contains quartz, sericite and sulfide. Assemblage group IV contains quartz, adularia, chlorite, sulfide which is associated with the highest gold grade. The high gold grade samples (greater than 8 ppm) usually belong to assemblage group IV including sample nos. A01, A02, A09-A13, A17, A24, A32 and A38 (see Table 4.5).

Gold (Au) contents range from 0.1-1.4 ppm with an average of 0.73 ppm in assemblage group I, 0.90-6.2 ppm with an average of 2.66 ppm in assemblage group II, 1.1-7.2 ppm with an average of 5.35 ppm in assemblage group III and 4.1-25 ppm with an average of 13.67 ppm in assemblage group IV.

Silver (Ag) contents range from 1.03-29.6 ppm with an average of 9.63 ppm in assemblage group I, 2.33-100 ppm with an average of 38.80 ppm in assemblage group II, 2.28-100 ppm with an average of 49.85 ppm in assemblage group III and 13.6-100 ppm with an average of 67.02 ppm in assemblage group IV.

Arsenic (As) contents range from 1-40.3 ppm with an average of 16.1 ppm in assemblage group I, 4.5-180.5 ppm with an average of 48.33 ppm in assemblage group II, 1-85.1 ppm with an average of 28.65 ppm in assemblage group III and 11.2-92.2 ppm with an average of 37.48 ppm in assemblage group IV.

Cadmium (Cd) contents range from 0.21-1.57 ppm with an average of 0.77 ppm in assemblage group I, 0.03-19.2 ppm with an average of 3.59 ppm in assemblage group II, 0.29-8.52 ppm with an average of 3.25 ppm in assemblage group III and 0.75-15.85 ppm with an average of 5.12 ppm in assemblage group IV.

Chromium (Cr) contents range from 62-723 ppm with an average of 439 ppm in assemblage group I, 493-799 ppm with an average of 629.2 ppm in assemblage group II, 228-1,250 ppm with an average of 673.92 ppm in assemblage group III and 148-1,220 ppm with an average of 676.77 ppm in assemblage group IV.

Copper (Cu) contents range from 19.2-79.5 ppm with an average of 55.8 ppm in assemblage group I, 9.2-188 ppm with an average of 58.06 ppm in assemblage group II, 15.4-199.5 ppm with an average of 77.24 ppm in assemblage group III and 34.3-510 ppm with an average of 181.39 ppm in assemblage group IV.

Mercury (Hg) contents range from 0.01-0.05 ppm with an average of 0.03 ppm in assemblage group I, 0.02-0.45 ppm with an average of 0.12 ppm in assemblage group II, 0.01-0.47 ppm with an average of 0.12 ppm in assemblage group III and 0.10-0.69 ppm with an average of 0.26 ppm in assemblage group IV.

Molybdenum (Mo) contents range from 0.48-3.42 ppm with an average of 1.73 ppm in assemblage group I, 3.78-19.8 ppm with an average of 8.22 ppm in assemblage

group II, 0.17-12.75 ppm with an average of 5.46 ppm in assemblage group III and 1.53-9.36 ppm with an average of 5.54 ppm in assemblage group IV.

Lead (Pb) contents range from 9.6-78.9 ppm with an average of 42.48 ppm in assemblage group I, 5.9-904 ppm with an average of 139.25 ppm in assemblage group II, 3.4-497 ppm with an average of 128.54 ppm in assemblage group III and 71.3-511 ppm with an average of 293.06 ppm in assemblage group IV.

Rubidium (Rb) contents range from 0.2-1.4 ppm with an average of 0.73 ppm in assemblage group I, 0.1-4.9 ppm with an average of 1.24 ppm in assemblage group II, 0.05-1.3 ppm with an average of 0.57 ppm in assemblage group III and 0.1-2.3 ppm with an average of 0.79 ppm in assemblage group IV.

Sulfate(S) contents range from 0.09-1.1 percent with an average of 0.49 percent in assemblage group I, 0.2-3.15 ppm with an average of 0.80 percent in assemblage group II, 0.04-1.51 percent with an average of 0.51 percent in assemblage group III and 0.22-0.94 percent with an average of 0.55 percent in assemblage group IV.

Selenium (Se) contents range from 0.5-0.9 ppm with an average of 0.63 ppm in assemblage group I, 0.9-4.3 ppm with an average of 2.43 ppm in assemblage group II, 0.7-5.2 ppm with an average of 2.3 ppm in assemblage group III and 1.2-6.2 ppm with an average of 3.16 ppm in assemblage group IV.

Antimony (Sb) contents range from 0.12-0.34 ppm with an average of 0.26 ppm in assemblage group I, 0.24-6.89 ppm with an average of 1.45 ppm in assemblage group II, 0.08-4.73 ppm with an average of 0.89 ppm in assemblage group III and 0.63-1.54 ppm with an average of 1 ppm in assemblage group IV.

Telluride (Te) contents range from 0.02-0.21 ppm with an average of 0.08 ppm in assemblage group I, 0.01-0.17 ppm with an average of 0.07 ppm in assemblage group II, 0.02-0.2 ppm with an average of 0.1 ppm in assemblage group III and 0.03-1.32 ppm with an average of 0.28 ppm in assemblage group IV.

Zinc (Zn) contents range from 49-225 ppm with an average of 120.25 ppm in assemblage group I, 38-1,740 ppm with an average of 297.2 ppm in assemblage group II, 59-1,290 ppm with an average of 311.85 ppm in assemblage group III and 212-1,540 ppm with an average of 691.23 ppm in assemblage group IV.

Table 4.4 Trace element analyses (in ppm except S in %) of the high grade vein samples from the Eastern A pit, determined using ICP-MS and ICP-AES.

Sample	Assemblage	Au	Ag	As	Cd	Cr	Cu	Hg	Mo	Pb	Rb	S%	Se	Sb	Te	Zn
A001	IV	25.00	88.00	15.00	15.90	922.00	349.00	0.69	5.78	341.00	1.30	0.65	2.60	1.44	0.04	1,540.00
A002	IV	25.00	84.00	49.00	4.60	148.00	510.00	0.61	8.61	254.00	0.80	0.59	3.90	0.87	1.32	852.00
A003	I	1.40	30.00	10.00	1.60	634.00	48.00	0.04	0.81	47.30	1.40	0.16	0.60	0.30	0.05	85.00
A004	I	0.40	2.00	13.00	0.20	723.00	19.00	0.01	2.22	9.60	0.40	0.62	0.50	0.27	0.02	49.00
A005	III	5.90	81.00	2.00	0.50	1,250.00	20.00	0.08	5.59	3.40	0.05	0.04	2.70	0.16	0.20	63.00
A006	III	6.60	100.00	19.00	6.80	894.00	137.00	0.47	6.02	236.00	0.10	0.31	5.20	4.73	0.07	664.00
A007	III	4.80	95.00	12.00	1.20	646.00	49.00	0.11	4.12	94.70	0.50	0.17	2.80	0.66	0.02	224.00
A008	I	1.00	5.00	1.00	0.80	62.00	80.00	0.05	0.48	78.90	0.20	0.09	0.90	0.12	0.21	225.00
A009	IV	9.10	100.00	11.00	3.00	366.00	62.00	0.19	1.53	177.00	0.50	0.32	3.10	0.81	0.04	380.00
A010	IV	9.60	14.00	22.00	2.50	188.00	70.00	0.09	7.85	208.00	0.40	0.36	1.20	0.89	0.05	400.00
A011	IV	25.00	100.00	53.00	6.70	1,130.00	160.00	0.31	9.36	511.00	0.80	0.54	6.20	1.30	0.39	1,080.00
A012	IV	14.00	100.00	36.00	3.90	1,080.00	110.00	0.26	7.69	331.00	0.90	0.46	5.90	0.87	0.19	802.00
A013	IV	14.20	56.00	43.00	3.40	1,220.00	144.00	0.17	7.64	294.00	0.10	0.61	3.90	0.63	0.09	501.00
A014	II	2.70	100.00	5.00	9.70	799.00	76.00	0.12	3.78	180.50	0.50	0.13	0.90	0.50	0.01	374.00
A015	III	5.20	100.00	24.00	5.90	793.00	96.00	0.17	7.53	207.00	0.80	0.35	2.70	0.99	0.17	416.00
A016	IV	6.00	80.00	55.00	3.10	865.00	123.00	0.21	6.57	207.00	1.60	0.63	2.40	1.25	0.06	418.00
A017	IV	16.70	65.00	92.00	6.30	652.00	162.00	0.31	4.51	457.00	0.20	0.94	3.10	1.54	0.05	655.00
A018	IV	4.10	100.00	21.00	3.10	551.00	57.00	0.10	2.24	145.50	0.30	0.22	1.80	0.82	0.03	302.00
A019	III	7.20	10.00	13.00	8.50	935.00	90.00	0.05	6.99	497.00	0.80	0.32	1.70	0.28	0.06	1,290.00
A020	III	5.80	25.00	37.00	1.10	831.00	37.00	0.09	5.63	79.60	0.30	0.37	1.40	0.39	0.13	163.00
A021	II	3.30	32.00	24.00	0.70	625.00	30.00	0.06	5.88	23.40	1.50	0.23	1.70	0.68	0.03	101.00
A022	III	7.00	63.00	4.00	0.30	546.00	15.00	0.15	3.81	27.90	1.30	0.09	4.10	0.81	0.02	59.00
A023	III	3.70	98.00	33.00	7.50	741.00	73.00	0.11	2.93	71.20	1.30	1.15	1.80	0.61	0.12	233.00
A024	IV	8.80	28.00	12.00	0.80	494.00	34.00	0.11	2.78	71.30	1.00	0.23	1.90	1.02	0.49	212.00
A026	III	1.10	2.00	1.00	1.20	290.00	77.00	0.01	3.43	14.70	0.10	0.53	0.70	0.09	0.08	124.00
A027	III	7.20	48.00	81.00	5.80	518.00	115.00	0.19	12.75	227.00	0.80	1.21	3.60	1.77	0.06	420.00
A028	II	4.00	45.00	67.00	0.50	522.00	30.00	0.06	4.52	29.00	2.40	0.64	4.20	2.13	0.06	76.00
A029	III	4.30	9.00	5.00	0.60	523.00	45.00	0.03	0.17	48.10	0.40	0.12	0.90	0.08	0.14	108.00
A030	II	0.80	3.00	31.00	0.00	602.00	9.00	0.02	9.40	5.90	0.60	0.67	0.90	0.43	0.01	65.00
A031	II	2.40	17.00	54.00	0.20	674.00	25.00	0.04	6.42	13.70	0.50	0.65	1.80	0.86	0.03	44.00
A032	IV	11.40	26.00	46.00	5.60	533.00	362.00	0.15	3.48	361.00	2.30	0.87	2.70	0.83	0.80	1,020.00
A033	II	3.30	84.00	11.00	1.90	695.00	44.00	0.08	5.46	64.90	0.60	0.20	3.80	0.24	0.03	191.00
A034	II	0.90	13.00	181.00	0.30	756.00	64.00	0.45	19.80	21.80	4.90	3.15	3.60	6.89	0.07	38.00
A036	II	6.20	87.00	68.00	2.10	584.00	33.00	0.26	3.04	56.50	0.90	0.79	1.90	1.39	0.08	151.00
A037	II	0.50	2.00	18.00	1.30	542.00	82.00	0.02	19.75	92.80	0.10	0.34	1.20	0.97	0.17	192.00
A038	IV	8.80	32.00	33.00	7.90	649.00	215.00	0.21	3.95	452.00	0.10	0.72	2.40	0.82	0.15	824.00
A039	II	2.50	4.00	25.00	19.20	493.00	188.00	0.10	4.17	904.00	0.40	1.22	4.30	0.39	0.13	1,740.00
A040	III	6.60	7.00	85.00	2.50	228.00	200.00	0.03	6.64	144.00	0.80	1.51	1.40	0.43	0.07	220.00
A041	III	4.20	11.00	58.00	0.50	566.00	51.00	0.07	5.32	20.40	0.20	0.43	1.00	0.63	0.11	70.00
A042	I	0.10	1.00	40.00	0.50	337.00	77.00	0.02	3.42	34.10	0.90	1.10	0.50	0.34	0.02	122.00

Table 4.5 Geochemical characteristics of top 11 high gold grade samples (higher than 8.0 ppm Au) in the Eastern A pit presented as ranges of trace elements and the remarks (/) for the high concentrations of each element.

Sample ID	Trace element (ppm)															
	Au	Ag	As	Cd	Cr	Cu	Hg	Mo	Pb	Rb	S%	Se	Sb	Te	Tl	Zn
A024	8.8													/		
A038	8.8			/		/										/
A009	9.1	/														
A010	9.6							/								
A032	11.4		/	/		/			/		/			/		/
A012	14.0	/		/	/			/	/			/				/
A013	14.2		/	/	/			/	/			/				
A017	16.7		/	/						/	/		/		/	
A011	25.0	/	/	/	/			/	/			/	/	/	/	/
A001	25.0	/		/		/	/		/				/			/
A002	73.0	/	/	/		/	/	/	/	/		/		/		/
Concentration range		13.6-100	11.2-92.2	0.75-15.85	148-1220	34.3-510	0.09-0.69	1.53-9.36	71.3-511	0.10-2.40	0.23-0.94	1.2-6.2	0.63-1.54	0.04-1.32	0.02-0.69	212-1540
Mean		62.88	37.39	5.49	671.09	198.01	0.28	5.74	314.30	0.79	0.57	3.35	1.00	0.33	0.25	751.45
Median		64.90	35.60	4.55	649.00	160.00	0.21	5.78	331.00	0.80	0.59	3.10	0.87	0.15	0.20	802.00

Probability plots using ioGAS Geochemical Analysis software were carried out for these trace analyses. The ioGAS is a famous tool for exploratory and geochemical analysis. It has been created by REFLEX's geochemistry team (reflexnow.com/iogas). Trace element dataset underconsideration must firstly be imported into ioGAS. For this study, Ag, As, Cd, Cu, Hg, Mo, Pb, Rb, Mo, Pb, Sb, Se, Te, Tl, Zn and Au were selected for comparison. Subsequently, each element was plotted for probability. Individual trace elements were plotted on y-axis versus Z score normal distribution on x-axis for statistical correlation data. The probability diagram can be used for more details in data classification and anomaly separation as suggested by Moradpouri and Ghavami-Riabi (2014). The probability plots are particularly useful for quickly and simply initial assessment of single data set (McQueen, 2006). That would be very helpful for elemental grouping prior to consideration of associations and identification of anomalies related to the gold mineralization.

Ag contents in high grade veins fall within in a range of 14-100 ppm. It appears to be inconsistent correlation with Au. Arsenic (As) is quite low in high grade zone then it cannot be correlated. Cd shows positive correlation with Au. The Cd contents reach up to 15.85 ppm in the middle part of ore shoot with the high Au assay of 25 ppm. Figure 4.2 shows the probability plots of Au versus Ag, As and Cd.

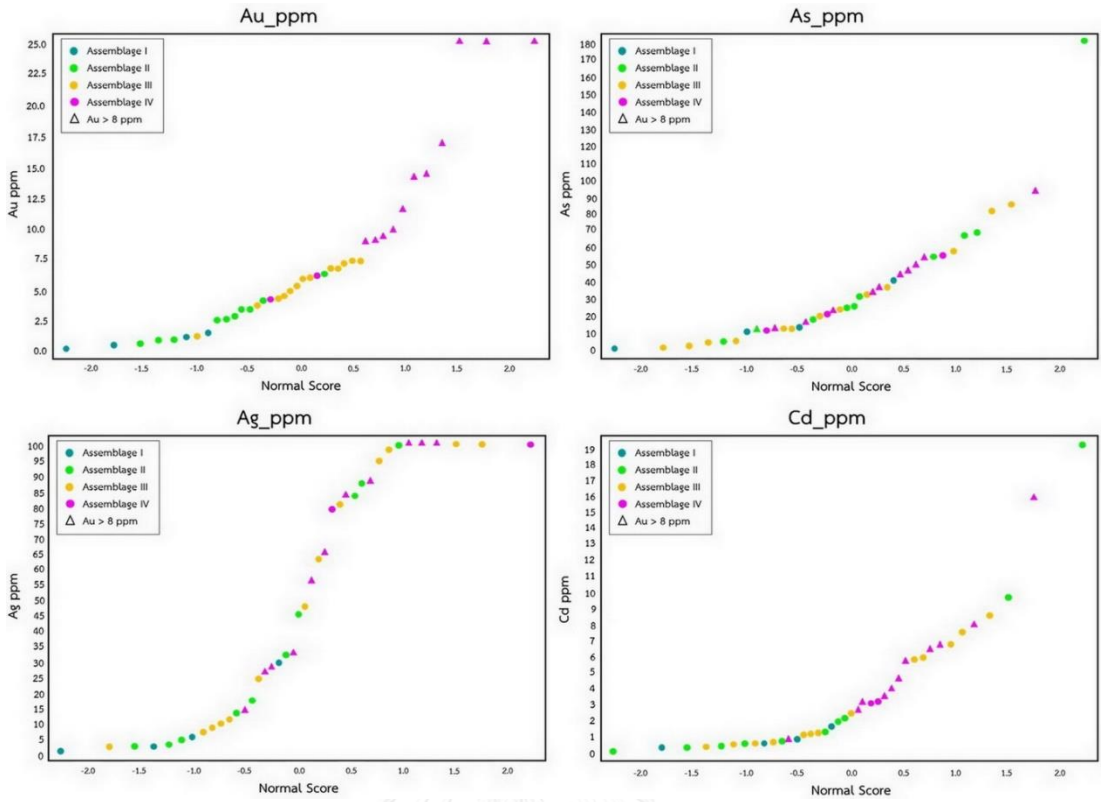

Figure 4.2 Probability plots of Au, Ag, As and Cd among different assemblage groups. Assemblage group IV (pink plots) is associated with the highest gold grade.

Copper (Cu) contents in the high-grade veins are yield a range of 34-510 ppm. The Cu contents reach up to 510 ppm in the highest gold grade. Most of the high gold values yield positive correlation to Cu. Molybdenum (Mo) has anomaly greater than 5.3 ppm (Normal Score or mean=0) and ranges between 7-9 ppm which their probability plots are consistent with the high-gold grade. Therefore, Mo appears to be the key pathfinder of gold mineralization. Anomalous lead (Pb) is compatible to the high gold content (greater than 8 ppm). Pb contents range between 254-511 ppm which are quite good positive correlation to Au. Figure 4.3 shows the probability plots of Au versus Cu, Mo and Pb.

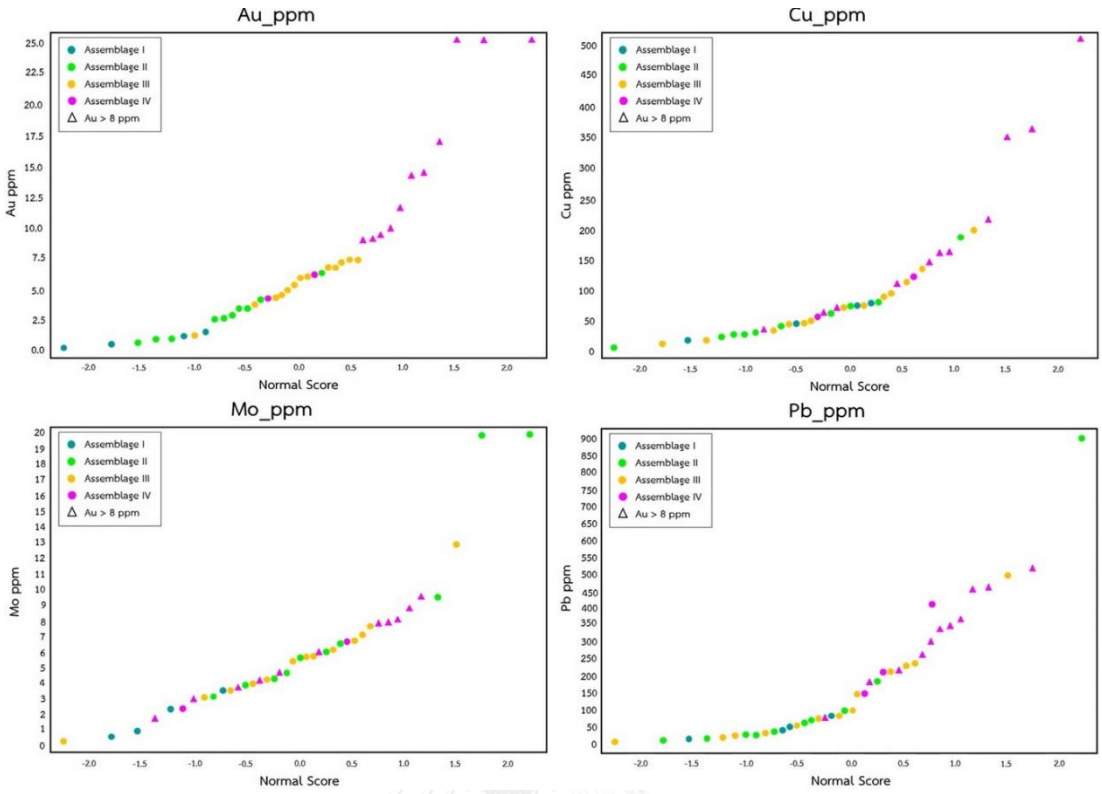

Figure 4.3 Probability plots of Au, Cu, Mo and Pb among different assemblage groups. Assemblage group IV (pink plots) is associated with the highest gold grade.

Most antimony (Sb) analyses are generally low contents with an average of 1 ppm. Sb seems to have no correlation to Au; although, anomalous Sb may have occurred within the altered wall rock and stock work vein as a mineralization halo (Braund, 2006). Selenium (Se) contents range between 3-6 ppm in the high gold grade (greater than 8 ppm). Selenium appears to have positive correlation to Au. Telluride (Te) ranges between 0.39-1.32 ppm and appears to have correlation to Au. Samples with high Au contents trend to have high zinc (Zn) which Zn contents range between 380-1,520 ppm when Au is greater than 8 ppm. Rubidium (Rb) appears to have no correlation. It presents discontinuously flat-step pattern. Figure 4.4 shows probability plots of Au, Sb, Se, Te, Zn and Rb. Correlation plots of Au against As, Ag, Cd, Zn, Cu, Mo, Pb Rb, Sb, Te, Tl and Se are present in Figures 4.5 and 4.6.

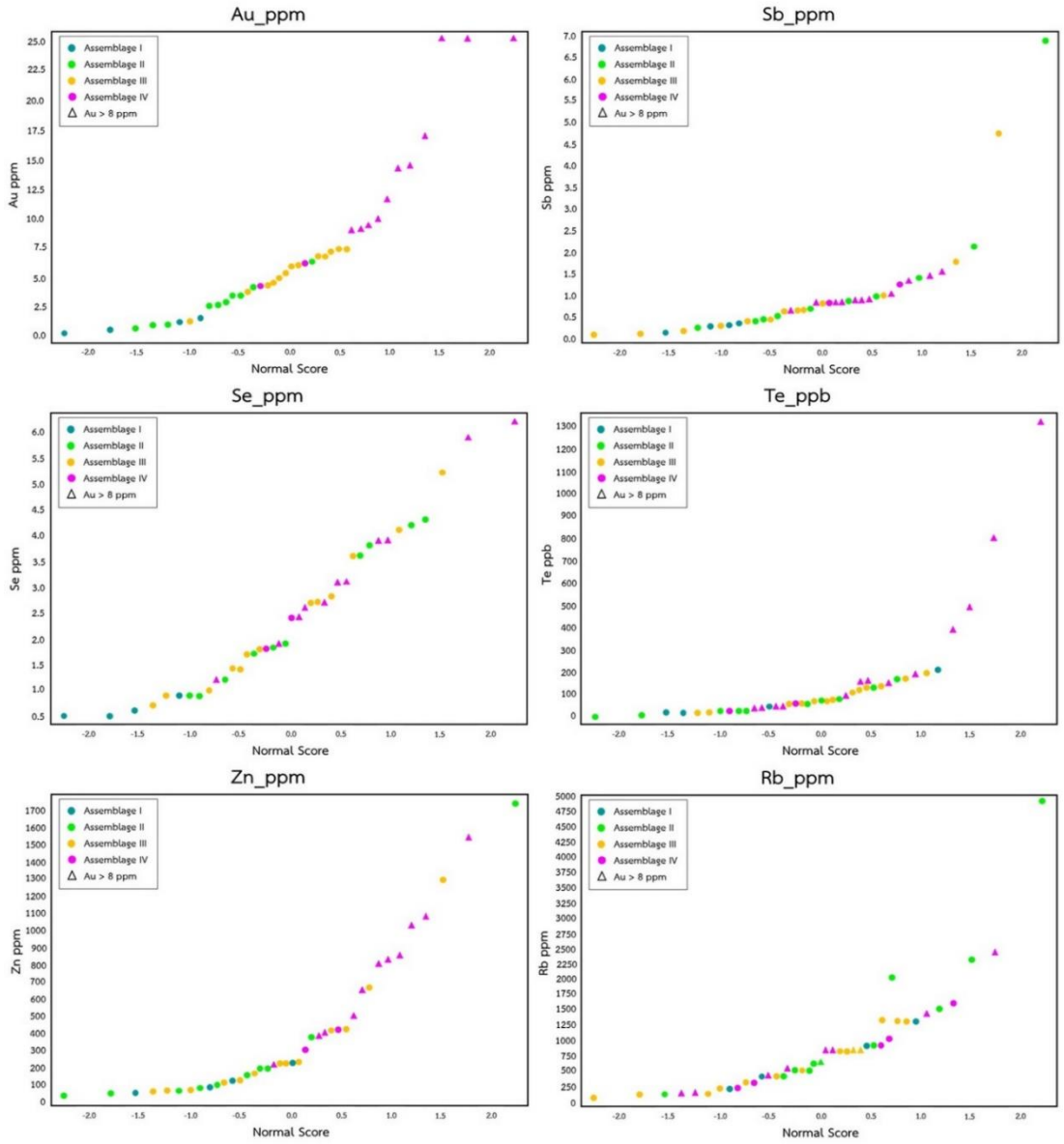

Figure 4.4 Probability plots of Au, Sb, Se, Te, Zn and Rb among different assemblage groups. Assemblage group IV (pink plots) is associated with the highest gold grade.

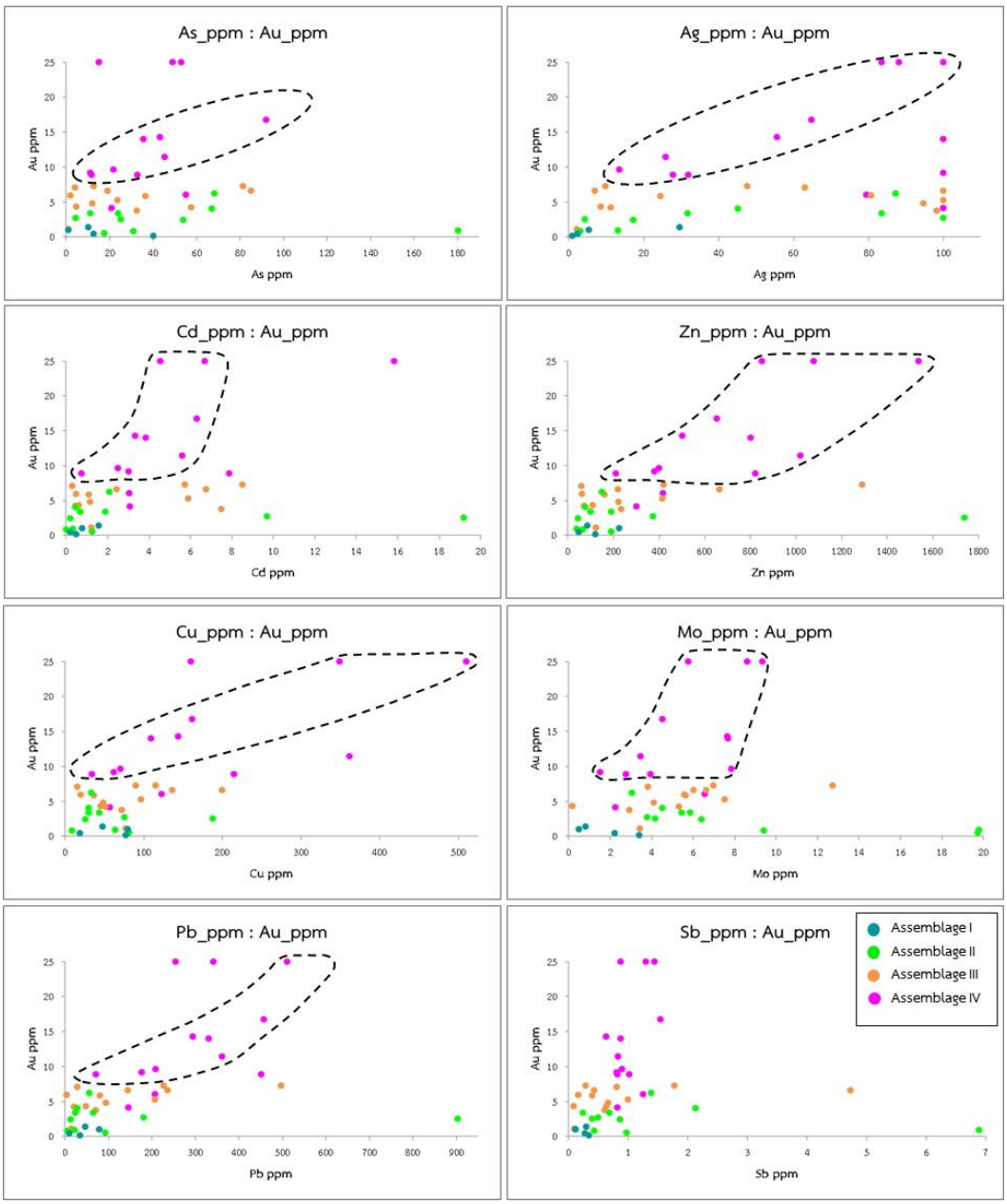

Figure 4.5 Correlation plots of Au versus As, Ag, Cd, Zn, Cu, Mo, Pb and Sb. The dashed lines show positive correlation data. Assemblage group IV (pink plot) is associated with the highest gold grade.

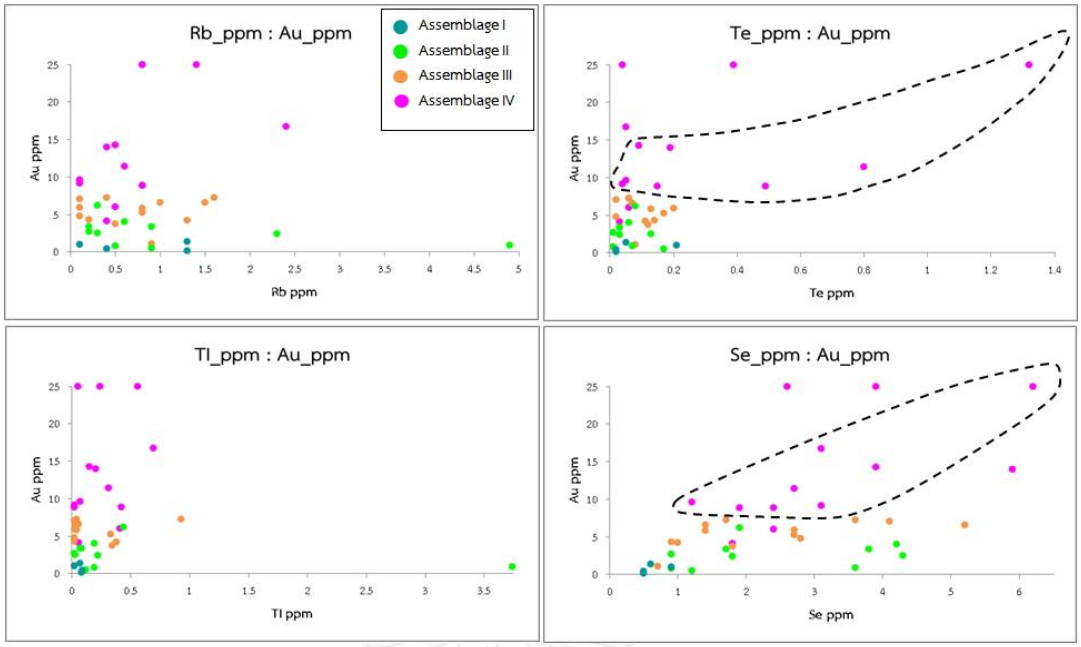

Figure 4.6 Correlation plots of Au versus Rb, Te, Tl and Se. The dashed lines show positive correlation data. Assemblage group IV (pink plot) is associated with the highest gold grade.

4.4 Statistical correlation coefficient

Statistical correlation coefficients were analyzed on the basis of whole-rock geochemical analyses of 40 core samples from the Eastern of A pit (Table 4.4). Subsequently, the correlation matrix can be determined. Correlation coefficients were interpreted using Pearson's correlation coefficient which is evaluation of relationship between two variables (as suggested by Ngeno and Simatwa (2015) in Table 4.6). The correlation coefficients may be positive (+) or negative (–) with values of 0.01-0.30 for weak relationship, 0.31-0.70 for moderate relationship and 0.71-0.99 for strong relationship. For perfect relationship, it can be +1 or -1. For value of 0.00, it indicates no relationship at all.

The correlation coefficient were determined for all 40 vein samples (see Tables 4.7). The statistical correlations of gold and other elements were also determined individually for each quartz texture type (see Tables 4.8-4.4.12).

Table 4.6 Pearson's correlation coefficients and their of the relationship (Ngeno and Simatwa, 2015).

Strength of the relationship	Positive (+)	Negative (-)
Weak/low/small	0.01-0.30	0.01-0.30
Moderate/medium	0.31-0.70	0.31-0.70
Strong/high	0.71-0.99	0.71-0.99
Perfect relationship	1.00	1.00
No relationship	0.00	0.00

Table 4.7 Correlation coefficients of selected trace elements of 40 high-grade vein samples from the Eastern A pit.

Element	*Ag*	*As*	*Au*	*Cd*	*Cr*	*Cu*	*Mo*	*Pb*	*S*	*Sb*	*Te*	*Zn*
Ag	1											
As	-0.09912	1										
Au	0.45404	0.10338	1									
Cd	0.25834	-0.07344	0.40205	1								
Cr	0.42991	0.01579	0.23612	0.20249	1							
Cu	0.15544	0.14861	**0.70730**	0.53769	-0.11513	1						
Mo	-0.11014	0.54609	0.07448	-0.03138	0.18509	0.10213	1					
Pb	0.12265	0.04069	0.49274	**0.83407**	0.18782	0.54573	0.04114	1				
S	-0.23944	**0.86098**	-0.04095	0.12771	-0.06428	0.19436	0.49743	0.12557	1			
Sb	0.13029	0.67233	0.04700	0.02266	0.15987	0.05637	0.53577	-0.00784	0.62080	1		
Te	0.08409	0.04371	0.52639	0.06982	-0.20334	**0.71357**	0.06455	0.19975	-0.01189	-0.03889	1	
Zn	0.18138	-0.05158	0.61349	**0.88013**	0.20952	0.68458	0.03257	**0.92170**	0.07237	0.00822	0.30163	1

Total 40 samples were used to generate elemental set for correlation matrix. Table 4.7 shows twelve elements having correlation with Au with different values. The correlation between Au and Cu is strong. Moderate positive correlation with Au is observed for Ag, Cd, Pb, Te and Zn. Moreover, weak positive correlation with Au is observed for As, Cr, Mo and Sb. Only S shows slightly negative correlation with Au.

Table 4.8 Correlation coefficients of banded quartz texture samples (10 samples).

Element	*Ag*	*As*	*Au*	*Cd*	*Cr*	*Cu*	*Mo*	*Pb*	*S*	*Sb*	*Te*	*Zn*
Ag	1											
As	0.15260	1										
Au	0.39174	0.32526	1									
Cd	0.43185	-0.00690	**0.76282**	1								
Cr	0.39455	0.09249	0.33808	0.52242	1							
Cu	0.34266	0.28224	**0.84330**	0.63001	-0.03876	1						
Mo	0.19981	0.61780	**0.73932**	0.39546	0.13547	0.58613	1					
Pb	0.50275	0.28534	**0.86422**	0.70576	0.53844	0.53454	**0.72605**	1				
S	0.25582	**0.73977**	0.69133	0.58987	0.20825	0.62825	0.68049	0.53198	1			
Sb	0.15980	**0.71671**	0.23605	0.28726	0.29011	0.10003	0.40564	0.19483	**0.79134**	1		
Te	0.06631	0.38033	0.56209	0.00637	-0.31063	**0.71895**	0.46737	0.23724	0.31174	-0.05987	1	
Zn	0.47012	0.15287	**0.92465**	**0.94611**	0.49902	**0.75122**	0.61014	**0.86023**	0.65599	0.26655	0.25101	1

The correlation matrix of banded quartz texture with gold contents between 3.8-73 g/t is presented in Table 4.8. Most elements have a strong positive correlation with Au. The Au has strong positive correlation with Cd, Cu, Mo, Pb and very strong

(0.92) positive with Zn, moderate positive with Ag, As, S and Te. However, weak positive correlation is also observed with Sb.

Table 4.9 Correlation coefficients of plumose quartz texture samples (15 samples).

Element	*Ag*	*As*	*Au*	*Cd*	*Cr*	*Cu*	*Mo*	*Pb*	*S*	*Sb*	*Te*	*Zn*
Ag	1											
As	0.09157	1										
Au	0.33837	0.42425	1									
Cd	0.07012	0.14841	0.48638	1								
Cr	0.33700	-0.03689	0.51187	0.22341	1							
Cu	-0.11294	0.19774	0.55983	0.62332	-0.00408	1						
Mo	0.14706	0.26418	0.09112	0.25476	0.36282	-0.09581	1					
Pb	0.04572	0.18842	**0.73087**	**0.91944**	0.40962	0.68171	0.16018	1				
S	-0.09015	**0.80106**	0.35590	0.37610	-0.23561	0.50762	0.27499	0.33604	1			
Sb	0.41280	**0.81002**	0.41589	0.27628	-0.12221	0.17315	0.33485	0.21164	**0.72147**	1		
Te	-0.11049	0.04053	0.27753	0.25913	-0.09248	**0.82044**	-0.22347	0.30048	0.25621	0.00452	1	
Zn	-0.04825	0.00392	0.58215	**0.87296**	0.37700	**0.69301**	0.12047	**0.93383**	0.21424	0.02831	0.46136	1

The correlation matrix of plumose quartz texture with gold contents between 3.0-14.5 g/t is presented in Table 4.9. The correlation matrix shows that Au has strong positive correlation with Pb. Moderate positive correlation with Au is observed in Ag, As, Cd, Cr, Cu, S, Sb and Zn. Mo and Te have a weak positive correlation with Au.

Table 4.10 Correlation coefficients of comb quartz texture samples (4 samples).

Element	*Ag*	*As*	*Au*	*Cd*	*Cr*	*Cu*	*Mo*	*Pb*	*S*	*Sb*	*Te*	*Zn*
Ag	1											
As	**-0.81694**	1										
Au	-0.37470	0.42685	1									
Cd	0.38180	-0.02430	0.66417	1								
Cr	**0.85052**	**-0.92598**	**-0.71017**	-0.14014	1							
Cu	-0.60855	**0.85441**	**0.80562**	0.46248	**-0.93475**	1						
Mo	-0.59391	**0.94910**	0.37734	0.16267	**-0.82241**	**0.85225**	1					
Pb	0.14824	0.37838	0.55700	**0.86003**	-0.38364	0.68307	0.60142	1				
S	**-0.91056**	**0.96602**	0.55731	-0.03884	**-0.97992**	**0.86712**	**0.84838**	0.27024	1			
Sb	0.57567	-0.29253	0.53288	**0.96285**	0.10817	0.21620	-0.10539	**0.71387**	-0.29186	1		
Te	0.20571	-0.68855	-0.60777	-0.66597	0.66554	**-0.87190**	**-0.84244**	**-0.93179**	-0.59171	-0.44631	1	
Zn	0.47156	-0.01664	0.50588	**0.97156**	-0.06200	0.41026	0.22488	**0.91351**	-0.09207	**0.92861**	**-0.70970**	1

correlation with Au is observed for Cu. On the other hand, Au shows moderate negative correlation with Ag and Te, and strong negative correlation with Cr.

Table 4.11 Correlation coefficients of moss/ghost-sphere quartz texture samples (4 samples).

Element	*Ag*	*As*	*Au*	*Cd*	*Cr*	*Cu*	*Mo*	*Pb*	*S*	*Sb*	*Te*	*Zn*
Ag	1											
As	-0.37385	1										
Au	0.61252	-0.62318	1									
Cd	0.13745	-0.53096	**0.86701**	1								
Cr	0.70415	0.33070	-0.04528	-0.49346	1							
Cu	-0.08537	-0.18664	0.69306	**0.92798**	-0.50794	1						
Mo	-0.41521	**0.96408**	**-0.79756**	**-0.72678**	0.34553	-0.42075	1					
Pb	-0.18823	-0.38079	0.66008	**0.94646**	-0.70574	**0.95666**	-0.56700	1				
S	-0.50960	**0.96708**	-0.53593	-0.33556	0.11656	0.03804	**0.89046**	-0.14229	1			
Sb	-0.22986	**0.98834**	-0.53914	-0.51545	0.45423	-0.18762	**0.93805**	-0.41060	**0.93628**	1		
Te	-0.51026	0.21595	0.24881	0.64204	-0.60557	**0.86932**	0.01295	**0.81624**	0.45310	0.16327	1	
Zn	-0.18693	-0.40473	0.66187	**0.94735**	**-0.71653**	**0.94835**	-0.58580	**0.99957**	-0.16702	-0.43583	**0.80232**	1

The correlation matrix of moss/ghost-sphere quartz texture with gold contents between 0.8-2.7 g/t is presented in Table 4.11. Various ranges of the results shows in both positive and negative correlations. Au has high positive correlation with Cd, moderate correlation with Ag, Cu, Pb and Zn, and weak correlation with Te. High negative correlation with Au is also observed in Mo whereas moderate negative correlation is present in As, S and Sb with weak negative correlation of Cr.

Table 4.12 Correlation coefficients of saccharoidal quartz texture samples (7 samples).

Element	*Ag*	*As*	*Au*	*Cd*	*Cr*	*Cu*	*Mo*	*Pb*	*S*	*Sb*	*Te*	*Zn*
Ag	1											
As	0.35254	1										
Au	**0.86610**	0.23256	1									
Cd	**0.94145**	0.36355	0.68452	1								
Cr	0.49879	0.28120	0.42738	0.39617	1							
Cu	0.05366	0.17745	-0.16085	0.29982	-0.57040	1						
Mo	-0.21888	0.10374	-0.16776	-0.08586	0.12955	0.30750	1					
Pb	0.17276	-0.19774	0.03212	0.38577	-0.35465	**0.83398**	0.46778	1				
S	0.41678	**0.83334**	0.09752	0.53403	0.26960	0.21499	-0.10994	-0.13929	1			
Sb	0.22561	0.35501	0.30525	0.25860	0.43529	0.16543	**0.86848**	0.35306	0.06847	1		
Te	0.04270	-0.45116	-0.00464	0.23464	-0.51324	0.69407	0.31606	**0.91099**	-0.30275	0.14091	1	
Zn	0.38935	0.01776	0.27202	0.57308	-0.40305	**0.82403**	0.22756	**0.87628**	0.12486	0.24104	**0.86193**	1

The correlation matrix of saccharoidal quartz texture with gold contents between 0.1-3.7 g/t is presented in Table 4.12. Correlation between Au and Ag is strong positive correlation. Moderate positive correlation with Au is observed in Cd, Cr and Sb. Weak positive correlation with Au is observed in As, Pb, S and Zn. On the other hand, Cu, Mo and Te have weak negative correlation with Au.

As a result, most of the datasets show that Au has positive correlation with Ag. However, comb texture samples show Au has negative correlation with Ag. Au has fairly positive correlation with Te in overall 40 vein samples and banded texture samples. Au shows weak positive correlation with Te in plumose and moss textures. For the comb and saccharoidal textures, they indicate negative correlation between Au and Te. Au has strong positive correlation with Mo in banded texture, moderate positive in comb texture but negative correlation in moss and saccharoidal textures. The fairly positive correlation between Au and As was also observed in band, plumose and comb textures.

CHAPTER 5
Discussion and Conclusions

5.1 Quartz texture and sulfide characteristics

The main goal of this study was to examine mineralization characteristics between mineralization texture and ore composition of the high-grade gold mineralization. Five types of quartz texture within mineralization vein observed in the Eastern A pit are defined from this study. Based on detailed petrographic study, the colloform banded quartz texture found in the higher gold grade (4-73 g/t) is usually associated with the sulfide assemblage IV (chlorite-adularia-pyrite-sphalerite-chalcopyrite-tennantite-electrum). This finding is similar to the main gold-silver mineralization stages of the Chatree deposit (reported by Salam, 2011), including Stage 4A (quartz - chlorite ± carbonate ± adularia - sulfide - electrum), Stage 4B (quartz ± carbonate - adularia -sulfide - electrum) and Stage 4C (carbonate ± quartz – adularia – sulfide - electrum - argentite - tetrahedrite) in which sulfide and electrum appear to be enriched in the quartz-chlorite rich band and subordinated in the quartz ± carbonate band. Moreover, the sulfide-rich chlorite - quartz band tends to have a high gold grade, based on petrographic investigation of Salam (2011).

The most common feathery-plumose quartz texture has a gold range of 3-14.5 g/t and mainly associates with sulfide assemblage groups III and IV. Both plumose and banded quartz textures are the most common feature observable in 25 samples from the total 40 samples of the high-grade vein of the Eastern A pit. Sangsiri (2010) suggested similarly that colloform banded texture is mostly associated with the high gold grade in the A pit of Chatree deposit. Kilias et al. (2013) have also suggested the colloform band and plumose texture are very closely associated with high concentration of gold found in Viper epithermal Au-Ag-Cu ore body, Greece. Epithermal silver-gold deposits at Guanajuato, Mexico (studied by Moncada et al. (2012)) also presents the plumose and banded textures related to the higher gold and silver grades. Vearncombe (1993) also revealed that the crustiform-colloform banding and plumose or acicular crystals are characteristics of open-space filling for gold deposition at Archaean lode-gold deposits of the Yilgarn Craton, Australia. These appear to be conclusive remark that the high gold grade should be associated with banded and plumose quartz textures which may be the most suitable for epithermal gold deposit.

The high-grade gold samples in Eastern A pit occur within the fine-grained quartz band with a large amount of sulphide. Rapid cooling and possible fluid mixing may pay the important role as reported by Ovenden et al. (2005). Mixing between hydrothermal fluid and bicarbonate leads to gold precipitation. Corbett and Leach (2008) introduced the term of high-grade (bonanza) gold in the epithermal vein deposits by mixing between ore fluid with low pH water. Corbett (2002) reported the bonanza gold often occurs in epithermal quartz-sulfide bands containing electrum-rich bands.

The sulfide assemblage III (sericite-pyrite-sphalerite-chalcopyrite-tennantite±electrum) also shows an association of comb and zonal textures related to the moderate gold grade within the range of 5.9-6.6 g/t Au. This is compatible to the study of quartz texture observed at the Q and A pits in Chatree deposit ((Tangwattananukul, 2012). The comb and flamboyant (plumose) textures usually associate with large amount of sulfide and electrum. However, the comb and zonal textures were identified as non- boiling textures with slow crystal growth related to the lower gold grade of the epithermal Ag–Au deposits at Guanajuato, Mexico (Moncada et al., 2012). However, the Pajingo epithermal vein systems in North Queensland Australia, studied by Pinder (2006), usually yield gold grade commonly below 1 g/t in the comb texture.

The moss and ghost-sphere textures have lower gold grade within a range of 0.8-2.7 g/t and relate to sulfide assemblage II (minor sulphide, i.e., pyrite and sphalerite). It may be developed by spherulitic crystallization within the wall rock. The moss (ghost-sphere) texture usually displays in the early stage vein texture which may have precipitated during or immediately after the banded quartz occurrences (Ovenden et al., 2005). Moncada et al. (2012) also suggested that the moss texture should occur in the less common non-boiling outside of the boiling zone. Therefore, the boiling zone may be good indicator of high-grade zone (Moncada et al., 2012).

Low gold concentration (0.1-1 g/t) of the saccharoidal quartz texture is associated with mineralization assemblage I (microcrystalline quartz with trace amount of pyrite). Microcrystalline quartz is classified as vein Stage 1 of Salam (2011) who reported the effect of rapid cooling on microcrystalline quartz precipitation. Its mineral assemblage can be regarded as a precursor stage of the main gold mineralization stages. Low sulphidation epithermal system at the Bunikasih Area, Pangalengan, West Java (studied by Subandrio and Basuki (2010)) shows the saccharoidal texture with relatively low gold contents (0.3-3.1 g/t). Braund (2006) introduced that the low gold grade is indicative of more quiescent condition. Therefore, saccharoidal texture in the

Eastern A pit may indicate lower gold grade. The saccharoidal texture generally does not have open space texture then it could not generate rapid opening fracture for deposition of high-grade gold.

In summary, the vein samples with low gold content in this study also appear to be recognized in the saccharoidal (assemblage I) and moss/ghost-sphere (assemblage II) textures. Both textures present traces of sulfide (pyrite-sphalerite-galena) referring to a low grade gold deposit. Because the moss and saccharoidal textures have minor fractures without deformation for mineralization. On the other hand, deformation feature is usually associate with boiling fluid as suggested by Moncada et.al. (2012). The most important indicator in the high-grade vein samples is indicated by quantity of sulfide. As mentioned by Salam (2011), sulfide is potential indicator of gold content.

The assemblage IV observed in the Eastern A pit is characterized by quartz, chlorite, feldspar (adularia), pyrite, sphalerite, chalcopyrite, tennantite and electrum in the plumose and colloform banded textures which indicate the main phase of gold deposition and high gold grade. Moreover, EPMA results of mineral assemblage IV can also determine mineral chemistry of sulfides related to gold mineralization. Five major types of mineral chemistry are recognized including (1) electrum inclusions in pyrite, (2) invisible Au-Ag in (Fe-rich) sphalerite, (3) invisible Au-Ag in K-feldspar (adularia), (4) invisible tellurium (Te) in electrum and (5) multiphase inclusions of tennantite and electrum.

Electrum occurs predominantly as inclusions in pyrite. Au: Ag ratio by EPM analyses of individual gold and electrum grains (> 8 g/t Au) in the Eastern A pit reaches up to 35.42 % (0.18 atomic proportion) Au and 34.03 % (0.32 atomic proportion) Ag with average Au: Ag ratio of about 1: 1.7. The Au: Ag is in the ranging from 1:1.4 to 1:1.7 which are higher than the Au: Ag ratio (1:0.6) of electrum grains in H zone of Chatree deposit (Kromkhun, 2005). Because the gold grade vein samples in Eastern A pit (> 8 g/t Au) are higher than H pit with 2-3 g/t Au containing.

Fe-rich sphalerite and tennantite are also observed in the main ore zone of Chatree deposit (Salam, 2011). In this study, electrum presents as invisible phase in sphalerite detected by EPMA spot analyses. The Fe-poor sphalerite has much lower Au content (0-0.07 % Au, 3-4 mole% FeS) than the Fe-rich sphalerite (0.44 % Au, 46 mole% FeS). Fine-grained gold bleb can also be found in late stage of Fe rich sphalerite which may be caused by low temperature and higher salinity ore fluids in sulfur reducing conditions as mentioned by Noku et al. (2012). Under such low temperature

(~ 200 °C) conditions, the ore fluids seem to be acidic (pH < 4) that probably increases gold solubility (in the form of Au $(HS)_2^-$) as suggested by Moss and Scott (2001).

Tennantite observed in this study has very low Sb (0.007 wt. %); however EPMA detected the main composition very close to tennantite formula ($Cu_{12}As_4S_{13}$) (as suggested by Moritz (2006)). Moreover, it is characterized by high As content reaching to 1.29 wt. % and also high Fe content, but their main compositions still fall within tennantite range. The tennantite associated with gold –electrum have also been mentioned by Salam (2011) from Chatree gold deposit and Braund (2006) from Cracow deposit in Queensland. Telluride probably formed as small inclusions (e.g., hessite (Ag_2Te), altaite (PbTe) and krennerite (Au, Ag)Te_2 in tennantite which intergrowths with electrum inclusions (up to 0.23 wt. % Te).

The gangue minerals such as adularia were also found in the main gold mineralization by Salam (2011); moreover adularia occurrence in Chatree deposit was reported previously by Sangsiri (2010). Crystalline quartz bands associated with adularia and disseminated sulfides and sulfide bands have also been reported in A pit. Dong et al. (1995) suggested that the adularia is a low temperature polymorphism of K-feldspar and is an indicator of boiling in the epithermal system. Besides, the adularia also precipitates in most gold-bearing quartz veins in A pit and Q prospect of the Chatree deposit (Tangwattananukul, 2012).

5.2 Trace element pathfinders

Baaku (2013) studied the geochemical data and applied the box plot method to identify pathfinder for gold deposit. Box plot or whisker diagram (Gutiérrez et al., 2012) is a common technique applied to trace element data analysis. The whisker plot can examine the frequency distribution of data sets and for comparison of the frequency distributions of multiple data sets, (McQueen, 2006). It shows the middle (median) value of data lies along with the upper and lower hinges (or limits) as mentioned by Tukey (1977) (See Figure 5.1-5.4). The box plot of each element may show the positive skew with a long tail towards higher values or the negative skew with a tail towards lower values (Moradpouri and Ghavami-Riabi, 2014). Based on whole-rock trace geochemistry, twelve elements (including Te, S, Sb, Mo, Cd, Au, Ag, As, Cu, Pb, Zn and Cr) were considered for comparative box plot in each quartz texture and mineral assemblage group. Detail of both comparative box plot of trace element for quartz texture and box plot of trace element of sulfide assemblage are described below.

5.2.1 Quartz Texture and Whole-Rock Geochemistry

Characteristics of gold mineralization and quartz texture in term of hydrothermal fluid have been described previously for epithermal gold exploration (e.g., (Henley and Hughes, 2000; Moncada et al., 2012; Richards et al., 1998)). They discussed on process of colloform texture generation related to gold precipitation. Henley and Hughes (2000) reported that colloform texture is a primary depositional texture. It may have occurred during the rapid opening of fracture associated with boiling. The boiling should be caused by de-pressuring of hot fluid forced into dilational zones during recurring fault activity. Epithermal banding and multiple brecciations may have also been related to gold-bearing fluids (Richards et al., 1998). Moncada et al. (2012) suggested that mineral textures may be the better indicators of mineralization in the epithermal deposit compared to fluid inclusion. In contrast, this study focused on quartz texture in association with trace element chemistry; consequently, colloform banded texture appear to be the most significant pathfinder of gold mineralization. This result is agree well with suggestion of
Pinder (2006).

Trace element data and associated quartz textures in high-grade vein from the Eastern A pit area demonstrated by box plot diagram (Figures 5.1 and 5.2).

Regarding to various element plots of vein textures samples (Figures 5.1 and 5.2). Te, Ag, Cu, Pb and Zn contents have positive correlation to Au values. Negative correlation with Au is observed for S, Sb, Mo, Cd, As and Cr contents. As the results, Ag, Cu, Te and Au show maximum concentration and tend towards higher contents of Zn, Pb and Cd in the banded quartz texture. The comb quartz has lower concentrations of Cu, Pb, Zn and Te than plumose texture. The comb texture appear to have the highest average Cr content against the lower Au content. S, Sb, Mo, Cd, As, Pb and Zn contents are enriched in moss/ghost-sphere. The saccharoidal texture seem to have the lowest contents of most twelve elements (i.e., Te, S, Sb, Cd, Au, Ag, As, Cu, Pb, Zn, Cr and Mo). Therefore, box plots correlation between quartz textures and trace elements with positive skewed indicate likely that As-Te-Pb-Zn can be considered as a pathfinders for gold deposits.

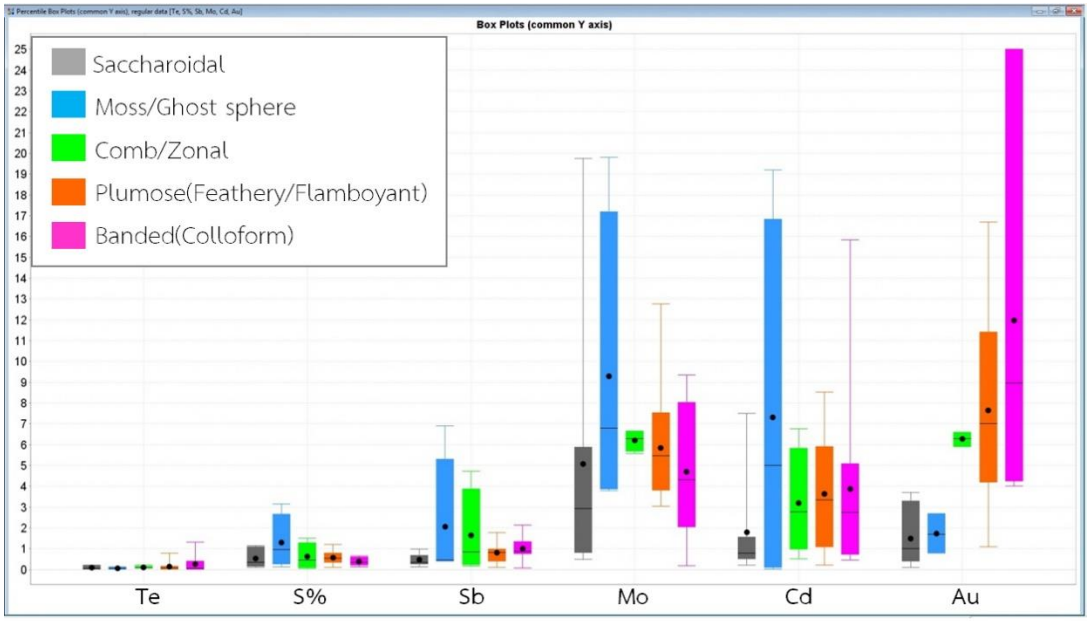

Figure 5.1 Box diagram of trace elements (Au, Te, Sb, Mo and Cd in ppm and S%) in correlation with different quartz textures.

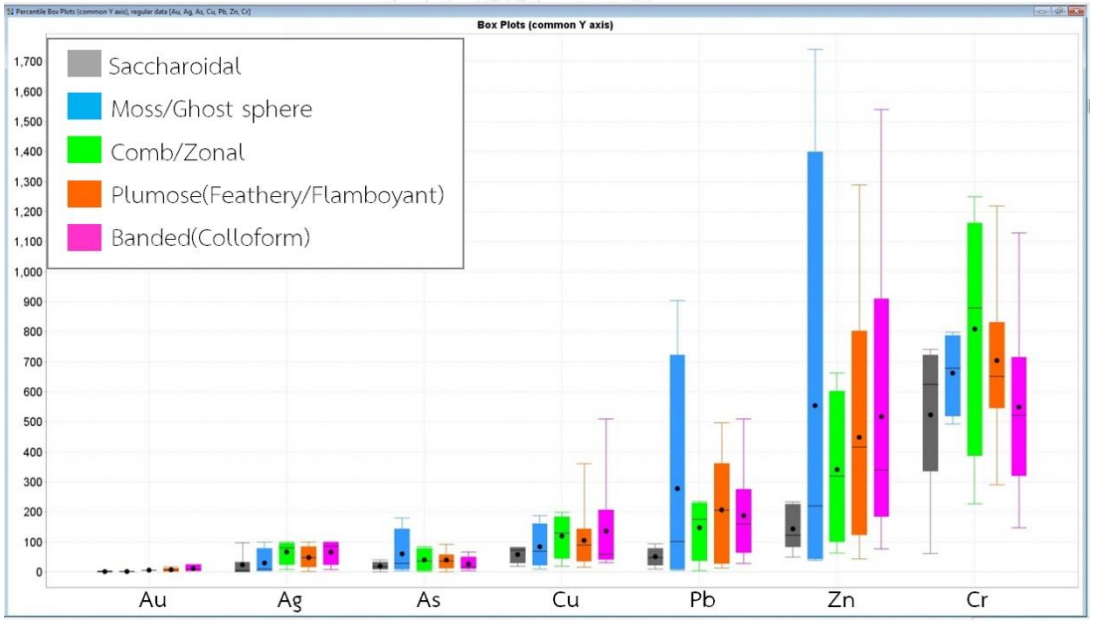

Figure 5.2 Box diagram of trace elements (Au, Ag, As, Cu, Pb, Zn and Cr in ppm) in correlation with different quartz textures.

5.2.2 Quartz-Sulfide Assemblage and Whole-Rock Geochemistry

The quartz-sulfide composition and whole-rock composition are also significant to gold grade and gold bearing vein. Regarding to sulfide assemblage, the high-gold grade samples are composed of quartz, chlorite, feldspar (adularia) and sulfide (pyrite-

sphalerite-chalcopyrite-tennantite-electrum) dominantly in mineralization assemblage IV (>8 ppm of Au content). The gold contents range between 4-8 ppm of mineralization assemblage III which is mainly composed of feldspar-sericite–sulfide. Mineralization assemblage II is characterized by pyrite and minor (common) base metals related to low gold content (1-4 ppm). Mineralization assemblage I yields the lowest range of gold (0.1-1 ppm) and It is characterized by grey quartz, massive carbonate with trace sulfide.

For correlation, the whole-rock trace elements are plotted versus quartz-sulfide assemblages in box diagram (Figures 5.3 and 5.4). Assemblages and trace element chemistry can be an useful tool to indicate high grade gold mineralization as suggested by Pinder (2006) and Braund (2006).

Figures 5.3-5.4 show positive correlation between Au against Te, Ag, Cd, Cu, Pb, Zn and Cr with positive skew. On the other hand, Mo, S, Sb and As are relatively negative correlation to Au. They are present as negative skew with a tail towards low values. The highest gold grade mineral assemblage IV contains also high contents of Te, Ag, Cu, Pb, Zn and Cr whereas the higher contents of Mo, S and As are recognized in mineral assemblage II with dominant Mo-As rich pyrite.

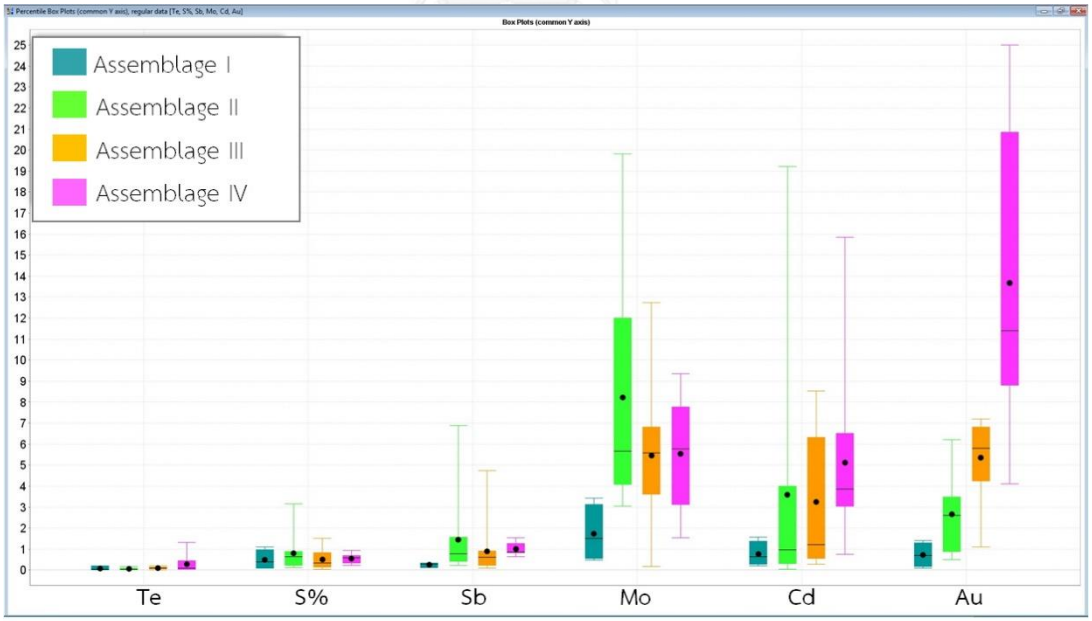

Figure 5.3 Box diagram of trace elements (Au, Te, Sb, Mo and Cd in ppm and S%) in correlation with different sulfide assemblages.

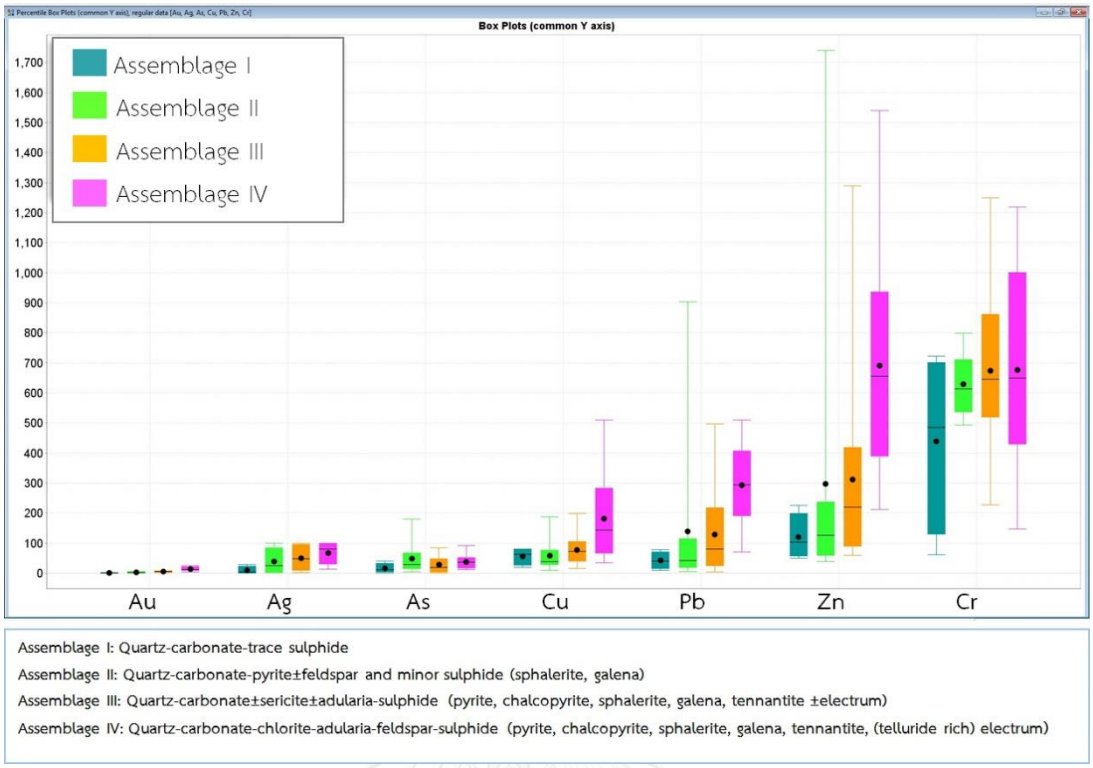

Figure 5.4 Box diagram of trace elements (Au, Ag, As, Cu, Pb, Zn and Cr in ppm) in correlation with different sulfide assemblages.

Whole-rock geochemistry present as box plot in quartz textures from Eastern A pit show clearly that Mo has negative correlation to Au. It shows higher median (line-horizontal bar) and maximum (top of box) of Mo (Figures 5.1 and 5.3) in assemblage group II and moss texture. Statistical correlation reported in Chapter 4 also indicated the high negative correlation between Mo and Au in moss texture. The moss texture is recognized significantly in the assemblage group II which is composed of predominant pyrite. In this regard, the high Mo in moss texture of assemblage II is a result of Mo-rich pyrite ($MoFeS_2$). The similar observation was previously reported by Pinder (2006) who also found the moss texture with high Mo content. In addition, most gold mineralization in Victorian gold deposit have unlikely association between gold and molybdenum (Phillips et al., 1996).

Based on the probability plot and box diagram, arsenic (As) has negative correlation to Au. This is agreeable to the statistical correlation that Au has negative correlation to As in moss and saccharoidal, and moderate positive correlation in band, plumose and comb textures. As the results, high As contents are observed in assemblage group II with dominant pyrite in moss texture without high gold occurrence. Morishita et al. (2008) reported similar result of Hishikari gold deposit in

which arsenic bearing pyrite is always incompatible with gold occurrence. Salam (2011) studied pyrite chemistry in Chatree deposit; subsequently, he suggested that molybdenum (Mo) occurred in the pre-mineralization stages (quartz-carbonate-sericite-pyrite and quartz-feldspar minor sulfide) whereas arsenic (As) had occurred in both pre-mineralization and main gold mineralization stages. In the Pajingo epithermal system, Pinder (2006) found that arsenic concentration was depleted in the main gold-silver mineralization. Taylor et al. (2010) suggested that arsenic pyrite tends to be concentrated along the margin of primary ore which these pyrites may have been subsequently modified from the primary ore. It should be noted that arsenic is not compatible to Au mineralization. Fleet et al. (1989) suggested that arsenic may be incorporated as a metastable solid solution in pyrite.

Sb (antimony) as demonstrated in the probability plot (Figure 4.4 in chapter 4) showed negative correlation to Au. The high values of Sb (>2 to 7 ppm) occurred outside the high gold grade zone. Similar to the box plot, Sb showed negative correlation to Au. The main gold mineralization studied by Salam (2011), showed weak correlation between Au against As and Sb. However, trace element plot (box plot) of ICP whole-rock analyses of altered volcanic rocks in the Chatree deposit (Lunwongsa et al., 2010) showed positive correlation of K, Ag, Mo, W, Sb and Pb contents to Au contents. The result of Lunwongsa et al. (2010) is agreeable to geochemical data of low sulfidation epithermal gold deposit in Cracow Queensland (Braund, 2006) which identified the Sb is anomalous within the altered wall rock and stock work vein adjacent to the high grade gold. It may indicate that concentrations of Sb and As are possibly higher in low grade gold deposition.

A significant correlation between Au and Ag from statically analysis and box plot show positive correlation. Gold and silver also correlate with Cu, Pb, Zn and Te. The box plot of trace elements show that Au and Ag progressively increase from the sulfide assemblage group I to group III and reach the highest values in sulfide assemblage group IV of the main gold mineralization. Salam (2011) also suggested that Au and Ag have strong correlation in the main gold mineralization of Chatree deposit. Cu, Pb and Zn may occur as sulfide assemblage or inclusion such as sphalerite, chalcopyrite and galena.

Cu has positive correlation to Au and show a maximum level at 510 ppm in the highest-gold grade. The highest-gold grade is recognized in banded quartz texture and assemblage group IV. Cu is significant composition of chalcopyrite ($CuFeS_2$), tennantite ($Cu_{12}As_4S_{13}$) and tetrahedrite ($Cu_{12}Sb_4S_{13}$). Gold mineralization in A pit (by

(Tangwattananukul et al., 2009)) also showed positive correlation between Cu and Au in the gold-bearing quartz vein.

Pb has positive correlation to Au which is similar to the previous study of Lunwongsa et at. (2010). The average contents of Pb is higher in assemblage group IV in banded texture of the main gold mineralization (Figure 5.4). Pinder (2006) also suggested that the banded texture hosts significant gold and contains high Pb contents.

The high average Zn content particularly part of sphalerite occurs in sulfide assemblage group IV of plumose and banded quartz textures (see Figure 5.4). The results of box plot indicated that base-metal (Cu-Pb-Zn) mineralization trends to increase gold content. Similar result was reported by Braund (2006) who reported positive correlation between base-metal and electrum.

Telluride (Te) has positive correlation to gold and has higher content in banded texture. The telluride was found as invisible inclusions within electrum grain. It may be formed as (hessite, Ag_2Te). Bogdanov et al. (2005) studied Au-Ag-Te-Se minerals in Bulgaria and described that hessite is closely associated with gold. Moreover, Cracow epithermal gold deposit also has hessite in association with electrum which they occur in the quartz banded vein (reported by Braund, 2006). Braund studied Ag-Te phase of low sulfidation. Salam (2011) also reported that Te probably formed as Au-Ag-Te inclusions in pyrite within Chatree gold deposit. In addition, Salam (2011) also reported that Au, Te, Zn contents are particularly high in the main gold stages. This is also consistent with the gold-telluride in Cripple Creek of Colorado, studied by Watterson et al. (1977) who suggested that Te useful for geochemical gold exploration.

For instant, geochemical characteristics of Eastern A pit indicate that Ag, Te, Cu, Pb, Zn and Au can be used as pathfinder elements or good indicators of the gold-rich mineralization. Arsenic (As) and antimony (Sb) may also be used to trend analysis. On the other hand, As and Sb seem to indicate depletion of gold mineralization.

5.3 Gold Mineralization System

The high grade vein deposit in Eastern A pit shows vertical zonation pattern (see Figures 5.5-5.7). Three zones can be recognized as shown in Figure 5.7, including upper gold-barren zone, gold-electrum (precious metal) zone and lower (or root) base metal zone. Precious and base metal zones are varied with depth from bottom of the ore shoot to the upper of gold mineralization zone.

As shown in Figure 5.7, the upper zone (6 to -13 RL) consist of a quartz vein breccia to stock work vein (saccharoidal, moss and plumose) and small amount of banded vein. The stock work vein may be closed to the surface depending on the

evolution of the epithermal system, as suggested by Camus (1990). Grey quartz, chalcedonic, pyrite and minor sulfide base-metal are enriched in the uppermost of silica ledge, Figure 5.7. Mo and As are founded in pyrite as Mo-rich pyrite ($Mo.Fe.S_2$) or arsenic-rich pyrite ($Fe(As.S)_2$) that present at the upper to central mineralize zone. In addition, the mineralization in Eastern A pit of Chatree deposit are enriched in silica as the phase of silicification. Sangsiri (2010) found silicification and K-feldspar alteration that are dominantly in the upper part of A pit in Chatree deposit.

The zone of gold-electrum (precious metal) zone underlines the gold-barren zone. It consists both banded vein and breccia to stock work vein. This central zone mainly has banded and plumose textures with subordinate comb and moss textures. Relatively high concentration of gold (up to 73 g/t Au) occurred in the central zone at -50 to -125 RL. This zone shows a well-developed quartz, Mo-rich pyrite, chalcopyrite, sphalerite, tennantite/tetrahedrite, adularia and sericite associated with gold and electrum. Some elements such as Cu, Mo, Sb and Te are enriched along the zone of K-feldspar (adularia) and sericite. They represent in the center to upper zone (-13 to -125m) of main ore zone. Sangsiri (2010) also found that the quartz-sericite or phyllic alteration presented in the distal to the ore zone of A pit. The sericite and illite are depleted from center to lower at feeder veins. The tetrahedrite and tennantite are mainly formed as inclusion in pyrite crystal. Spycher and Reed (1989) suggested that the low temperature sulfosalt (tennantite and tetrahedrite) is composed of arsenic and antimony at the shallow levels in the epithermal system. Electrum are less abundant in the upper level compared to the middle level of the vein system. Gold-silver minerals is highly concentrated in the middle part and tends to decrease slightly in the upper part. It may also result from loss of H_2S product to a gas phase during boiling (Moss and Scott, 2001). Moss and Scott (2001) suggested that the solubility of gold as the $Au(HS)_2^-$ complex is dependent to the activity of H_2S. Very high activity of H_2S or $Au(HS)_2^-$ complex is flavored and gold solubility can reach to high gold contents.

The lower zone is characterized by breccia to quartz-carbonate vein-massive vein. This root of mineralization zone (-125 to-200 RL) shows both low and high gold grades in a range of 0.1-3.7 ppm in saccharoidal and moss textures and in a range of 6.6-7.2 ppm in comb and plumose textures. The base metals (Cu, Pb, Zn) from the Eastern A pit occur at shallow in minor amounts and constrain in the deeper levels of the gold shoots. Lead and zinc yield anomalous concentrations reached up to 904 ppm Pb and 1,740 ppm Zn whereas Cu is usually in a range of 73-200 ppm. These base metals are mainly in the near lower (between middle to lower) zone to deeper zone around -70 to -170 RL. Base metals of Pajingo gold deposit, Queensland Australia

have occurred similarly in the lower zone (Pinder, 2006). This similarity has also been occurred in epithermal quartz vein in Cracow studied by Braund (2006) who suggested that Cu, Pb, Zn have occurred at the deeper levels near the base of gold shoots (Figure 5.8). Salam (2011) reported that the base metal-rich zone is found at the deeper part of the Chatree gold deposit which may have occurred at the depth below boiling level. In addition, the shallow level above the boiling zone should be part of precious metal which is the main gold mineralization stage as identified by Salam (2011).

Electrum in Eastern A pit occurred in the phases of Au-Ag, Au-Te, Ag-Te and Au-Ag-Te, and may be formed as inclusions in pyrite. They are mainly associated with banded vein and presenting at the center to upper level of ore shoots around –s to -130 RL. The electrum in main gold mineralization were suggested to have occurred at shallow level (Salam, 2011). Au, Ag and Te occurred in the banded texture which mainly hosts significant gold grades as suggested by Braund (2006); and Pinder (2006). Braund (2006) studied geochemical vector to gold and subsequently reported that Ag and Te occur adjacent to the gold shoots and should be formed as elemental halo to the gold shoots. Pinder (2006) inferred that the electrum at the upper zone of mineralization has higher silver contents. Au-(Ag)-Telluride deposit at Quadrilateral (Romania) at a volcano of Neogene calc-alkaline magmatism has telluride-rich ore forming the high grade in the middle part of vein (Cook et al., 2009).

Moreover, various quartz textures were found in both horizontal and vertical zonation from the surface to below between 6RL to -200RL. The drilled-core samples were selected mainly from the deeper part rather than from the near surface samples. The near surface samples mainly contain rock chips caused by reversed circulation drilling. They are not suitable for selective samples for this study. The colloform banded quartz generally occurs between -70 to -93RL below the surface. This zone, located in the gold shoot level, has significantly high gold content. Small amounts of band texture occur near the surface at 6.4RL. The plumose (flamboyant/feathery) quartz texture mainly occurs in the middle to deeper between -65 to-191RL; however, some of them are found near the surface. The comb texture occurs at -16RL to the deeper part up to -200RL. It may be implied that the banded, plumose and comb textures mainly occurred at the middle gold mineralization zone and deeper root gold. On the other hand, moss texture should be occurred at various depths close to the surface (at about -5 RL) and the deeper part (at about-170RL). Saccharoidal texture is similarly observed at the shallow depth (about -15RL) and deeper part (at about -130RL).

Figure 5.5 Strip logs of trace element in each quartz texture.

Figure 5.6 Strip logs of trace element in each mineral assemblage group.

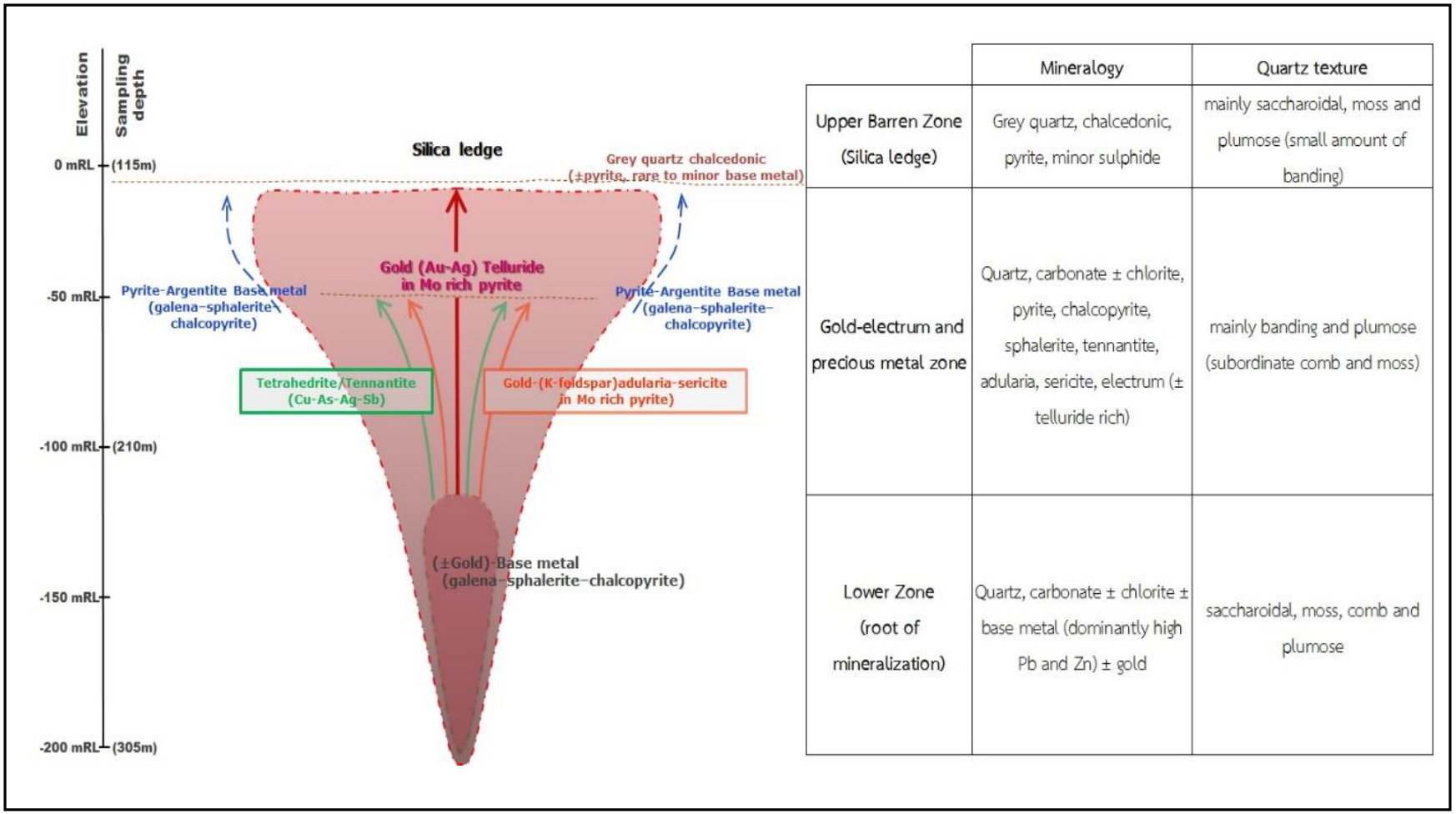

	Mineralogy	Quartz texture
Upper Barren Zone (Silica ledge)	Grey quartz, chalcedonic, pyrite, minor sulphide	mainly saccharoidal, moss and plumose (small amount of banding)
Gold-electrum and precious metal zone	Quartz, carbonate ± chlorite, pyrite, chalcopyrite, sphalerite, tennantite, adularia, sericite, electrum (± telluride rich)	mainly banding and plumose (subordinate comb and moss)
Lower Zone (root of mineralization)	Quartz, carbonate ± chlorite ± base metal (dominantly high Pb and Zn) ± gold	saccharoidal, moss, comb and plumose

Figure 5.7 Empirical model for gold mineralization epithermal vein system in Eastern A pit of Chatree deposit.

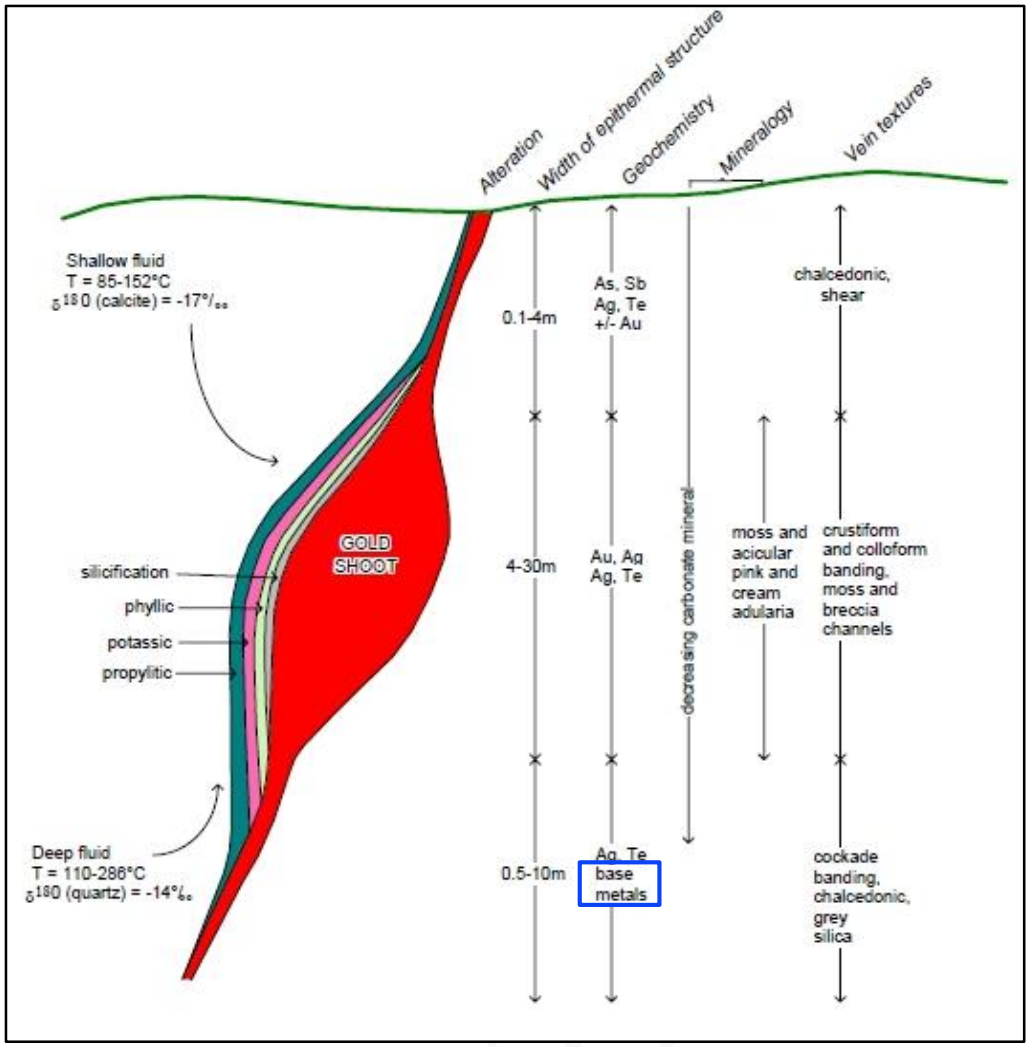

Figure 5.8 Epithermal system in Cracow Queensland (after Braund, 2006).

5.4 Conclusions

Based on vein characteristics, e.g., quartz texture, mineral assemblage, ore mineral chemistry and whole-rock trace element in this study can be concluded below.

(1) Colloform quartz texture is closely related to higher gold grades and it is characterized by high contents of Te, Cu, Pb, Zn, Ag and Au in the Eastern A pit, Chatree deposit.

(2) Mineral assemblage IV of quartz-chlorite-feldspar (adularia)-pyrite-sphalerite-tennantite-electrum is important to the gold deposition in this study area. This is because high concentrations of sulfide and electrum formed in this are related to the high gold grade.

(3) Assemblage group IV of the main Au-Ag mineralization is recognized in colloform banded quartz and subordinate plumose texture, and usually occur in the middle ore zone.

(4) Au-Ag-Te-Cu-Pb-Zn can be used as pathfinder elements of the Au-rich mineralization.

(5) The best indicators of high gold grade are Ag, Te, and Zn.

(6) Electrum of high-gold grade vein is concentrated in pyrite, iron-rich sphalerite (Zn.Fe)S, adularia, tennantite, and telluride (Te)-rich electrum.

REFERENCES

Adam, S.F., 1920. A microscopic study of vein quartz. Economic Geology, 15.

Amstutz, G.C., Gasparrini, C. and Gray, P.M.J., 2012. Gold and Other Precious Metals: From Ore to Market. Springer Berlin Heidelberg.

Audley-Charles, M.G., 1988. Evolution of the southern margin of the Tethys (North Australian region) from Early Permian to Late Cretaceous: In Audley-Charles. Gondwana and Tethys: Geological Society, London, Special Publications, 37: 79-100.

Baaku, E.K., 2013. Determination of Anomalous Gold Targets by use of Geochemical Exploration and Multivariate Statistics Methods in Chirano Gold Mining Area of the Western Region, Ghana. Thesis (MSc) Thesis, University of Ghana, 130 pp.

Barber, A.J. and Crow, M.J., 2003. An evaluation of plate tectonic models for the development of Sumatra. Gondwana Research 6: 1-28.

Barber, A.J., Ridd, M.F., and Crow, M.J., 2011. The origin, movement and assembly of the pre-Tertiary tectonic units of Thailand. Geological Society of London: 507-537.

Barr, S.M. and Charusiri, P., 2011. Volcanic rocks, In Ridd, M.F., Barber, A.J., and Crow, M.J., eds. The geology of Thailand, The Geological Society of London: 415-440.

Barr, S.M. and Macdonald, A.S., 1987. Nan River suture zone, northern Thailand. Geology, 15: 907-910.

Barr, S.M., Macdonald, A.S., Dunning, C.R., Ounchanum, P. and Yaowaloiyothin, W., 2000. Petrochemistry, U-Pb (zircon) age, and palaeotectonic setting of the Lampang Volcanic Belt, northern Thailand. Geological Society of London 157: 553-563.

Barr, S.M., MacDonald, A.S., Ounchanum, P. and Hamilton, M.A., 2006. Age, tectonic setting and regional implications of the Chiang Khong volcanic suite, northern Thailand. Journal of the Geological Society 163 (6): 1037–1046.

Bogdanov, K., Filipov, A. and R., K., 2005. Au-Ag-Te-Se minerals in the Elatsite porphyry-copper deposit, Bulgaria, Geochemistry, Mineralogy and Petrology, 43, Sofia, IGCP Project 486, Field Workshop, Kiten, Bulgaria, pp. 13-19.

Braund, K.G., 2006. Geology, Geochemistry and paragenesis of the Royal, Crown and Roses Pride low sulphidation epithermal quartz vein structures, Cracow, South-East Queensland. unpublished Thesis, University of Queensland, 1-334 pp.

Buffetaut, E., Suteethorn, V., Tong, H., Chaimanee, Y. and Khunsubha, S., 1997. New dinosaur discoveries in the Jurassic and Cretaceous of Northeastern Thailand. In: Dheradilok, P., Hinthong, C., Chaodumrong, P., Puthaphiban, P., Tansathien, W., Utha-aroon, S., Sattayarat, N., Nutchanong, T., Techawan, S. (Eds.), Proceeding of the International Conference on Stratigraphy and Tectonic Evolution of Southeast Asia and the South Pacific (Geothai 97), Bangkok, Thailand, pp. 177–187.

Bunopas, S., 1981. Paleogeographic history of Western Thailand and adjacent parts of Southeast Asia-a plate tectonic interpretation. Unpublished PhD thesis Thesis, Victoria University of Wellington, New Zealand.

Bunopas, S., 1991. The pre-Late Triassic collision and stratigraphic belts of Shan-Thai and Indochina microcontinents in Thailand. In Proceeding of the 1st International Symposium of the IGCP Project 321, Gondwana Dispersal and Accretion of Asia, Kumming, China: 25-30.

Bunopas, S. and Vella, P., 1978. Late Paleozoic and Mesozoic structural evolution of northern Thailand-a plate tectonics model: In Nutalaya, P., ed., Proceedings of the Third Regional Conference on geology and mineral resources of SE Asia, Asia Institute of Technology, pp. 133-140.

Bunopas, S. and Vella, P., 1983. Tectonic and geology evolution of Thailand, In Nutalaya, P., ed., Proceedings of a workshop on stratigraphic correlation of Thailand and Malaysia, Haad Yai, Thailand. Geological Society of Thailand and Geological Society of Malaysia: 307-322.

Burrett, C., Long, J. and Stait, B., 1990. Early–Middle Palaeozoic biogeography of Asian terranes derived from Gondwana. Geological Society of London, Memoirs 12: 163–174.

Camus, F., 1990. The geology of hydrothermal gold deposits in Chile. Journal of Geochemical Exploration, 36(1–3): 197-232.

Charoenpravat, A., Sripongpan, P., Thammadusadee, V. and Wolfart, R., 1987. Geology of Amphoe Sop Prap and Amphoe Wang Chin, Thailand. Geo 13.2. B65, Hannover.

Charusiri, P., 1989. Lithophile metallogenetic epochs of Thailand: a geological and geochronological investigation. Unpublished PhD thesis Thesis, Queen's University, Ontario, Canada, 819 pp.

Charusiri, P., Daorerk, V., Archibald, D., Hisada, K. and Ampaiwan, T., 2002. Geotectonic evolution of Thailand, a new Tectonic feature of Eastern Thailand synthesis. Geological Society of Thailand, 1: 1-20.

Christie, A. and Brathwaite, R., 2011. Mineral Commodity Report 14 Institute of geological and Nuclear sciences Ltd.

Chuaviroj, S., Chaturongkawanich, S. and Sukawattananan, P., 1980. Geology of Geothermal Resources of Northern Thailand (Part I, San Kamphaeng), Department of Mineral Resources, Bangkok, Thailand, Unpublished report of Geological Survey Division.

Cook, N., Ciobanu, C., Spry, P. and Voudouris, P., 2009. Understanding gold-(silver)-telluride-(selenide) mineral deposits. Episodes 32(4): 249-263.

Cooke, T.D., 1982. The Demand for Gold by Industry. Gold bulletin, 15(2): 38-42.

Corbett, G., 2002. EPITHERMAL GOLD FOR EXPLORATIONISTS. AIG: 1-26.

Corbett, G.J., 2004. Comments on controls to gold prospects in the vicinity of the Chatree Gold Mine, Thailand, Unpublished Report, Kingsgate Consolidated Limited.

Corbett, G.J. and Leach, T.M., 2008. Fluid mixing as a mechanism for bonanza grade epithermal gold formation, Terry leach Symposium, Australian Institute of Geoscientists, pp. 83-92.

Crossing, J., 2004. Geology of the Chatree District, Thailand, Kingsgate Consolidated Limited.

Crossing, J., 2006. Additional Geological Mapping Of The Chatree Regional Thailand, Company Report.

Cumming, G.V., 2004. Analysis of volcanic facies at the Chatree gold mine and in the Loei- Phetchabun Volcanic Belt, central Thailand. Unpublished Honours thesis Thesis, University of Tasmania, 84 pp.

Cumming, G.V., Allen, S., McPhie J. and Zaw., K., 2006. Polymictic andesitic lithic breccias from centralThailand: evidence for the collapse of a volcanic edifice, In: Geochronology, Metallogenesis and deposit styles of the Loei foldbelt in Thailand and Laos PDR, ARC Linkage Project report, Centre for Ore deposit research.

Cumming, G.V., James, R., Salam, A., Khin Zaw, Meffre, S., Lunwongsa, W. and Nuanla-Ong, S., 2008. Geology and mineralisation of the Chatree epithermal Au-Ag deposit, Phetchabun and Phichit Provinces, central Thailand, Proceeding of PACRIM Congress 2008, Australian Institute of Mining and Metallurgy, Gold Coast, Australia, pp. 409-416.

Dedenczuk, D., 1998. Epithermal gold mineralisation at Khao Sai, Phichit, Thailand. Unpublished Honours thesis Thesis, University of Tasmania, Australia.

Department of Mineral Resources (DMR), 1976. Geologicalmap of Phetchabun area, Scale 1:250,000. In: D.o.M.R. Geological Survey Division, Bangkok, Thailand.

Department of Mineral Resources (DMR), 2004. Geological map of Thailand, Scale 1:250,000, Geological Survey Division, Department of Mineral Resources, Bangkok, Thailand.

Diemar, M.G. and Diemar, V.G., 1999. Geoloogy of the Chartee Epithermal Gold deposit, Thailand, Pacific Rim Conference 1999, Indonesia, pp. 227-231.

Dong, G., Morrison, G. and Jaireth, S., 1995. Quartz Texture in epithermal veins, Queensland: classification, origin, and implication, 90, 1841-1856 pp.

Feng, Q., Chonglakmani, c., Helmcke. D., Ingavat-Helmcke, R. and Liu, B., 2005. Correlation of Triassic of Stratigraphy between the Simao and Lampang-Phrae basins: implications for the tectonopaleogeography of Southeast Asia. Journal of Asian Earth Sciences, 24: 777-785.

Fleet, M.E., MacLean, P.J. and Barbier, J., 1989. Oscillatory-zoned As-bearing pyrites from stratabound gold deposits: An indication of the fluid evolution. Econ. Geol. Mon., 6: 356-362.

Gatinsky, Y.G., Hutchison, C.S., Nguyen, M.N. and Tri, T.V., 1984. Tectonic evolution of Southeast Asi: 27th International Geological Congress Report.

Gatinsky, Y.G., Mischina, A.V., Vinogradov, I.V. and Kovaley, A.A., 1978. The main metallogenic belts of SE Asia as the result of different geodynamic conditions in interference, 3rd regional conference on geology and mineral resources of SE Asia, Bangkok, pp. 313-318.

Gutiérrez, M., Victor, M., Teresa, A. and López, D., 2012. Exploratory Analysis of Sediment Geochemistry to Determine the Source and Dispersion of Ba, Fe, Mn, Pb and Cu and in Chihuahua, Northern Mexico. Journal of Geography and Geology, 4(4).

Hada, S., Bunopas, S., Ishii, K. and Yoshikura, S., 1997. Riftdrift history and the amalgamation of Shan-Thai and Indochina/East Malaya block, In: P. Dheeradilok et al. (eds.),, Proceedings of the International Conference on Stratigraphy and Tectonic Evolution of Southeast Asia and the South Pacific, Department of Mineral Resources, Ministry of Industry, Bangkok, Thailand, pp. 273-286.

Hada, S., Bunopas, S., Ishii, K. and Yoshikura, S., 1999. Rift-drift history and the amalgamation of Shan-Thai and Indochina/East Malaya blocks. Gondwana dispersion and Asian accretion: IGCP, 321: 67-87.

Hara, H., Kurihara, T., Kuroda, J., Adachi, Y., Kurita, H., Wakita, K., Hisada, K., Charusiri, P., Charoentitirat, T. and Chaodumrong, T., 2010. Geological and geochemical aspects of a Devonian siliceous succession in northern Thailand: implications for the opening of the Paleo-Tethys. Palaeogeography, Palaeoclimatology, Palaeoecology, 297: 452–464.

Henley, R.W. and Hughes, G.O., 2000. Underground fumaroles: “Excess heat” effects in vein formation. Economic Geology 95(3): 453–466.

Hutchison, C.S., 1975. Ophiolites in Southeast Asia. Geological Society of American Bulletin 86: 797–806.

Hutchison, C.S., 1989. Geological evolution of South-east Asia. Oxford Monographs on Geology and Geophysics, 13: 368.

Intasopa, S., 1993. Petrology and geochronology of the volcanic rocks of central Thailand volcanic belt. Unpublished PhD thesis Thesis, University of New Brunswick, Canada, 242 pp.

Intasopa, S. and Dunn, T., 1994. Petrography and Sr-Nd isotope systems of the basalts and rhyolites, Loei, Thailand. Southeast Asian Earth Sciences, 9: 167-180.

Intasopa, S., Dunn, T. and Lux, D.R., 1990. 40Ar/39Ar geochronology of the Central Thailand Volcanic Belt. Trans, Am. Geophys. Union EOS, 71: 1700.

Jame, R., Bradley, B., Munoz, M. and Suphananthi, S., 2014. Quaterly Report 2014 for three months ended 30 September 2014, Institution of Kingsgate Consolidated Limited, Sydney, NSW 2000 Australia.

Jungyusuk, N. and Khositanont, S., 1992. Volcanic rocks and associated mineralisation in Thailand, Proceedings of National Conference on Geologic Resources of Thailand: Potential for Future Development, pp. 522-538.

Kamvong, T., Charusiri, P. and Intasopa, S.B., 2006. Petrochemical characteristics of igneous rocks from Wang Pong area, Phetchabun, north-central Thailand: Implications for tectonic setting. Journal of Geological Society of Thailand, 1: 9-26.

Kilias, S.P., Paktsevanoglou, M., Giampouras, M., Stavropoulou, A., Apeiranthiti, D. and Mitsis, I., 2013. Gold occurrence, mineral textures and ore fluid properties at the Viper (Sappes) epithermal Au–Ag–Cu orebody, Thrace, Greece, 12th SGA Biennial Meeting 2013. The Society for Geology Applied to Mineral Deposits (SGA), At Uppsala, Sweden.

Kromkhun, K., 2005. Geological setting, mineralogy, alteration, and nature of ore fluid of the H-zone, the Chatree deposit, Thailand. Unpublished M.Sc. Thesis, University of Tasmania, Australia.

Lunwongsa, W., Nuanla-ong, S., Charusiri, P. and Sangsiri, P., 2010. Alteration Study of the Chatree Epithermal Au-Ag Deposit, Central Thailand by a Combination of Methods; ASDSpectrometry, Conventional and Whole Rock ICP Geochemistry, International Conference on Geology, Geotechnology and Mineral Resources of Indochina (GEOINDO 2011), Khon Kaen, Thailand, pp. 89-96.

Marhotorn, K., Mizuta, T., Ishiyama, D., Yoshida, H. and Charusiri, P., 2008. Petrochemistry of Igneous rocks in the Southern Parts of the Chatree Gold Mine, Pichit, Central Thailand, International Symposium on Geoscience Resources and Environments of Asian Terranes (GREAT 2008), Bangkok, Thailand, pp. 289-298.

McQueen, K.G., 2006. Identifying geochemical anomalies, Department of Earth and Marine Sciences Australian National University, ACT 0200.

Meesook, A. and Saengsrichan, W., 2011. Jurassic. In: Ridd, M.F., Barber, A.J., Crow, M.J. (Eds.), Geology of Thailand. Geological Society of London: 151–168.

Meesook, A., Suteethorn, V. and Wongprayoon, T., 1995. Early Cretaceous non-marine bivalves of the Sao Khua Formation, Khorat Group, Northeastern Thailand, 3rd Symposium, IGCP, Manila, Philippines, pp. 10-11.

Metcalfe, I., 1984. Stratigraphy, palaeontology and palaeogeography of the Carboniferous of Southeast Asia. Mem. Soc. Geol. France 147: 107–118.

Metcalfe, I., 1988. Origin and assembly of south-east Asian continental terranes; In Audley-Charles M.G. and Hallam A. ed., Gondwana and Tethys. Geological Society Special Publications, 37: 101-118.

Metcalfe, I., 1991. Late Palaeozoic and Mesozoic palaeogeography of Southeast Asia. Palaeogeography, Palaeoclimatology and Palaeoecology, 87: 211-221.

Metcalfe, I., 1996. Gondwanaland dispersion, Asian accretion and evolution of eastern Tethys. Journal of Asian Earth Sciences, 43: 605-623.

Metcalfe, I., 1999. Gondwana dispersion and Asia accretion, an overview, In: I. Metcafe (ed.). Gondwana Dispersion and Asian Accretion. A.A. Balkema Publishers, Rotterdam, Netherlands, 9-36 pp.

Metcalfe, I., 2002. Permian tectonic framework and palaeogeography of SE Asia. Journal of Asian Earth Sciences 20: 551–566.

Metcalfe, I., 2006. Palaeozoic and Mesozoic tectonic evolution and palaeogeography of East Asian crustal fragments: the Korean Peninsula in context. Gondwana Research, 9: 24-46.

Metcalfe, I., 2013. Gondwana dispersion and Asian accretion: Tectonic and palaeogeographic evolution of eastern Tethys. Journal of Asian Earth Sciences, 66: 1-33.

Moncada, D., Mutchler, S., Nieto, A., Reynolds, T.J., Rimstidt, J.D. and Bodnar, R.J., 2012. Mineral textures and fluid inclusion petrography of the epithermal Ag–Au deposits at Guanajuato, Mexico: Application to exploration. Journal of Geochemical Exploration, 114(0): 20-35.

Moradpouri, F. and Ghavami-Riabi, R., 2014. Geochemical Exploration at Qolqola Shear Zone Gold Deposit: North-West of Iran. Open Transactions on Geosciences, 1(1): 1-6.

Morishita, Y., Shimada, N. and Shimada, K., 2008. Invisible gold and arsenic in pyrite from the high-grade Hishikari gold deposit, Japan. Applied Surface Science, 255(4): 1451-1454.

Moritz, R., 2006. Fluid salinities obtained by infrared microthermometry of opaque minerals: implications for ore deposit modeling. Journal of Geochemical Exploration 89: 284–287.

Moss, R. and Scott, S.D., 2001. Geochemistry and mineralogy of gold-rich hydrothermal precipitates from the eastern Manus Basin, Papua New Guinea. Can. Mineral, 39: 957–978.

Ngeno, V.C. and Simatwa, M.W., 2015. Influence of Free Secondary Education Policy on Dropout Rates in Kenya: A Case Study of Kericho County Greener Journal of Educational Research, Vol. 5 (4)(ISSN: 2276-7789 ICV: 6.05): 152-175.

Noku, S.K., Matsueda, H., Akasaka, M. and Espi, J.O., 2012. Petrology, Geochemistry, and Fluid Inclusion Microthermometry of Sphalerite from the Laloki and Federal Flag Strata-Bound Massive Sulfide Deposits, Papua New Guinea: Implications for Gold Mineralization. Resource Geology 62(2): 187–207.

Nuanla-ong, S., 2012. Report on vein orientation in A pit of Chatree Issara Mining Limited, Phetchabun, Thailand.

Ovenden, A., Baker, T., Mustard, R. and Bolt, S., 2005. Textural and geochemical analysis of veins in the Pajingo epithermal system, Queensland, Australia in Discrimination of barren versus gold-bearing epithermal systems and vectoring of ore in the Pajingo mining area, 63,, EGRU (Economic Geology Research Unit) Contribution, 63, James Cook University.

Palomera, A.D., Ruitenbeek P. V., A., F.J., van der Meer, Freek D. and Fernández, R., 2012. Geochemical indicators of gold-rich zones in the La Josefina epithermal deposit, Deseado Massif, Argentina. Ore Geology Reviews, 45(0): 61-80.

Panjasawatwong, Y., Chantaramee, S., Limtrakun, P. and Pirarai, K., 1997. Geochemical and tectonic setting of eruption of central Loei volcanics in the Pak Chom area, Loei, northeast Thailand: Proceeding of International conference on Stratigraphy and tectonic evolution of Southeast Asian and the South Pacific, Bangkok, Proceeding of International conference on Stratigraphy and tectonic evolution of Southeast Asian and the South Pacific, Bangkok, pp. 287-302.

Panjasawatwong, Y., Khin Zaw, Chantaramee, S., Limtrakun, P. and Pirarai, K., 2006. Geochemistry and tectonic setting of the Central Loei volcanic rocks, Pak Chom area, Loei, northeastern Thailand. Journal of Asian Earth Sciences, 26: 77-90.

Phillips, G., Hughes, N. and J., M., 1996. The geology and gold deposits of the Victorian gold province. Ore Geology Reviews, 11(5): 255-302.

Pinder, J., 2006. Geochemical evaluation and modelling of the macro to micro-scale variations of the Vera Nancy system, Pajingo, North Queensland Australia. Unpublished Thesis, School of Earth Sciences, James Cook University of North Queensland, 1-107 pp.

Piyasin, S., 1972. Geology of Changwat Lampang. 1:250,000. Royal Thai Department of Mineral Resources, Report of Investigation.

Piyasin, S., 1975. Geology of Changwat Uttaradit. 1:250,000. Royal Thai Department of Mineral Resources, Report of Investigation.

Racey, A., Goodall, J.G.S., Love, M.A., Polachan, S. and Jone, P.D., 1994. New age data for the Mesozic Khorat Group of Northeast Thailand, In Proceeding of the Internation Symposium on Stratigraphic Correlation of Southeast Asia, pp. 245–252.

Richards, D.R., Elliott, G.J. and Jones, B.H., 1998. Vera North and Nancy gold deposits, Pajingo. Geology of Australia and Papua New Guinea Mineral Deposits, The Australasian Institute of Mining and Metallurgy, Melbourne, 685-690 pp.

Richards, T.H., Ketu Gede Suyadnya., I., T., N., D., D., and Muryanto, A., 2005. The Discovery of the Kencana Low Sulphidation Epithermal Deposit, Gosowong

Goldfields, Halmahera Island, East, Indonesia, NewGen Gold Conference, Perth, Western Australia, pp. 151-167.

Salam, A., 2006. A Geological, Geochemical and Metallogenic study of the Northern Chatree area, Phetchabun province, Loei fold Belt, Central Thailand – progress report, In: Geochronology, Metallogenesis and Deposit Styles of Loei Foldbelt in Thailand and Laos PDR, CODES: ARC Linkage Project, CODES Centre for Excellence in Ore deposit Research, University of Tasmania.

Salam, A., 2011. A Geological, Geochemical and Metallogenic study of the Chatree epithermal deposit, Phetchabun province, Central Thailand. unpublished Thesis, University of Tasmania (UTAS), Australia, 1-251 pp.

Salam, A., Zaw, K., Meffre, S., McPhie, J. and Lai, C.-K., 2014. Geochemistry and geochronology of the Chatree epithermal gold–silver deposit: Implications for the tectonic setting of the Loei Fold Belt, central Thailand. Gondwana Research, 26(1): 198-217.

Salyapongse, S., 1992. Foliated contact metamorphic rocks of the eastern gulf Thailand. Geological Society of Thailand, 2: 35-42.

Salyapongse, S., Fontaine, H., Putthapiban, P. and A., L., 1997. Geology of eastern Thailand (Route No. 1), Guidebook for Excursion of the International Conference on Stratigraphy and Tectonic Evolution of Southeast Asia and the South Pacific, Department of Mineral Resources, Ministry of Industry, Bangkok, Thailand.

Sander, M.V. and Black, J.E., 1988. Crystallization and recrystallization of growth zoned vein quartz crystals from Epithermal systems-implication for fluid inclusion studies. Economic Geology, 83.

Sangsiri, P., 2010. Wallrock Alteration and Mineralization of the A and the H West Prospects, Chatree Gold Deposit, Phichit and Phetchabun, Province, Central Thailand. Unplubished Msc. Thesis Thesis, Chulalongkorn University.

Sangsiri, P. and Pisutha-Arnond, V., 2008. Host rock alteration at the A prospect of the Chatree gold deposits, Phichit province, central Thailand: A preliminary re-evaluation, In Proceedings of the International Symposia on Geoscience Resources and Environments of Asian Terranes (GREAT 2008), 4th IGCP526 and 5th APSEG, Bangkok, Thailand, pp. 258-261.

Singharajwarapan, S. and Berry, R., 2000. Tectonic implications of the Nan Suture Zone and its relationship to the Sukhothai Fold Belt, Northern Thailand. Journal of Asian Earth Sciences 18: 663-673.

Sone, M. and Metcalfe, I., 2008. Parallel Tethyan sutures in mainland Southeast Asia: New insights for Palaeo-Tethys closure and implications for the Indosinian orogeny. Comptes Rendus Geoscience, 340(2–3): 166-179.

Sone, M., Metcalfe, I. and Chaodumrong, P., 2012. The Chanthaburi terrane of southeastern Thailand: stratigraphic confirmation as a disrupted segment of the Sukhothai Arc. Journal of Asian Earth Sciences, 61: 16–32.

Spycher, N.F. and Reed, M.H., 1989. Evolution of a Broadlands-type epithermal ore fluid along alternative P-T paths: Implications for the transport and deposition of base, precious and volatile metals. Economic Geology, 84: 328-359.

Subandrio, A.S. and Basuki, N.I., 2010. Alteration and Vein Textures Associated with Gold Mineralization at the Bunikasih Area, Pangalengan, West Java. Indonesian Journal on Geoscience, 5(4): 247-261.

Tangwattananukul, L., 2012. Characteristic features of gold mineralization at the Chatree deposit, Central Thailand. Unpublished Thesis, Akita University, Japan 1-103 pp.

Tangwattananukul, L., Ishiyama, D., Matsubaya, O., Mizuta, T., Charusiri, P. and Sera, K., 2009. Gold mineralization of Q prospect at Chatree deposit, central Thailand, NMCC Annual Report 16.

Taylor, C.D., Sutley, S.J. and Lichte, F.E., 2010. Mineralogical, textural, and metal residence studies of primary, recrystallized, and remobilized ores of the greens creek deposit. US Geological Survey Professional Paper: 187-236.

Tukey, J.W., 1977. Exploratory Data Analysis. Addison. . Addison-Wesley Publishing Company Reading, Mass, Menlo Park, Cal., London, Amsterdam, Don Mills, Ontario, Sydney.

Tulyatid, J. and Charusiri, P., 1999. The ancient Tethys in Thailand as indicated by nationwide airborne geophysical data, In: B. Ratanasthien and S.L. Rieb (eds.). Proceedings of International Symposium on Shallow Tethys (ST) 5, Chiang Mai, Thailand: 380-388.

Ueno, K., 2002. Geotectonic linkage between West Yunnan and Mainland Thailand:Toward the Unified Geotectonic Evolution Model of East Asia. Fourth Symposium of IGCP Project no. 411, Geodynamic Processes of Gondwanaland-derived terranes in East & Southeast Asia, Phitsanulok, Thailand: 35–42.

Ueno, K. and Hisada, K., 1999. Closure of the Paleo-Tethys caused by the collision of Indochina and Sibumasu. Chikyu Monthly, Japanese, 21: 832–839.

Vearncombe, J.R., 1993. Quartz vein morphology and implications for formation depth and classification of Archaean gold-vein deposits. Ore Geology Reviews, 8(5): 407-424.

Wakita, K. and Metcalfe, I., 2005. Ocean plate stratigraphy in East and Southeast Asia. Journal of Asian Earth Sciences, 24: 679-702.

Watterson, J.R., Gott, G.B., Neuerburg, G.J., Lakin, H.W. and Cathrall, J.B., 1977. Tellurium, a Guide to Mineral Deposits. In: B. C.R.M and W. I.G.P (Editors), Developments in Economic Geology. Elsevier, pp. 31-48.

Wu, Haoruo, Boulter, C.A., Ke, Baojia, Stow, D.A.V., Wang and Zhongcheng, 1995. The Changning–Menglian Suture Zone; a segment of the major Cathaysian–Gondwana divide in Southeast Asia. Tectonophysics, 242: 267–280.

Yang, K., Mo, X. and Zhu, Q., 1994. Tectono-volcanic belts and late Paleozoic-early Mesozoic evolution of southwestern Yunnan, China. Journal of Southeast Asian Earth Sciences, 10: 245-262.

Zaw, K., Meffre, S. and students., h.d., 2007. Metallogenic relations and depositscale studies, final report: geochronology, metallogenesis and deposit styles of Loei Fold Belt in Thailand and Laos PDR, ARC Linkage Project, CODES with Industry Partners.University of Tasmania, Hobart.

APPENDIX

APPENDIX A

List of Samples Analysis

Mineralogy (Core logging)	Sample no.	Au (g/t) Chatree Lab	Au (ppm)_ICP (ALS Lab)	Thin section	Polish section	EPMA
quartz-chalcgrey-co3	HG_A001	16.0	25.0	HG1-1	HG1	A01_El1, A01_Sf1, A01_Sf2
quartz-chalc-grey-co3	HG_A002	73.0	25.0	HG2-1	HG2	A02_Py1, A02_Py2, A02_Au (1, 2), A02_Sf1, A02_fsp (1, 2, 3, 4)
quartz-chalc-grey-co3(zeolite)	HG_A003	0.7	1.4	HG3-1	-	-
quartz-grey-chl(mainly grey si)	HG_A004	0.1	0.4	HG4-1	-	-
quartz-(+/-chal)-chl fracture	HG_A005	5.7	5.9	HG5-1	HG5	-
quartz-chalc-grey-co3-chl	HG_A006	7.0	6.6	HG6-1	HG6	-
quartz-grey-co3-(colloform chl)	HG_A007	4.1	4.8	HG7-1	HG7 (1, 2)	-
massive co3(+/-chl)	HG_A008	1.1	1.0	HG8-1	-	-
quartz-(+/-grey)-chl	HG_A009	9.8	9.1	HG9-1	-	-
quartz-chalc-grey-co3-(+/-chl)	HG_A010	12.0	9.6	HG10-1	HG10	A10-Sf (1, 2, 3, 4, 5), A10_Au (1, 2), A10_Sp1, A10_Py (1, 2)
quartz(+/-grey silica)-strong blk sulfide-chl-co3 replace	HG_A011	21.1	25.0	HG11-1	HG11	A11-Cp (1, 2, 3), A11-Sf (1,2), A11 Sp (1, 2), A11 Ga (1, 2, 3)
quartz-chl(+/-chalc and co3)-strong sul	HG_A012	14.5	14.0	HG12-1	HG12	A12-Au (1, 2, 3), A12 Cp (1,2), A12-Ga1
quartz(+/-grey silica) sulfide vein-co3 late	HG_A013	11.1	14.2	HG13-1, HG13-2, HG13-3	HG13 (1, 2)	A13-Au1, A13-Ga1
quartz-chalc(strong opaline chalc)-chl some co3 fill	HG_A014	2.6	2.7	HG14-1	-	-
quartz-chl	HG_A015	3.7	5.2	HG15-1	-	-
quartz-chl(+/-grey and co3)-sulfide stringer	HG_A016	6.0	6.0	HG16-1	HG16	-
quartz-grey-chl with yell/blk sulfide	HG_A017	12.4	16.7	HG17-1, HG17-2, HG17-3	HG17 (1, 2, 3)	A17-Au1, A17-El1, A17-Sf1, A17-Sp1
quartz-chalc-grey-co3-chl	HG_A018	3.8	4.1	HG18-1, HG18-2, HG18-3	HG18 (1, 2)	-
quartz-chalc-grey(quartz-sericite domi)-chl minor	HG_A019	6.9	7.2	HG19-1	-	-
quartz-chl	HG_A020	5.5	5.8	HG20-1	-	-

Mineralogy (Core logging)	Sample no.	Au (g/t) Chatree Lab	Au (ppm)_ICP (ALS Lab)	Thin section	Polish section	EPMA
quartz-(+/-chal, grey, late co3)+/-chl alt fragm	HG_A021	2.3	3.3	HG21-1	HG21 (1, 2)	-
quartz-chalc-chl	HG_A022	5.3	7.0	HG22-1	-	-
quartz-grey	HG_A023	5.1	3.7	HG23-1	HG23	-
quartz-(+/-chal and grey)-late co3-chl fracture	HG_A024	6.4	8.8	HG24-1	HG24	A24_El (1, 2, 3, 4), A24-Cp1, A24-Sf1
grey-co3	HG_A026	9.8	1.1	HG26-1	HG26	-
quartz-grey-co3	HG_A027	8.6	7.2	HG27-1	HG27	-
quartz-grn chalc-co3-chl	HG_A028	3.9	4.0	HG28-1	-	-
quartz-chl-chalc-co3	HG_A029	4.6	4.3	HG29-1	-	-
quartz-chalc-chl-late co3(host rock more than)	HG_A030	5.6	0.8	HG30-1	-	-
quartz-chalc-grey-co3(matrix)	HG_A031	5.5	2.4	HG31-1	HG31 (1, 2)	-
quartz-chalc-grey-co3(late)	HG_A032	14.3	11.4	HG32-1	HG32 (1, 2)	A32-Au (1, 2), A32-Sp (1, 2), A32-Sf (1, 2)
quartz+/-grey-chl(co3 late)	HG_A033	3.0	3.3	HG33-1	HG33 (1, 2, 3)	-
quartz-chalc-co3-strong sufide stringer(host rock more than)	HG_A034	6.5	0.9	HG34-1	HG34 (1, 2, 3)	-
quartz-sulfide	HG_A036	7.0	6.2	HG36-1	HG36	-
quartz-chalc-grey-strong sulph	HG_A037	0.6	0.5	HG37-1	-	-
quartz-grey-pyr-cpy-late co3-(chl fill*thin)	HG_A038	8.8	8.8	HG38-1	HG38	A38-El (1,2, 3, 4), A38-Sp (1, 2, 3), A38-Sf-1
quart-co3-chl fracture	HG_A039	1.8	2.5	HG39-1	HG39	-
quart-co3(more than qtz)	HG_A040	6.8	6.6	HG40-1	-	-
quart-co3	HG_A041	4.0	4.2	HG41-1	HG41	-
quart-co3(late and zeolite) matris is host rock	HG_A042	0.1	0.1	HG42-1	-	-

APPENDIX B

Trace elements (in ppm) by ICP from ALS Lab

in variable quartz texture of Eastern A pit

Hole ID	From (m)	To (m)	Sample no.	E(x)	N(y)	RL(z)	Texture classification	Au	Ag	As	Cd	Cr	Cu	Hg	Mo	Pb	Rb	S%	Se	Sb	Te	Tl	Zn
03371RD	214.60	215.50	HG_A001	5349	19623	-87	Banded	25.00	88.00	15.00	15.90	922.00	349.00	0.69	5.78	341.00	1.30	0.65	2.60	1.44	0.04	0.07	1,540.00
03371RD	216.35	217.80	HG_A002	5350	19623	-89	Banded	25.00	84.00	49.00	4.60	148.00	510.00	0.61	8.61	254.00	0.80	0.59	3.90	0.87	1.32	0.05	852.00
03371RD	218.90	223.60	HG_A003	5353	19623	-94	Saccharoidal/massive	1.40	30.00	10.00	1.60	634.00	48.00	0.04	0.81	47.30	1.40	0.16	0.60	0.30	0.05	0.24	85.00
02554RD	126.55	128.00	HG_A004	5384	19650	-13	Saccharoidal/massive	0.40	2.00	13.00	0.20	723.00	19.00	0.01	2.22	9.60	0.40	0.62	0.50	0.27	0.02	0.09	49.00
02554RD	128.10	132.40	HG_A005	5382	19650	-17	Comb	5.90	81.00	2.00	0.50	1,250.00	20.00	0.08	5.59	3.40	0.05	0.04	2.70	0.16	0.20	0.01	63.00
02534RD	141.00	148.00	HG_A006	5385	19724	-33	Comb	6.60	100.00	19.00	6.80	894.00	137.00	0.47	6.02	236.00	0.10	0.31	5.20	4.73	0.07	0.07	664.00
02561RD	201.00	209.60	HG_A007	5384	19719	-81	Banded	4.80	95.00	12.00	1.20	646.00	49.00	0.11	4.12	94.70	0.50	0.17	2.80	0.66	0.02	0.15	224.00
02561RD	210.00	213.00	HG_A008	5382	19719	-83	Saccharoidal/massive	1.00	5.00	1.00	0.80	62.00	80.00	0.05	0.48	78.90	0.20	0.09	0.90	0.12	0.21	0.01	225.00
02561RD	213.30	213.70	HG_A009	5381	19719	-84	Banded	9.10	100.00	11.00	3.00	366.00	62.00	0.19	1.53	177.00	0.50	0.32	3.10	0.81	0.04	0.41	380.00
02561RD	222.85	225.85	HG_A010	5374	19720	-94	Banded	9.60	14.00	22.00	2.50	188.00	70.00	0.09	7.85	208.00	0.40	0.36	1.20	0.89	0.05	0.06	400.00
06231RD	193.00	193.66	HG_A011	5400	19770	-74	Banded	25.00	100.00	53.00	6.70	1,130.00	160.00	0.31	9.36	511.00	0.80	0.54	6.20	1.30	0.39	0.04	1,080.00
06231RD	193.66	194.65	HG_A012	5400	19770	-75	Feathery	14.00	100.00	36.00	3.90	1,080.00	110.00	0.26	7.69	331.00	0.90	0.46	5.90	0.87	0.19	0.08	802.00
06231RD	194.65	196.50	HG_A013	5401	19770	-77	Feathery	14.20	56.00	43.00	3.40	1,220.00	144.00	0.17	7.64	294.00	0.10	0.61	3.90	0.63	0.09	0.01	501.00
06231RD	196.50	198.00	HG_A014	5401	19770	-78	Moss	2.70	100.00	5.00	9.70	799.00	76.00	0.12	3.78	180.50	0.50	0.13	0.90	0.50	0.01	0.34	374.00
06216RD	215.40	217.10	HG_A015	5392	19767	-86	Feathery	5.20	100.00	24.00	5.90	793.00	96.00	0.17	7.53	207.00	0.80	0.35	2.70	0.99	0.17	0.02	416.00
06216RD	220.00	222.35	HG_A016	5395	19767	-91	Comb	6.00	80.00	55.00	3.10	865.00	123.00	0.21	6.57	207.00	1.60	0.63	2.40	1.25	0.06	0.93	418.00
06216RD	228.40	230.10	HG_A017	5399	19767	-97	Flamboyant	16.70	65.00	92.00	6.30	652.00	162.00	0.31	4.51	457.00	0.20	0.94	3.10	1.54	0.05	0.01	655.00
02771RD	205.30	216.70	HG_A018	5390	19782	-88	Banded	4.10	100.00	21.00	3.10	551.00	57.00	0.10	2.24	145.50	0.30	0.22	1.80	0.82	0.03	0.44	302.00
02771RD	221.00	222.50	HG_A019	5387	19783	-93	Feathery	7.20	10.00	13.00	8.50	935.00	90.00	0.05	6.99	497.00	0.80	0.32	1.70	0.28	0.06	0.42	1,290.00
02771RD	225.00	225.80	HG_A020	5385	19783	-96	Feathery	5.80	25.00	37.00	1.10	831.00	37.00	0.09	5.63	79.60	0.30	0.37	1.40	0.39	0.13	0.03	163.00

Hole ID	From (m)	To (m)	Sample no.	E(x)	N(y)	RL(z)	Texture classification	Au	Ag	As	Cd	Cr	Cu	Hg	Mo	Pb	Rb	S%	Se	Sb	Te	Tl	Zn
02537RD	160.00	163.50	HG_A021	5370	19681	-43	Saccharoidal/massive	3.30	32.00	24.00	0.70	625.00	30.00	0.06	5.88	23.40	1.50	0.23	1.70	0.68	0.03	0.06	101.00
02564RD	120.50	122.20	HG_A022	5374	19677	-8	Plumose	7.00	63.00	4.00	0.30	546.00	15.00	0.15	3.81	27.90	1.30	0.09	4.10	0.81	0.02	0.38	59.00
02626RD	260.50	264.00	HG_A023	5369	19674	-126	Saccharoidal/massive	3.70	98.00	33.00	7.50	741.00	73.00	0.11	2.93	71.20	1.30	1.15	1.80	0.61	0.12	0.08	233.00
00959RD	142.15	143.05	HG_A024	5385	19704	-29	Banded	8.80	28.00	12.00	0.80	494.00	34.00	0.11	2.78	71.30	1.00	0.23	1.90	1.02	0.49	0.03	212.00
03217RD	326.10	327.20	HG_A026	5374	19693	-192	Feathery	1.10	2.00	1.00	1.20	290.00	77.00	0.01	3.43	14.70	0.10	0.53	0.70	0.09	0.08	0.02	124.00
03368RD	276.00	278.00	HG_A027	5387	19705	-145	Feathery	7.20	48.00	81.00	5.80	518.00	115.00	0.19	12.75	227.00	0.80	1.21	3.60	1.77	0.06	0.56	420.00
02535RD	102.00	103.10	HG_A028	5389	19718	6	Banded	4.00	45.00	67.00	0.50	522.00	30.00	0.06	4.52	29.00	2.40	0.64	4.20	2.13	0.06	0.69	76.00
02560RD	188.00	189.30	HG_A029	5387	19725	-71	Banded	4.30	9.00	5.00	0.60	523.00	45.00	0.03	0.17	48.10	0.40	0.12	0.90	0.08	0.14	0.04	108.00
06186RD	120.00	121.00	HG_A030	5384	19724	-5	Moss	0.80	3.00	31.00	0.00	602.00	9.00	0.02	9.40	5.90	0.60	0.67	0.90	0.43	0.01	0.19	65.00
02504RD	110.00	117.00	HG_A031	5376	19750	-3	Flamboyant	2.40	17.00	54.00	0.20	674.00	25.00	0.04	6.42	13.70	0.50	0.65	1.80	0.86	0.03	0.19	44.00
02562RD	243.30	247.00	HG_A032	5387	19752	-120	Feathery	11.40	26.00	46.00	5.60	533.00	362.00	0.15	3.48	361.00	2.30	0.87	2.70	0.83	0.80	0.22	1,020.00
03224RD	217.40	224.15	HG_A033	5388	19744	-89	Feathery	3.30	84.00	11.00	1.90	695.00	44.00	0.08	5.46	64.90	0.60	0.20	3.80	0.24	0.03	0.31	191.00
02559RD	169.30	171.00	HG_A034	5395	19778	-53	Moss	0.90	13.00	181.00	0.30	756.00	64.00	0.45	19.80	21.80	4.90	3.15	3.60	6.89	0.07	3.74	38.00
07554RD	157.40	158.50	HG_A036	5419	19777	-65	Feathery	6.20	87.00	68.00	2.10	584.00	33.00	0.26	3.04	56.50	0.90	0.79	1.90	1.39	0.08	0.12	151.00
07554RD	203.00	206.40	HG_A037	5394	19778	-106	Saccharoidal/massive	0.50	2.00	18.00	1.30	542.00	82.00	0.02	19.75	92.80	0.10	0.34	1.20	0.97	0.17	0.01	192.00
07554RD	208.50	209.25	HG_A038	5392	19779	-108	Feathery	8.80	32.00	33.00	7.90	649.00	215.00	0.21	3.95	452.00	0.10	0.72	2.40	0.82	0.15	0.02	824.00
07555RD	267.70	269.00	HG_A039	5388	19776	-167	Moss	2.50	4.00	25.00	19.20	493.00	188.00	0.10	4.17	904.00	0.40	1.22	4.30	0.39	0.13	0.20	1,740.00
07555RD	305.75	307.00	HG_A040	5370	19777	-201	Comb	6.60	7.00	85.00	2.50	228.00	200.00	0.03	6.64	144.00	0.80	1.51	1.40	0.43	0.07	0.33	220.00
07556RD	179.40	180.31	HG_A041	5365	19624	-91	Plumose	4.20	11.00	58.00	0.50	566.00	51.00	0.07	5.32	20.40	0.20	0.43	1.00	0.63	0.11	0.07	70.00
07556RD	226.00	229.00	HG_A042	5341	19624	-133	Saccharoidal/massive	0.10	1.00	40.00	0.50	337.00	77.00	0.02	3.42	34.10	0.90	1.10	0.50	0.34	0.02	0.01	122.00

APPENDIX C

Analytical Techniques for Trace element data

by ICP-MS and AES from ALS Lab analysis

Trace element or whole rock geochemistry analysis is completed at Australian Laboratory Service (ALS) using procedure ME-MS41. In order to report the widest possible concentration range, this method uses both ICP-MS (Inductively Coupled Plasma Mass Spectrometer) and ICP-AES (Inductively Coupled Plasma Atomic Emission Spectrometer). They provides the element values in totally 51 elements including Ag, Al, As, Au, B, Ba, Be, Bi, Ca, Cd, Ce, Co, Cr, Cs, Cu, Fe, Ga, Ge, Hf, Hg, In, K, La, Li, Mg, Mn, Mo, Na, Nb, Ni, P, Pb, Rb, Re, S, Sb, Sc, Se, Sn, Sr, Ta, Te, Th, Ti, Tl, U, V, W, Y, Zn, Zr, Ag. Prior to both the ICP-MS and ICP-AES techniques, minimum 1 g of milled samples was digested using an aqua regia with ultra-low detection limit and multi-element package useful for exploration (ALS Chemex, 2011).

51 elements by aqua regia digestion, ICP-MS and ICP-AES (ME-MS41 method)

Although some base metals may dissolve quantitatively, in the majority of geological matrices, data reported from an aqua regia leach should be considered as representing only the leachable portion of the particular analyze. The recovery percentages for many analyze from more resistive minerals can be very low, but the acid leachable portion can also be an excellent exploration tool. In order to report the widest possible concentration range, this method uses both the ICP-MS and the ICP-AES techniques. Minimum sample size is 1g. (ALS Chemex, 2011)

Sample ID	Ag ppm ME-MS41	Al % ME-MS41	As ppm ME-MS41	Au ppm ME-MS41	B ppm ME-MS41	Ba ppm ME-MS41	Be ppm ME-MS41	Bi ppm ME-MS41	Ca % ME-MS41	Cd ppm ME-MS41	Ce ppm ME-MS41	Co ppm ME-MS41
HG_A1	88.1	0.29	15	>25.0	<10	20	0.05	0.01	3.22	15.85	5.99	2.7
HG_A2	83.6	0.27	49	>25.0	<10	10	0.05	0.01	19.35	4.55	31.8	1.3
HG_A3	29.6	0.27	10.3	1.4	<10	10	<0.05	0.01	3.62	1.57	4.38	1.2
HG_A4	2.41	1.66	12.8	0.4	<10	10	0.25	0.02	2.72	0.21	1.63	4.5
HG_A5	80.8	0.26	2	5.9	<10	<10	0.12	0.01	4.25	0.5	2.64	1.8
HG_A6	>100	0.51	19.1	6.6	<10	<10	0.15	0.01	5.12	6.75	3.13	1.5
HG_A7	94.8	0.52	12.2	4.8	<10	<10	0.17	0.01	5.61	1.16	1.37	1.4
HG_A8	5.48	0.08	<2	1	<10	<10	0.08	0.01	>25.0	0.78	3.25	0.3
HG_A9	>100	0.65	11.2	9.1	<10	<10	0.1	0.01	9.53	3.01	2.1	0.9
HG_A10	13.6	0.24	22	9.6	<10	<10	0.06	0.01	20.4	2.5	1.95	0.7
HG_A11	>100	0.17	53	>25.0	<10	10	0.06	0.01	2.93	6.7	3.4	2.1
HG_A12	>100	0.33	35.6	14	<10	20	0.08	0.01	2	3.86	1.13	2
HG_A13	55.7	0.29	43.1	14.2	<10	10	0.07	0.01	1.28	3.35	1.28	2.3
HG_A14	>100	0.36	4.5	2.7	<10	<10	0.13	0.01	4.54	9.69	0.8	1.5
HG_A15	>100	0.45	23.7	5.2	<10	<10	0.09	0.01	2.51	5.9	1.75	1.6
HG_A16	79.5	0.51	55.1	6	<10	10	0.08	0.01	2.45	3.06	3.01	3.3
HG_A17	64.9	0.63	92.2	16.7	<10	30	0.13	0.01	0.4	6.32	1.7	5.8
HG_A18	>100	0.39	20.8	4.1	<10	<10	0.07	0.01	2.4	3.1	1.8	0.8
HG_A19	9.81	0.39	12.7	7.2	<10	10	0.1	0.06	1.02	8.52	1.24	2.6
HG_A20	24.5	1.53	36.5	5.8	10	10	1.57	0.2	2.35	1.09	3.61	4.5
HG_A21	31.8	0.46	24	3.3	<10	<10	0.14	0.01	2.2	0.69	2.64	0.9
HG_A22	63.1	0.32	4	7	<10	<10	0.08	0.01	11.55	0.29	1.21	1
HG_A23	98.3	0.66	32.6	3.7	<10	20	0.06	0.02	1.84	7.51	1.32	4.7
HG_A24	27.8	0.31	11.9	8.8	<10	10	0.09	0.01	4.15	0.75	2.41	0.8
HG_A26	2.28	0.52	<2	1.1	200	20	<0.05	0.02	19.85	1.22	4.23	2.2
HG_A27	47.7	0.45	81.4	7.2	<10	10	0.06	0.01	4.69	5.75	2.19	4.1
HG_A28	45.2	0.32	67	4	<10	10	0.07	0.01	12.9	0.47	3.5	1.7
HG_A29	8.65	0.56	4.6	4.3	<10	<10	0.11	0.01	5	0.63	2.13	0.6
HG_A30	3.06	1.41	30.9	0.8	<10	10	0.21	0.02	4.91	0.03	4.42	1.7
HG_A31	17.3	0.33	54	2.4	<10	10	0.13	0.01	2.43	0.22	2.38	2.6
HG_A32	26	0.42	45.5	11.4	<10	10	0.06	0.01	4.4	5.62	2.39	2.6
HG_A33	83.6	0.5	11.2	3.3	<10	10	0.1	0.02	5.13	1.91	2.69	1.7
HG_A34	13.1	0.32	180.5	0.9	<10	40	0.08	0.02	0.55	0.33	5.23	11.6
HG_A36	87.2	0.35	68.3	6.2	<10	<10	0.08	0.01	2.46	2.1	3.09	2.2
HG_A37	2.33	0.2	17.6	0.5	<10	10	0.07	0.01	5.75	1.25	19.35	1.3
HG_A38	32	0.26	32.8	8.8	<10	10	0.24	0.01	3.04	7.88	2.58	1.5
HG_A39	4.35	1.02	25.3	2.5	<10	<10	0.05	0.01	5.66	19.2	1.87	2.1
HG_A40	7.02	1.88	85.1	6.6	<10	220	0.14	0.01	6.83	2.46	7.52	13
HG_A41	11.15	0.2	57.5	4.2	<10	50	<0.05	0.01	2.29	0.45	3.6	2.6
HG_A42	1.03	1.59	40.3	<0.2	20	50	0.14	0.01	3.11	0.51	6.78	10.2

Sample ID	Cs	Cu	Fe	Ga	Ge	Hf	Hg	In	K	La	Li	Mg
	ppm	ppm	%	ppm	ppm	ppm	ppm	ppm	%	ppm	ppm	%
	ME-MS41	ME-MS41	ME-MS41	ME-MS41	ME-MS41	ME-MS41	ME-MS41	ME-MS41	ME-MS41	ME-MS41	ME-MS41	ME-MS41
HG_A1	<0.05	349	1.34	1.98	<0.05	<0.02	0.69	0.018	0.03	3.1	2.8	0.39
HG_A2	0.05	510	0.68	1.39	<0.05	0.03	0.61	0.015	0.04	19.6	2.3	0.38
HG_A3	<0.05	47.5	0.8	1.79	<0.05	<0.02	0.04	<0.005	0.04	2.5	2.2	0.34
HG_A4	0.06	19.2	1.7	7.53	0.06	0.06	0.01	0.013	0.02	0.8	11.7	3.02
HG_A5	<0.05	19.8	1.13	1.89	<0.05	<0.02	0.08	0.022	<0.01	1.5	3.2	0.32
HG_A6	<0.05	136.5	1.12	3.48	<0.05	<0.02	0.47	<0.005	0.02	1.8	6.1	0.78
HG_A7	<0.05	48.8	0.89	3.7	<0.05	<0.02	0.11	<0.005	<0.01	0.9	4.8	0.96
HG_A8	<0.05	79.5	0.15	0.73	<0.05	<0.02	0.05	<0.005	<0.01	3.1	0.6	0.13
HG_A9	<0.05	62.1	0.89	3.81	<0.05	<0.02	0.19	<0.005	<0.01	1.5	6.4	1.2
HG_A10	<0.05	70.2	0.58	1.33	<0.05	<0.02	0.09	<0.005	<0.01	1.4	2	0.37
HG_A11	<0.05	160	1.36	1.35	<0.05	<0.02	0.31	0.008	0.03	1.9	1.7	0.24
HG_A12	<0.05	109.5	1.34	2.35	<0.05	<0.02	0.26	<0.005	0.02	0.6	3.7	0.58
HG_A13	<0.05	144	1.55	1.89	<0.05	<0.02	0.17	<0.005	0.02	0.7	3.3	0.4
HG_A14	<0.05	75.6	0.89	4.04	<0.05	<0.02	0.12	<0.005	<0.01	0.6	5	0.71
HG_A15	<0.05	96.4	1.11	2.99	<0.05	<0.02	0.17	<0.005	0.02	1.1	4.6	0.73
HG_A16	<0.05	123	1.49	3.01	<0.05	<0.02	0.21	0.005	0.02	1.7	4.7	0.86
HG_A17	0.06	162	1.55	2.93	<0.05	0.03	0.31	0.012	0.11	0.7	6.4	0.9
HG_A18	<0.05	57	0.76	2.98	<0.05	<0.02	0.1	<0.005	0.01	1.1	3.3	0.71
HG_A19	<0.05	90.2	1.22	2.24	<0.05	0.02	0.05	0.019	0.02	0.6	3.4	0.55
HG_A20	<0.05	36.5	1.95	8.17	0.12	0.03	0.09	0.047	0.04	1.5	7	0.98
HG_A21	<0.05	29.8	0.86	2.98	<0.05	<0.02	0.06	<0.005	0.02	1.5	6.2	0.71
HG_A22	<0.05	15.4	0.65	2.27	<0.05	<0.02	0.15	<0.005	<0.01	0.8	2.7	0.61
HG_A23	<0.05	72.6	1.62	3.67	<0.05	0.03	0.11	0.013	0.03	0.7	5.3	1.25
HG_A24	<0.05	34.3	0.74	1.9	<0.05	<0.02	0.11	<0.005	0.03	1.4	3.2	0.44
HG_A26	<0.05	77.3	1	2.93	<0.05	0.09	0.01	0.008	0.06	2.8	1.7	0.52
HG_A27	0.08	115	1.66	2.32	<0.05	0.02	0.19	0.008	0.03	1.3	3.2	0.61
HG_A28	<0.05	30.2	1.1	1.99	<0.05	<0.02	0.06	<0.005	0.02	2.1	2.6	0.51
HG_A29	<0.05	45.4	0.79	3.45	<0.05	<0.02	0.03	<0.005	0.01	1.3	6.5	0.95
HG_A30	0.05	9.2	1.48	7.49	<0.05	0.13	0.02	0.011	0.03	1.8	9.8	2.96
HG_A31	0.12	25.4	1.16	1.38	<0.05	<0.02	0.04	<0.005	0.06	1.2	3.6	0.39
HG_A32	<0.05	362	1.42	2.58	<0.05	<0.02	0.15	0.014	0.02	1.2	3.2	0.65
HG_A33	<0.05	43.5	0.95	3.31	<0.05	0.02	0.08	0.014	0.01	1.7	3.7	0.81
HG_A34	0.13	63.8	3.27	1.31	<0.05	0.05	0.45	0.014	0.18	2.5	1.4	0.21
HG_A36	<0.05	33.3	1.32	2.37	<0.05	0.02	0.26	0.006	0.01	1.7	3.2	0.51
HG_A37	0.06	81.8	0.64	1.03	<0.05	<0.02	0.02	0.006	0.02	10.3	2.1	0.26
HG_A38	<0.05	215	1.34	1.08	<0.05	0.03	0.21	0.01	0.03	1.3	3.2	1.46
HG_A39	0.1	188	2.03	7.32	<0.05	<0.02	0.1	0.016	0.01	1.3	5.1	1.91
HG_A40	0.11	199.5	3.53	10.75	<0.05	0.07	0.03	0.023	0.08	4	12.9	2.62
HG_A41	<0.05	50.7	1.01	1.14	<0.05	<0.02	0.07	0.006	0.07	1.8	1.6	0.22
HG_A42	0.1	77	2.81	7.06	<0.05	0.04	0.02	0.016	0.05	3.2	15.2	2.04

Sample ID	Mn ppm ME-MS41	Mo ppm ME-MS41	Na % ME-MS41	Nb ppm ME-MS41	Ni ppm ME-MS41	P ppm ME-MS41	Pb ppm ME-MS41	Rb ppm ME-MS41	Re ppm ME-MS41	S % ME-MS41	Sb ppm ME-MS41	Sc ppm ME-MS41
HG_A1	751	5.78	0.01	0.05	18.2	20	341	0.8	0.003	0.65	1.44	1.4
HG_A2	5180	8.61	0.01	<0.05	1.5	30	254	1.4	0.004	0.59	0.87	2.4
HG_A3	921	0.81	0.01	<0.05	4.5	20	47.3	1.3	0.001	0.16	0.3	1.3
HG_A4	1480	2.22	0.02	<0.05	7.1	100	9.6	0.4	0.011	0.62	0.27	2.8
HG_A5	911	5.59	0.01	0.06	21	10	3.4	0.1	0.004	0.04	0.16	1.2
HG_A6	1520	6.02	0.01	0.05	16.8	10	236	1	0.002	0.31	4.73	1
HG_A7	1600	4.12	0.01	<0.05	12.9	20	94.7	0.1	0.001	0.17	0.66	0.6
HG_A8	5100	0.48	0.01	0.05	1.4	10	78.9	<0.1	0.001	0.09	0.12	0.3
HG_A9	2350	1.53	0.01	<0.05	2.7	30	177	0.1	0.001	0.32	0.81	1.1
HG_A10	3200	7.85	0.01	<0.05	1.2	40	208	0.1	0.003	0.36	0.89	0.8
HG_A11	661	9.36	0.01	0.06	22.1	30	511	0.8	0.004	0.54	1.3	0.8
HG_A12	712	7.69	0.01	0.05	22	20	331	0.4	0.002	0.46	0.87	0.8
HG_A13	565	7.64	0.01	0.06	24.4	40	294	0.5	0.003	0.61	0.63	1.1
HG_A14	1460	3.78	0.01	<0.05	15.5	10	180.5	0.2	0.001	0.13	0.5	0.4
HG_A15	837	7.53	0.01	<0.05	15.6	30	207	0.8	0.003	0.35	0.99	0.6
HG_A16	761	6.57	0.01	<0.05	19.2	90	207	0.5	0.006	0.63	1.25	2.5
HG_A17	488	4.51	0.01	<0.05	7.3	120	457	2.4	0.006	0.94	1.54	3.2
HG_A18	769	2.24	0.01	<0.05	3.8	10	145.5	0.4	0.002	0.22	0.82	0.8
HG_A19	357	6.99	<0.01	<0.05	18.5	30	497	0.4	0.002	0.32	0.28	1.4
HG_A20	449	5.63	0.01	<0.05	18.2	50	79.6	0.8	0.002	0.37	0.39	2.6
HG_A21	718	5.88	0.01	<0.05	4.5	30	23.4	0.9	0.003	0.23	0.68	1.4
HG_A22	1920	3.81	0.01	<0.05	11	60	27.9	0.1	0.001	0.09	0.81	0.3
HG_A23	918	2.93	0.01	<0.05	7.1	20	71.2	0.5	0.001	1.15	0.61	3
HG_A24	1060	2.78	0.01	<0.05	3.3	20	71.3	0.8	0.001	0.23	1.02	1
HG_A26	2850	3.43	0.01	0.07	5.8	140	14.7	0.9	0.002	0.53	0.09	2
HG_A27	1060	12.75	0.01	<0.05	5.6	50	227	1.6	0.006	1.21	1.77	3
HG_A28	2330	4.52	0.01	0.05	10.3	160	29	0.6	0.002	0.64	2.13	0.9
HG_A29	1370	0.17	0.01	<0.05	3.4	10	48.1	0.2	<0.001	0.12	0.08	2.4
HG_A30	2430	9.4	0.01	<0.05	4.8	80	5.9	0.5	0.004	0.67	0.43	3.1
HG_A31	659	6.42	0.01	<0.05	5.7	110	13.7	2.3	0.004	0.65	0.86	1.2
HG_A32	1230	3.48	0.01	<0.05	4.7	120	361	0.6	0.004	0.87	0.83	2.4
HG_A33	1220	5.46	0.01	<0.05	13.4	20	64.9	0.2	0.001	0.2	0.24	1
HG_A34	277	19.8	0.01	<0.05	9.7	1110	21.8	4.9	0.017	3.15	6.89	3.7
HG_A36	796	3.04	0.01	<0.05	12.9	160	56.5	0.3	0.003	0.79	1.39	1.6
HG_A37	1460	19.75	0.01	<0.05	11.6	30	92.8	0.9	0.008	0.34	0.97	1.8
HG_A38	917	3.95	0.01	<0.05	4.7	30	452	0.8	0.001	0.72	0.82	2.4
HG_A39	2600	4.17	0.01	<0.05	14.4	20	904	0.3	0.002	1.22	0.39	1.7
HG_A40	2370	6.64	0.01	<0.05	8.1	230	144	1.5	0.007	1.51	0.43	12.3
HG_A41	658	5.32	<0.01	<0.05	9.7	40	20.4	1.3	0.003	0.43	0.63	1.4
HG_A42	1580	3.42	0.02	<0.05	7.3	190	34.1	1.3	0.003	1.1	0.34	8.4

Sample ID	Se	Sn	Sr	Ta	Te	Th	Ti	Tl	U	V	W	Y	Zn	Zr	Ag
	ppm	ppm	ppm	ppm	ppm	ppm	%	ppm	ppm	ppm	ppm	ppm	ppm	ppm	ppm
	ME-MS41	ME-MS41	ME-MS41	ME-MS41	ME-MS41	ME-MS41	ME-MS41	ME-MS41	ME-MS41	ME-MS41	ME-MS41	ME-MS41	ME-MS41	ME-MS41	Ag-OG46
HG_A1	2.6	0.3	15.2	<0.01	0.04	<0.2	<0.005	0.05	<0.05	16	0.69	6.18	1540	<0.5	
HG_A2	3.9	0.2	91.9	<0.01	1.32	<0.2	<0.005	0.24	<0.05	9	<0.05	42	852	<0.5	
HG_A3	0.6	<0.2	18.1	<0.01	0.05	<0.2	<0.005	0.07	<0.05	10	<0.05	3.72	85	<0.5	
HG_A4	0.5	0.2	42.5	<0.01	0.02	<0.2	0.017	0.09	0.11	26	0.12	2.04	49	1.8	
HG_A5	2.7	0.4	29.6	<0.01	0.2	<0.2	<0.005	<0.02	0.05	12	0.98	3.32	63	<0.5	
HG_A6	5.2	0.3	27.6	<0.01	0.07	<0.2	<0.005	0.03	0.07	15	0.87	3.72	664	<0.5	379
HG_A7	2.8	0.2	34.9	<0.01	0.02	<0.2	<0.005	0.02	0.08	9	0.62	1.5	224	<0.5	
HG_A8	0.9	<0.2	164.5	<0.01	0.21	<0.2	<0.005	<0.02	<0.05	2	0.13	2.37	225	<0.5	
HG_A9	3.1	<0.2	60.3	<0.01	0.04	<0.2	<0.005	0.02	0.05	13	0.08	2.73	380	<0.5	139
HG_A10	1.2	<0.2	120	<0.01	0.05	<0.2	<0.005	0.07	<0.05	10	0.06	2.55	400	<0.5	
HG_A11	6.2	0.4	18.6	<0.01	0.39	<0.2	<0.005	0.56	<0.05	10	0.99	2.49	1080	<0.5	140
HG_A12	5.9	0.5	14.1	<0.01	0.19	<0.2	<0.005	0.2	<0.05	13	1.17	1.19	802	<0.5	162
HG_A13	3.9	0.4	7.8	<0.01	0.09	<0.2	<0.005	0.15	<0.05	20	1.15	1.01	501	<0.5	
HG_A14	0.9	0.2	24.8	<0.01	<0.01	<0.2	<0.005	<0.02	0.11	9	0.77	1.31	374	<0.5	168
HG_A15	2.7	0.3	14.2	<0.01	0.17	<0.2	<0.005	0.33	0.07	11	0.72	2.06	416	<0.5	101
HG_A16	2.4	0.4	14.7	<0.01	0.06	<0.2	<0.005	0.41	<0.05	26	0.73	3.71	418	<0.5	
HG_A17	3.1	0.2	6.3	<0.01	0.05	<0.2	0.005	0.69	0.1	28	0.06	2.35	655	0.8	
HG_A18	1.8	<0.2	15.9	<0.01	0.03	<0.2	<0.005	0.06	0.15	9	0.11	3.51	302	<0.5	95
HG_A19	1.7	0.6	9.6	<0.01	0.06	<0.2	<0.005	0.04	<0.05	14	0.71	2	1290	0.6	
HG_A20	1.4	0.9	19.7	<0.01	0.13	<0.2	0.014	0.04	0.11	20	0.73	8.14	163	1	
HG_A21	1.7	0.2	14.5	<0.01	0.03	<0.2	<0.005	0.08	0.05	18	<0.05	3.29	101	<0.5	
HG_A22	4.1	0.2	65.2	<0.01	0.02	<0.2	<0.005	<0.02	<0.05	7	0.61	1.09	59	<0.5	
HG_A23	1.8	<0.2	25.8	<0.01	0.12	<0.2	0.011	0.34	<0.05	21	<0.05	1.69	233	0.8	
HG_A24	1.9	<0.2	20.3	<0.01	0.49	<0.2	<0.005	0.02	<0.05	15	<0.05	1.45	212	<0.5	
HG_A26	0.7	0.2	118.5	<0.01	0.08	<0.2	0.021	<0.02	<0.05	21	0.36	3.75	124	2.8	
HG_A27	3.6	<0.2	26.4	<0.01	0.06	<0.2	<0.005	0.93	<0.05	22	<0.05	2.77	420	0.5	
HG_A28	4.2	0.2	72.1	<0.01	0.06	<0.2	<0.005	0.19	0.21	11	0.56	4.13	76	<0.5	
HG_A29	0.9	<0.2	28.4	<0.01	0.14	<0.2	<0.005	<0.02	<0.05	15	<0.05	1.44	108	<0.5	
HG_A30	0.9	0.3	49.3	<0.01	0.01	0.2	0.005	0.19	0.68	32	0.05	3.66	65	3.1	
HG_A31	1.8	<0.2	18.9	<0.01	0.03	<0.2	<0.005	0.22	0.17	11	0.08	3.23	44	<0.5	
HG_A32	2.7	<0.2	23.7	<0.01	0.8	<0.2	<0.005	0.31	<0.05	25	0.07	2.58	1020	<0.5	
HG_A33	3.8	0.3	30	<0.01	0.03	<0.2	<0.005	0.07	<0.05	13	0.69	2.94	191	<0.5	
HG_A34	3.6	<0.2	8.7	<0.01	0.07	<0.2	<0.005	3.74	0.86	62	0.19	4.61	38	1.5	
HG_A36	1.9	0.3	12.4	<0.01	0.08	<0.2	<0.005	0.44	0.15	33	0.93	2.92	151	0.6	
HG_A37	1.2	0.2	26.1	<0.01	0.17	<0.2	<0.005	0.12	<0.05	7	0.83	19.8	192	<0.5	
HG_A38	2.4	<0.2	59	<0.01	0.15	<0.2	<0.005	0.42	<0.05	12	0.06	5.36	824	1.4	
HG_A39	4.3	0.3	38.3	<0.01	0.13	<0.2	<0.005	0.03	<0.05	61	1.14	3.38	1740	<0.5	
HG_A40	1.4	0.2	55.9	<0.01	0.07	<0.2	0.032	0.06	<0.05	152	0.09	8.9	220	1.6	
HG_A41	1	0.2	12.6	<0.01	0.11	<0.2	<0.005	0.38	<0.05	15	0.69	2.8	70	<0.5	
HG_A42	0.5	<0.2	29.4	<0.01	0.02	<0.2	0.007	0.08	<0.05	87	<0.05	6.43	122	0.9	

APPENDIX D

Box Plot of Trace element

Trace element (Au, Te, Sb, Mo, Cd in ppm and S %) using box diagram correlation to quartz texture.

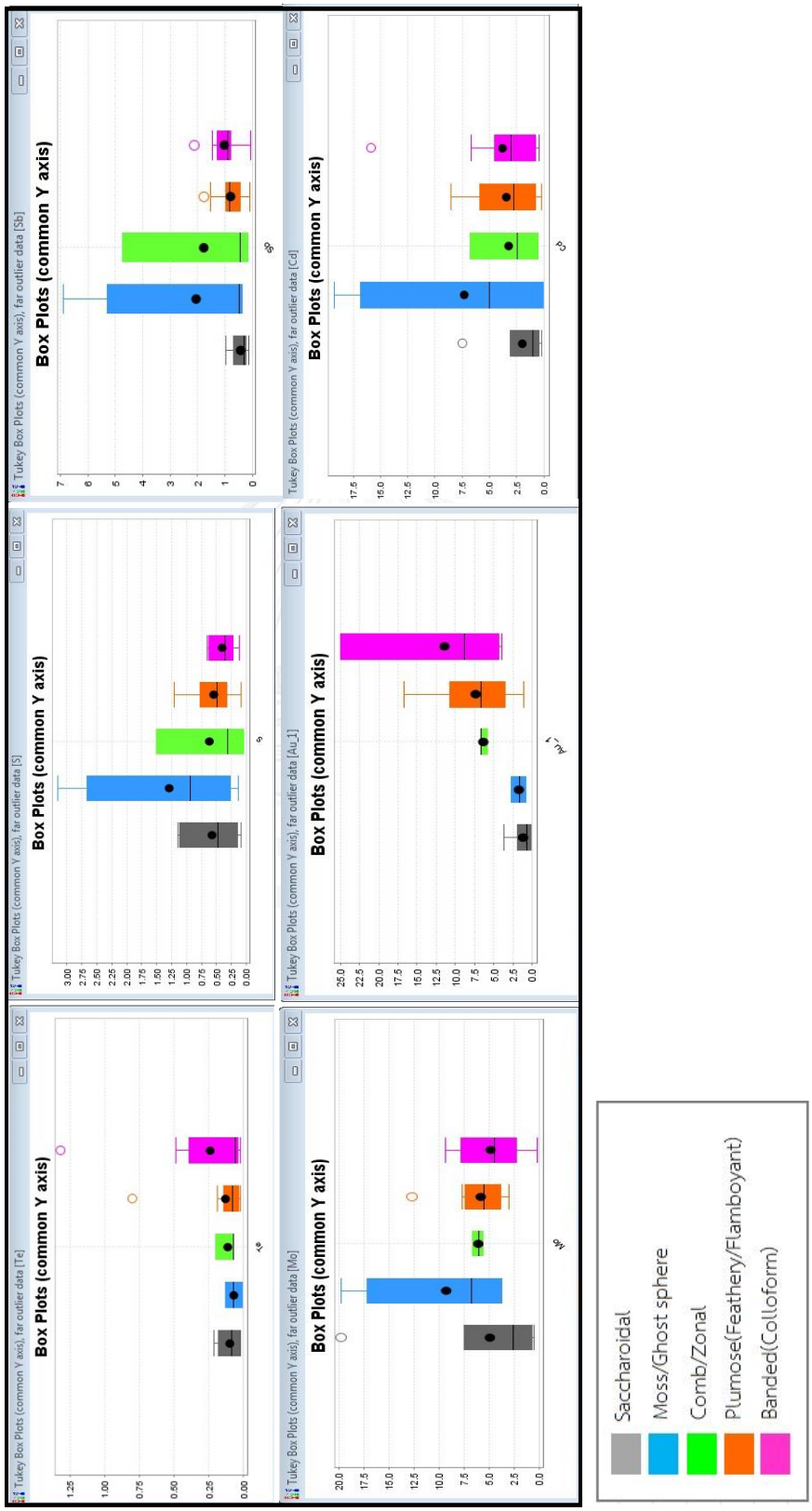

Trace element (Ag, As, Cu, Pb, Zn and Cr in ppm) using box diagram correlation to quartz texture.

Trace element (Ag, As, Cu, Pb, Zn and Cr in ppm) using box diagram correlation to sulphide assemblage, (zooming scale on the bar graph).

Trace element (Au, Te, Sb, Cd, Mo in ppm and S in %) using box diagram correlation to sulphide assemblage, (zooming scale on the bar graph).

VITA

Miss Phinyaphat Rongkhapimonpong was born in Phetchaburi, central provinces of Thailand, on February 4, 1984. After finishing the high school from Benchamatheputit School, Phetchaburi in 2003; she was chosen to study in Chulalongkorn University, where she acquired the B.Sc. degree in Geology from the Department of Geology, Faculty of Science, Chulalongkorn University in 2007. After graduation, she worked with Akara Mining Ltd. and Issara Mining Ltd. She continued her study in the M.Sc. program in geology at Graduate School, Chulalongkorn University, in 2011. The research work has been focused on mineralization and geochemistry.